CATALYTIC CARBONYLATION OF TERMINAL ALKYNE WITH AMINE: COMPUTATIONAL AND EXPERIMENTAL INVESTIGATIONS OF REGIOSELECTIVITY

JAMEEL AL-THAGFI

CHEMISTRY

MAY 2004

KING FAHAD UNIVERSITY OF PETROLEUM AND MINERALS
DHAHRAN 31261, SAUDI ARABIA

DEANSHIP OF GRADUATE STUDIES

This thesis, written by Jameel Al-Thagfi under the direction of his thesis advisor and approved by the thesis committee, has been presented to and accepted the Dean of Graduate Studies, in partial fulfillment of the requirements for the degree of MASTER OF SCIENCE IN CHEMISTRY.

Thesis committee

m. a. morsy
Dr. Mohamed Morsy
Thesis Advisor

Prof. Bassam El Ali
Member

A. Sanyan
Prof. Abdulaziz Al-Suwaiyan
Member

Dr. Mohammad Fettouhi
Member

Prof. Salah Sultan
Member

Dr. Zaki Seddagi
Department Chairman

for
Dr. Mohammad Al-Ohali
Dean of Graduate Studies

٢٨/١١/٢٠٠٤
Nov. 28th, 2004
Date

To my parents,
my wife and
my family

ACKNOWLEDGMENT

Praise and thanks be to Allah for helping me to accomplish this thesis and in all of my life.

A great thank is to King Fahad University of Petroleum and Minerals for supporting and providing facilities of the study.

Sincere appreciation and grateful thank to my thesis advisor Dr. Mohamed Morsy. The achievements of this research are due to his supporting efforts, criticism, encouragement and valuable discussion time. I would like to express my gratitude to the co-advisor Prof. Bassam El Ali for his assistance during the experimental work and his qualified suggestions. I also express my deep thanks to the thesis committee members: Prof. Abdulaziz Al-Suwaiyan, Dr. Mohammad Fettouhi and Prof. Salah Sultan for professional guidance, valuable discussions and talented ideas.

I wish to thank the chairmen of the chemistry department Dr. Zaki Seddigi and Dr. Assad Al-Thukair (previous chairman) for their support and assistance. My thanks are also to Dr. I. Forristal and Dr. H. Perzanowski for their useful discussions.

I would like to thank Mr. Tijani and Mr. Bahauddin for their helping in the experimental setup and related dissections. My thank is also to the department staffs: Mr. Arab, Mr. Baig, Mr. Fayyaz, Mr. Mazhar, Mr. Ismail, Mr. Al-Gushiri for their helpful supports.

TABLE OF CONTENTS

LIST OF TABELS

LIST OF FIGURES

THESIS ABSTRACT

Name: Jameel Al-Thagfi
Title: Catalytic Carbonylation of Terminal Alkyne with Amine: Computational and Experimental Investigations of Regioselectivity
Major Field: Chemistry
Date: May 2003

The catalytic carbonylation reaction is one of the most important applications of homogenous catalysts. Many catalytic carbonylation processes of alkynes are activated using complexes of nickel, palladium, and platinum with phosphine ligands. Different products can be formed from the carbonylation reactions depending on the type of the nucleophile. Recently, the Pd-catalytic carbonylation reaction of terminal alkynes conducted with aniline forms gem- and trans-α,ß-unsaturated amides with a total control of the regioselectivity under certain reaction conditions. The products' distribution (regioselectivity) was affected by the variation of the experimental conditions of the catalytic systems. The explanation of the detailed mechanism of this palladium carbonylation process is not developed yet. Theoretical calculations provide the best approach to reveal the detailed mechanism of this catalytic process.

In this study, density function calculations have been carried out to investigate the mechanism of this catalytic carbonylation process. The computed results show that an oxidative-addition mechanism with the possibility of phosphine ligand to coordinate/decoordinate over the process is the major pathway of the process that use syngas (CO/H_2) and terminal alkyne. Several experiments were performed to test the proposed reaction routes and the rate-determining step.

ملخص الرسالة

الاســـــم: جميل رده الثقفي
عنوان الرسالة: دراسة حسابية و عملية لتفاعل أول أكسيد الكربون مع الألكاينات في وجود مادة الأمين و المحفز بمركبات عنصر الباليديوم
التخصص: كيمياء
تاريخ التخرج: مايو 2004

يعتبر التفاعل المحفز لأول أكسيد الكربون من أهم تطبيقات المحفزات المتجانسة. حيث ُيسرع الكثير من هذه التفاعلات بواسطة مركبات النيكل والباليديوم والبلاتين مع الفوسفين. و تنتج تفاعلات الألكاينات مع أول أكسيد الكربون في وجود الأنيلين مركبات الأمايد غير المشبع ذات توزيع فراغي يعرف باسم جم (gem) و ترانس (trans). وتم التحكم في نسبة كل منتج على حده تحت ظروف معملية معينة.

لم تتم الدراسة الميكانيكية المفصلة للتفاعلات المحفزة لأول أكسيد الكربون من قبل لصعوبة فصل المواد الوسيطة ولكون التفاعل يتم تحت ضغط عالي من الغاز. لذلك تكون الدراسة الحسابية مهمة لفهم التفاعل بصورة أوضح. و لقد استخدمت عدة طرق حسابية من أفضلها طريقة كثافة الدالة (density function) لدراسة بعض التفاعلات المشابهة و التي عرضت طريقتين مختلفتين لميكانيكية هذه التفاعلات وهي: طريقة الإضافة بالأكسدة لمادة الألكاينات إلي مركبات الباليديوم أو طريقة تكوين متراكب من مركبات الباليديوم و الرابطة الثنائية لمادة الألكينات.

في هذا البحث ستتم دراسة ميكانيكية تفاعل أول أكسيد الكربون مع الألكاينات في وجود مادة الأنيلين و المحفز بمركبات عنصر الباليديوم بواسطة الحاسب الآلي لتحديد الحالة الانتقالية و المواد الوسيطة المشاركة في دائرة التحفيز و ارتباطها بسرعة التفاعل.

أوضحت الدراسة أن طريقة الإضافة بالأكسدة لمادة الألكاينات إلي مركبات الباليديوم هي الطريقة الأساسية لإجراء التفاعل وأن ارتباط و انفصال مجموعة الفوسفين له دور رئيسي في ميكانيكية التفاعل.

و لقد تم إجراء عدد من التجارب لاختبار الميكانيكية المقترحة. مثل استخدام الألكاين الطرفى وغير الطرفي لاختبار طريقة التفاعل. و لتأكد من الخطوة المحددة لسرعة التفاعل تم إجراء تجارب أخرى مع تغير ضغط غاز الهيدروجين و أيضاً تغير تركيز الأنلين

CHAPTER ONE

INTRODUCTION

The catalytic carbonylation process involves reactions of carbon monoxide with saturated or unsaturated organic substrates in the presence of a catalyst [1-5] and it can include nucleophilic species [6-8]. The catalytic carbonylation reaction can be considered as one of the most important applications of homogenous catalysts [1,4]. This process was revealed by Reppe in late of 1930s where carbon monoxide reacted with acetylene to form mono- or dialdehyde [5]. The first example of a commercial utilization of Reppe carbonylation was the production of acrylic acid derivatives (Eq. 1.1) [9]. Group VIII transition metal complexes with carbonyls or other types of ligands have been extensively utilized as catalysts in carbonylation reactions [2,6,9].

$$CH_3—C\equiv C—H + CO + H_2O \xrightarrow{Ni(CO)_4} H_2C=C(CH_3)COOH \qquad 1.1$$

Different products can be formed from carbonylation reactions depending on the type of a nucleophile (Scheme 1.1) [5,9,10]. The scheme shows that the catalytic carbonylation of acetylene gives unsaturated carboxylic acid derivatives such as esters, thioesters, amides and anhydrides.

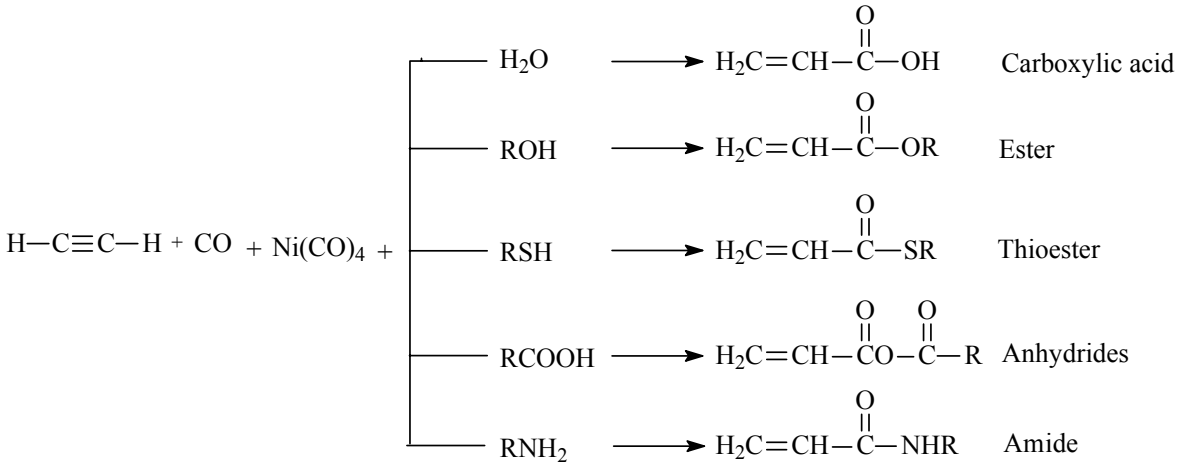

Scheme 1.1: Carbonylation reactions using different types of nucleophiles.

The following sections will summarize the major catalytic carbonylation processes of alkenes and alkynes using different transition metals. It will also include the recent computational models of some catalytic cycles.

1.1 Catalytic Carbonylation of Alkenes

The hydroxycarbonylation of olefins in presence of water affords a mixture of linear and branched carboxylic acids (Eq. 1.2) in good yields [4,9,10]. The ratio of linear and branched esters depends on the reaction conditions such as carbon monoxide pressure, temperature, kind and amount of phosphine ligands and additives [9-11]. For example, the carbonylation of styrene in the presence of triphenyl phosphine ligand (PPh_3) affords mainly branched esters (Eq. 1.3) whereas the use of bidentate phosphine ligands leads to linear ester as major products (Eq. 1.4) [11].

$$RCH{=}CH_2 + CO + H_2O \longrightarrow RCH_2CH_2CO_2H + RCH(CH_3)\,CO_2H \qquad 1.2$$

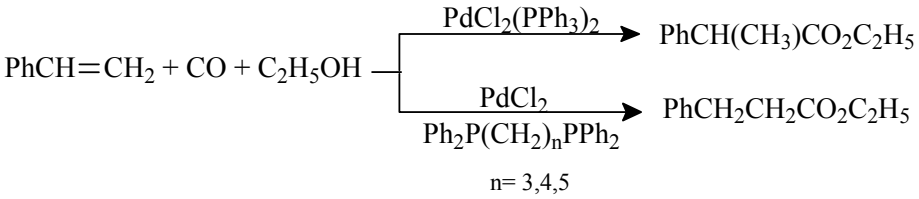

1.3

1.4

The industrial application of the olefins hydroxycarbonylation process is limited because other alternative processes existed for the production of large-scale carboxylic acids. However, propionic acid is produced by hydroxycarbonylation of ethylene (BASF process) [9]. In addition, fatty acid esters are commercial manufactured by cobalt-catalyzed methoxycarbonylation reactions of long-chain olefins, such as 1-octene and internal dodecenes (Eq. 1.5) [9].

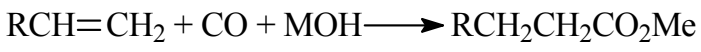

1.5

The direct hydroxycarbonylation of butadiene to adipic acid using an iodide-promoted rhodium catalyst at 75 bar and 200°C has also been reported (Eq 1.6) [9].

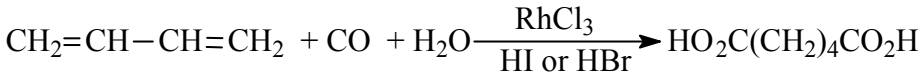

1.6

The hydrocarboxylation of isoprene occurs under 6.2 atm of CO and at 110°C to form the corresponding β,γ-unsaturated acid in 52% yield [12].

Under certain reaction conditions, keto esters and ketones are produced [9,11]. Ketones can be also formed by the hydroxycarbonylation of olefins. For example, the conversion of ethylene into diethyl ketone (Eq. 1.7) occurs with both rhodium and ruthenium

catalysts [9]. The carbonylation of ethylene in alcohol affords propionate as a main product and a considerable amount of 4-oxohexanoate (Eq. 1.8).

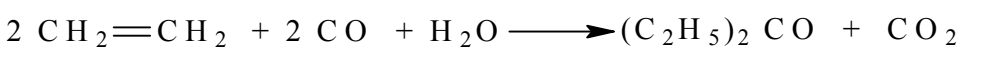

1.7

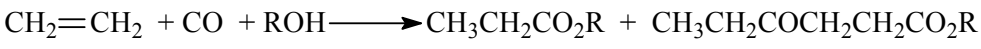

1.8

In addition, keto esters are formed by the carbonylation of certain diolefins which act as a bidentate ligand. The cyclic keto ester was produced from 1,5-hexadiene (Eq. 1.9). The carbonylation of 1,5-cyclooctadiene (1,5-COD) in alcohol gave mono-and diesters (Eq.1.10), but bicycle[3,3,1]-2-nonen-9-one was formed in 40% yield in THF (Eq. 1.11) [11].

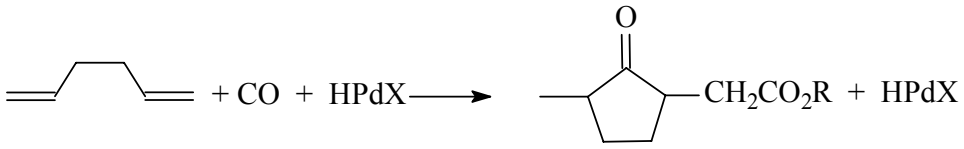

1.9

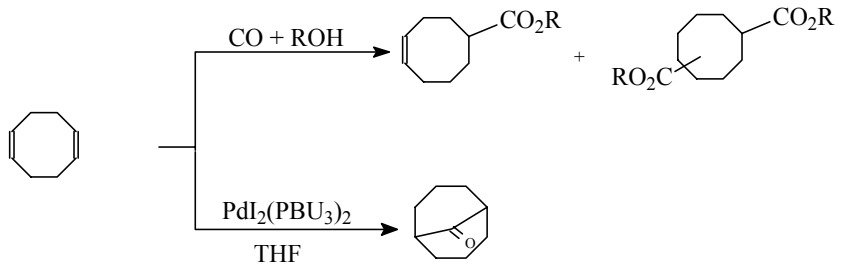

1.10

1.11

The products of the carbonylation of conjugated dienes depend strongly on the catalyst system (Eq. 1.12). For example, butadiene has potential commercial application as a route to adipic acid [9].

$$CH_2{=}CH{-}CH{=}CH_2 + CO + MeOH \xrightarrow[C_5H_5N]{Co_2(CO)_8} MeO_2C(CH_2)_4CO_2Me \qquad 1.12$$

1.2 Catalytic Carbonylation of Alkynes

Most of catalytic carbonylation processes of alkynes are activated using complexes of nickel, palladium, and platinum with phosphine ligands [13]. Different products can be formed from the carbonylation reactions depending on the type of the nucleophile [5,9,10]. The following subsections summarize the major catalytic processes of alkynes.

1.2.1 Hydroformylation of Alkynes

The carbonylation reaction of alkynes in presence of syngas (CO/H_2) is called hydroformylation process. These reactions produce aldehydes and ketones (aliphatic or cyclic). The first hydroformylation of acetylene was described by Roelen to synthesis acrolein from acetylene by using metallic cobalt as catalyst at 140-150°C and 1-10 atm. The hydroformylation of alkynes was slower than that of olefins. Acetylene acted as a poison of the hydroformylation of olefins [14]. The hydrocarbonylation of acetylene is usually catalyzed by nickel, cobalt, ruthenium, or rhodium catalysts.

1.2.2 Hydroesterification of Alkynes

The carbonylation reactions of alkynes, which are performed in presence of alcohols to produce esters, are known as hydroesterification reactions. However, different products can be formed depending on the catalyst system, solvent and reaction conditions, (Scheme 1.2). It was found that water is essential for the reaction. Under anhydrous conditions,

the reaction is delayed until water is produced from ether synthesis at high temperature [2].

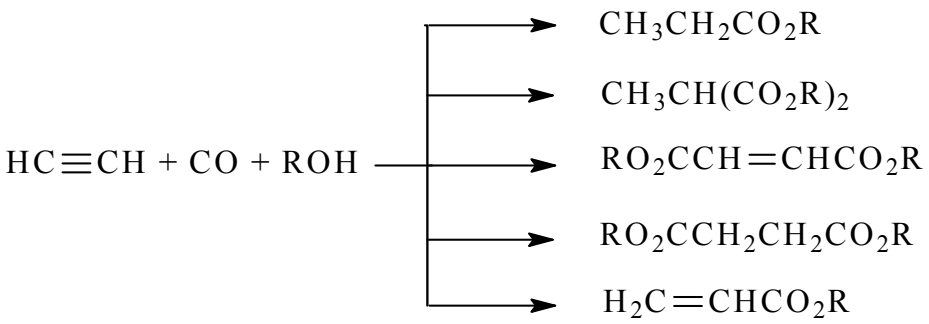

Scheme 1.2: The hydroesterification reactions of alkynes

The most commonly used metals as catalyst are Ni, Co, Fe, Rh, and Pd. Palladium is the most used metal in the catalytic hydrocarboxylation of alkynes. Using Pd/C under mild conditions, substituted acrylates were obtained in high yields from alkynes (Eq. 1.13). In the presence of a palladium complex such as $PdBr_2[P(OPh)_3]_2$ and perchloric acid, acetylene readily reacts to produce the corresponding acrylate in 95% yield [2].

$$RC{\equiv}CH + CO + R'OH \xrightarrow{Pd/C/R''X} H_2C{=}CRCO_2R' \qquad 1.13$$

The conversion of alkynes into tert-alkyl esters was realized using $Pd(OAc)_2$ and dppb at 150°C and 80 atm of CO. the use of primary and secondary alcohols gave low yields of esters[15]. However, the regioselective hydroesterification of alkynes and alkynols was achieved by the use of formate esters and the catalytic system, $Pd(OAc)_2$-dppb-PPh_3 in the presence of p-TSOH at 20 atm of CO and 100°C [16].

1.2.3 Hydrocarboxylation of Alkynes

The Hydrocarboxylation reactions of acetylene are very important carbonylation reactions [2]. These reactions have significant interest for both academic researches and industrial applications. The following processes are some selected models of hydrocarboxylation reactions.

1.2.3.1 Synthesis of Carboxylic Acids

In presence of water, the hydrocarboxylation reaction of alkynes produces substituted α,ß-unsaturated acids [2], e.g., the formation of acrylic acid and its derivatives (Eq. 1.14).

$$HC{\equiv}CH + CO + H_2O \xrightarrow{Ni(CO)_4} H_2C{=}CHCO_2H \qquad 1.14$$

The metal catalysts, ligand type, pH of reaction medium, and/or solvent can affect seriously the products yield and distribution. In the carbonylation reactions of alkynes, the isomerisation of triple bond takes place while it is not possible for the hydroformylation reaction. $Ni(CO)_4$ was an important catalyst in the hydrocarboxylation of alkynes where initially, a stoichiometric amount of the catalyst was used as CO source without pressure at room temperature. The hydrogen is not released but it reacts with the substrate to produce ethane and ethylene in addition to propionic acid [2].

1.2.3.2 Synthesis of Acid Chlorides

Sauer described the first production of acylchloride from the reaction of acetylene with CO and HCl. Acryloyl chloride was obtained as a major product at 120-200°C and high pressure (500-1000 atm) of CO. The reaction was catalyzed by rhodium or ruthenium complexes in the absence of solvents or in the presence of aportic solvents. In toluene, ß-

chloropropionyl chloride and succinoyl chloride were obtained (Eq. 1.15). The same type of reactions occurred with HF instead of HCl; both reactions are typical hydrocarboxylations [14].

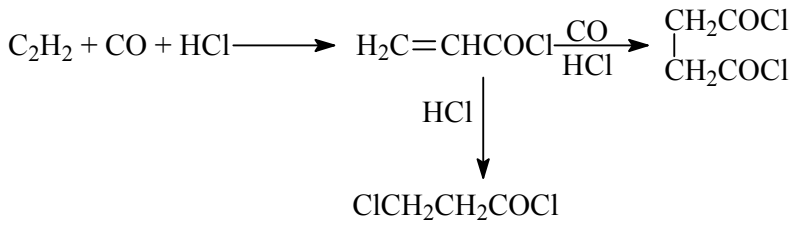

1.15

1.2.3.3 Synthesis of Thioesters

The carbonylation reaction of alkynes in the presence of thiols produces thioesters (Eq. 1.16) [2,14]. A stoichiometric synthesis of a series of thioesters from acetylene at 40-45°C in toluene with $Ni(CO)_4$ as CO source was described by Reppe [10]. The best yield (77%) was obtained by using benzyl mercaptan ($PhCH_2SH$) as the active hydrogen compound [2,14].

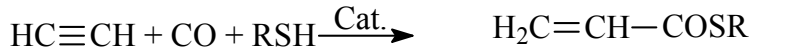

1.16

1.2.3.4 Synthesis of Anhydrides

The catalytic carbonylation reactions of alkynes in the presence of organic acids produce a mixture of anhydrides (Eq. 1.17). However, the reaction of 1-octyne instead of acetylene with $Ni(CO)_4$ in the presence of a large excess of organic acid gives side products (Eq. 1.18) [14].

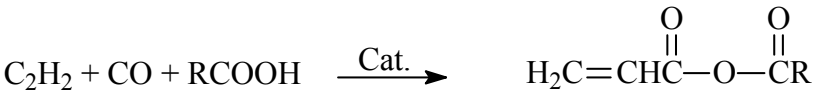

1.17

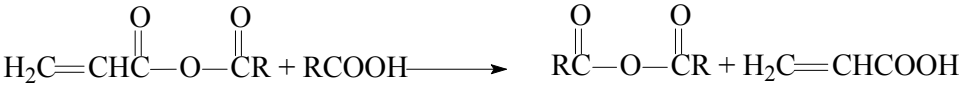

1.18

Acrylic anhydride is obtained in 88% yield from the reaction of acetylene with acrylic acid catalyzed by $Ni(CO)_4$ in an inert solvent at 40-50°C [14].

1.2.3.5 Synthesis of Amides

The carbonylation of alkynes in the presence of primary, secondary or aryl amines mainly affords amides [2]. For instance, substituted acrylamides can be synthesized from acetylene and various amines, aniline, urea, pyrolidone or acetamide in presence of stoichiometric amount of $Ni(CO)_4$ or nickel catalysts with polymerization inhibitors such as hydroquinone and CO pressure. This reaction was initialized by Reppe [4,14]. Free acids were formed during the reactions [14]. The yield obtained from secondary amines is higher than primary amines [2]. Ammonia reacts slowly. Neher, Specht, and Newman introduced a semi-catalytic synthesis of acrylamide. They reacted acetylene with $Ni(CO)_4$ in acrylic acid and then added CO, acetylene, $Ni(CO)_4$, HCl and an excess of ammonia at 50-90°C. In general, the best yields were obtained when using aniline or secondary amines while side reactions occurred for primary amines (Eq. 1.19). The reactions were catalyzed by NiI_2 or $Ni(CN)_2$. Acrylamide can further react with acetylene and CO to form bisacryloylamines (Eq. 1.20). Acetamide was successfully used in place of amines, whereas urea gave only polymers [14].

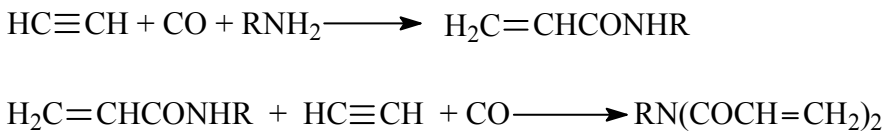

1.19

1.20

The carbonylation of different terminal alkynes with diethyl amine in the presence of an organic iodide or HI salt was catalyzed by palladium complexes to produce 2-substituted acrylamides [17]. β,γ-Unsaturated amides were formed via the Pd-catalytic carbonylation of alkynes with amines at 50 atm and 110°C. The linear amide products of this reaction were obtained with high selectivity [18]. Palladium(0) catalyzed the insertion of carbon monoxide into an inactivated carbon-nitrogen bond of propargylamines (Eq. 1.21) and 2,3-dienylamines to form selectively α,ß-unsaturated amides [4].

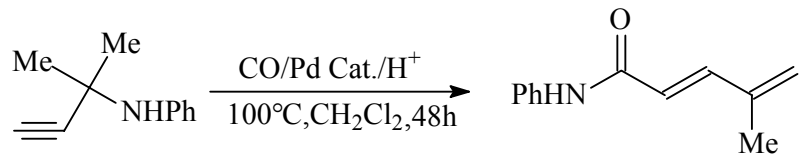

1.21

The reaction of substituted amines (or derivatives of aniline or acrylonitrile) with acryloyl chlorides or substituted acrylic acids affords 2-substituted acrylamides (Eq. 1.22). On the other hand, the olefination of aldehyde with carbamidomethylene triphenylphosphorane produces α,ß-unsaturated amides (Eq. 1.23) [4].

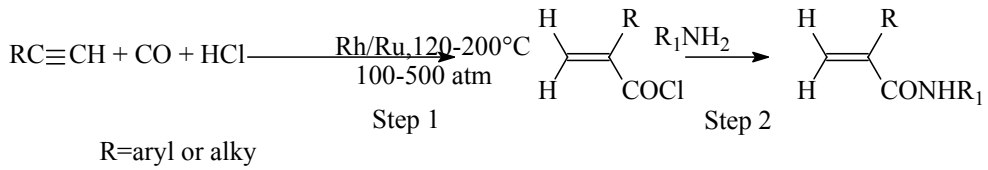

1.22

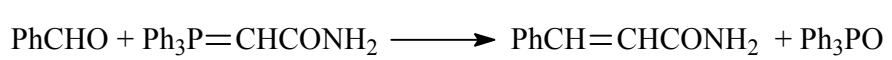

1.23

1.3 Computational Models of Some Catalytic Cycles

Computational chemistry is a large area of research, which is considered as a subfield of theoretical chemistry. Using this technique, some problems can be further investigated and studied to get better understanding of research problems [19,23]. Recently, some reactions are modeled. Where, thermodynamics and kinetics of a reaction have been determined successfully by means of computer. Also, many chemical concepts have been studied theoretically in qualitative or semi-quantitative manner [19]. Molecular properties, geometrical arrangement, relative energies and time dependence of molecular structures can computationally be determined faster and easier than with experimental technique [23].

The complexity of homogeneous catalytic reactions including the difficulty of isolation of the intermediate species has encouraged theoreticians to model these reactions using molecular orbital calculations [24-26]. Additionally, most of the palladium catalytic carbonylation reactions can only be performed at high pressure system [17,27-29]. Therefore, many research teams have recently carried out molecular mechanics, ab initio, and density function calculations to shed more light on Pd-catalytic cycles [30-33]. Some of investigated models of homogeneous catalytic reactions using computational facilities are described hereafter.

1.3.1 Brookhart's Olefin Polymerization Catalyst

Ni(II) diimine-based single site homogenous catalysts of the type $(\mathrm{ArN=C(R)\text{-}C(R)=NAr)Ni\text{-}R'^{+}}$ have been an alternative to both traditional Ziegler-

Natta and metallocene catalysts for olefin polymerization. The combined quantum mechanics/molecular mechanics (QM/MM) and the ab initio molecular dynamics methods (AIMD) were used to model the Brookhart's catalyst. Both methods allow for the incorporation of effects that are often ignored in high-level calculations, but may be critical to the real chemistry of the simulated system. In the combined QM/MM method part of the system, which is the active site, is treated quantum mechanically whereas the remainder of the system is treated with a faster molecular mechanics force field. This allows high level of calculations to was performed where the effects of the environment was incorporated in a computationally good manner. With the ab initio molecular dynamics methods, the system was simulated at a finite temperature with no empirical force field. Rather, the forces at each time step were determined with a full electronic structure calculation at the density functional level. Thus, simulations of chemical reactions were performed where finite temperature effects are realistically represented [24].

1.3.2 DFT-Mechanistic Study Of Pd(0)-Catalyzed Thioboration Reaction of Alkynes

The hybrid density functional (B3LYP) calculations were carried out to study the mechanism of acetylene thioboration reactions catalyzed by Pd(0)/Pt(0) complexes. The main findings can be summarized as follows: (i) No oxidative-addition product of the S-B bond to the $Pd(PH_3)_2$ was found. (ii) a new mechanism was proposed involving the following steps: (a) acetylene coordination to $Pd(PH_3)_2$, (b) dissociation of a phosphine ligand, (c) addition of the S-B bond to the metal center via a metathesis-like transition state, (d) isomerization of the resultant complex, accompanied by recoordination of the

phosphine ligand, and (e) the reductive elimination of the alkenyl-thioboron product. The rate-determining stage was found to be the addition of the S-B bond to the metal center via a metathesis-like transition state. (iii) The Pd(0) complexes catalyzed alkyne thioboration but not diboration, because the rate-determining barrier at the metathesis-like transition state is much higher for the latter, which has been explained in terms of the lack of hypervalency character of boron compared to sulfur. Due to the weaker C-S bond energy compared to C-B, the reductive-elimination step is highly exothermic for diboration but only slightly exothermic for thioboration. Consequently, the reductive-elimination step proceeds with a high barrier for thioboration but is barrierless for diboration. (iv) The Pt(0) complex is not expected to be a good catalyst for thioboration but is efficient for diboration. The reason behind this is the high barrier for reductive elimination, which in part comes from the promotion energy required for the metal during the process [30,31].

1.3.3 The Mechanism of Pd-Insertion Into Alkynyl/Aryl Carbon-Fluorine Bonds

An ab initio molecular orbital study using both gas-phase and B3LYP/CZVP-COSMO salvation models of the mechanism of palladium insertion into alkyne and aryl carbon-halogen was performed. The mechanism of palladium insertion into alkyne species can proceed via concerted oxidative addition across the carbon-halogen bond. A stepwise mechanism via an σ-complex is favored when a nitro group is introduced onto the alkyne. The palladium insertion into variously substituted aryl fluoride was again found to proceed via a single-step concerted mechanism, and although an σ-complex was located when 2,4-dinitro and 2-nitro substitution was present, the energy of this stepwise route was very similar to the concerted pathway and no clear decision on the pathway can be

made. No intermediate σ-complex could be located for η^6-tricarbonylchromium-complexes fluorobenzene, and only a concerted pathway was identified [32].

1.4 Aim of Investigations

Recently, the Pd-catalytic carbonylation reaction of terminal alkynes conducted with aniline forms gem- and trans-α,ß-unsaturated amides with a total control of the regioselectivity under certain reaction conditions (Eq. 1.24) [29].

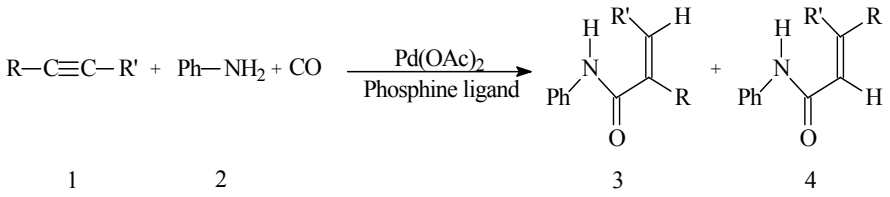

1.24

This catalytic process is an important reaction and has many industrial potential. The dependency of the products' distribution (regioselectivity) was found to be affected by the variation of the experimental conditions of the catalytic systems. The experimental results [18] of this process indicated that the compound 3 in Eq. 1.24 (gem-α,ß-unsaturated amide) was predominant with the catalytic system: $Pd(OAc)_2$/1,3-bis(diphenylphosphino) propane (dppp)/p-toluenesulfonic acid (p-TsOH)/CO in tetrahydrofuran (THF) as a solvent. While the use of catalytic system: $Pd(OAc)_2$/1,4-bis(diphenylphosphino)butane (dppb), under syngas (CO/H_2) conditions in CH_2Cl_2 as a solvent, afforded the compound 4 (Eq. 1.24) (trans-α,ß-unsaturated amide) as the major product. The examination of the detailed mechanism of this carbonylation process is not developed yet because of the well-known complexity of homogeneous catalytic system at high-pressure reactions and the difficulty of the separation of the active intermediates. Theoretical calculations provide the best approach to reveal the detailed mechanism of this catalytic process.

Other palladium catalytic processes were determined computationally. Jaket et al,[32] suggested that the insertion of palladium into alkynyl carbon-fluorine bonds should proceed via oxidative addition reaction across the carbon-halogen bond. On the other hand, Cui et al studies [30,31] on thioboration or diboration of alkyne using Pd-catalyst reveal that no oxidative addition takes place at the first step of the speculated mechanism while acetylene coordinates to the active catalyst (PdL_2).

Based on the above mentioned, two possible approaches for the unsaturated amides formation can be investigated (Eq.1.24). These results encourage us to perform a detailed investigation on the formation of amides by Pd-catalytic carbonylation reaction of terminal alkynes with aniline. The procedure will be conducted as follows:

1- Select a method of calculation and a level of theory that are suitable for the studied reaction system.
2- Use the selected method and level of theory to reveal the detailed mechanism of Pd-catalytic carbonylation process of the formation of unsaturated amides.
3- Perform series of experiments to test the validity of the proposed mechanism.
4- Verify the influence of ligand type and substrates that may affect the catalytic process.

Finally, a comparative analysis will take place between the experimental findings and the proposed reaction mechanism model(s) to verify the distribution of the unsaturated amides and the factors affect this distribution.

CHAPTER TWO

THEORETICAL BACKGROUND

Theoretical chemistry is the combination of mathematical methods and fundamental lows of physics [19]. There are two types of theoretical methods: molecular mechanics and quantum mechanics calculations. The quantum mechanics methods include semi-empirical, ab initio, and density function theory. In quantum mechanics, the Schrödinger equation 2.1 gives the wave functions and energies of a molecule.

$$H\Psi = E\Psi \qquad 2.1$$

Where H is the molecular Hamiltonian operator, Ψ is wave function, and E is the energy. The quantum mechanics methods differ in the approximation of the solution of the Schrödinger equation and in calculation of potential energy.

The molecular mechanics and semi-empirical quantum mechanics methods have several advantages over ab initio and density function theory. The most important, these methods are fast. Although this may not be significant for small molecules, it is certainly important for large systems such as biomolecules and polymers. Moreover, for specific and well-parameterized molecular systems, these methods can calculate values that are comparable to experimental results than low level of ab initio and density function methods.

The accuracy of molecular mechanics or semi-empirical methods is highly depending on the database used for parameterizing the method. This is true for the type of moleculesand the physical and chemical data in the database. Frequently, these methods give the best results for a limited class of molecules or phenomena. The main disadvantage of these methods is the parametization process where all of parameters must be available before running a calculation. Unfortunately, developing parameters is time-consuming.

The ab initio or density functional methods could overcome this problem. However, they are slower than any molecular mechanics and semi-empirical methods. Ab initio quantum mechanics methods have evolved for many decades. The speed and the accuracy of ab initio calculations have been greatly improved by developing new algorithms and introducing better basis functions. Density functional methods are modern techniques that have a lot in common with ab initio methods. The Density Functional Theory (DFT) has been used to predict how the energy depends on the electron density rather than the wavefunction in the ab initio method. In particular, the Hartree-Fock potential of ab initio calculations has been replaced with an exchange-correlation potential that is a functional of the electron density. The effects of electron correlation are included and hence, DFT can, in principal, be more accurate than ab initio Hartree-Fock calculations. Its results can be compared with ab initio Hartree-Fock or Mølar- Plesset (MP) perturbation theory.

Computational chemistry, as with other disciplines in chemistry, is used as a tool to understand chemical reactions and processes. The challenges for computational chemistry are to characterize and predict the structure and stability of chemical systems, to estimate energy differences between different states, and to explain reaction pathways and

mechanisms at the atomic/molecular level. For example, examination of potential energy surfaces of a reaction computationally needs to perform several single point calculations, optimizations of ground and transition states, frequency, and intrinsic reaction coordinates (IRC) calculations.

The following sections will concentrate on the commonly used methods in computational chemistry calculations that can be applied for the studied reaction system.

2.1 Universal Force Fields

Force Field (FF) methods are based on parametric function of the nuclear coordinates. The parameters that enter the function are fitted to experimental or high level of quantum mechanics results. A default force field was originally developed only for molecular mechanics 2 (MM2). One of the major difficulties of molecular mechanics procedures (MM2 or others) is that force constants are not available for the molecule of interest. As the number N of atom types increases, the number of force constants needed to describe all possible occurrences of these atom types becomes very large. For example, for torsions angle, N^4 force constants are needed. This does not even include all possibility of an atom type that have not been defined for the particular chemical situation at hand [19].

In computational chemistry, it can be very useful to have a general model that can be applied to any situation. Even if less accurate, such a computational tool is very useful for comparing results between molecules. This occurs universally with the periodic table so all possible molecules could be computed. Results of a calculation are realistic if the default parameters and the particular molecular situation are examined and compared with experimental data.

The combination of many atom types and lack of sufficient number of reference data have initiated developments of force field with reduced parameters sets, such as the Universal Force Fields (UFFs). The idea is to derive di-, tri-, and tetra- atomic parameters ($E_{str}, E_{bend}, E_{tors}$) from atomic constants (such as atom radii, ionization potentials, electronegativities, polarizabilities, etc.). In principle, the UFFs are capable of covering molecules composed of elements from the whole periodic table. They give less accurate results compared to conventional force fields, but geometries are often computed qualitatively and almost correctly. However, relative energies are much more difficult to obtain accurately. In addition, for organic molecules, conformational energies are generally quite poor. Recently, the UFFs have been implemented and it may likely be improved in future [19].

2.2 Hartee-Fock Method

The Hartree-Fock procedure or Self-Consistent Field (SCF) method introduces well-defined mathematical approximations to solve the Schrödinger equation. However, this leads to a one-electron eigenvalue problem that must be solved iteratively to self-consistency. The Hartree-Fock method introduces an effective one-electron Hamiltonian, as in equation 2.2.

$$F\psi_i = \varepsilon_i\psi_i \qquad 2.2$$

Where the Fock operator, F, depends implicitly on the solutions ε_i. The Fock operator is a sum of the kinetic energy operator for an electron, a potential energy that a single

electron would feel coming from the fixed nuclei, and an average of the effects of all the other N-1 electrons.

$$f(x_1) = h(x_1) + \sum_i J_i(x_1) - K_i(x_1) \qquad 2.3$$

Introducing a basis set transforms the Hartree-Fock equations into the Roothaan equations where the simplified form of the Roothaan equation as matrices is

$$FC = SC \in \qquad 2.4$$

Where $\in$ is a diagonal matrix of the orbital energies $\in_i$. This is like an eigenvalue equation except for the overlap matrix S. One performs a transformation of basis to go an orthogonal basis to make S vanish. Then, it is just a matter of solving an eigenvalue equation (or, equivalently, diagonalizing F). Since F depends on its own solution (through the orbitals), the process must be done iteratively. This is why the solution of the Hartree-Fock-Roothaan equations is often called the self-consistent-field procedure.

Hartree-Fock is a simple theory, which satisfies the commonly known features of fermionic wavefunctions. The theory generates wavefunctions that are antisymmetric with respect to the exchange of two electron positions and includes exchange between like-spin electrons. The cost of a Hartree-Fock calculation formally scales with the cube of the number of basis functions, but depending on implementation, the scaling can be between linear and quadratic with system size. It is insufficiently accurate for quantitative predictions of the properties of many compounds. By neglecting electron correlation, interaction energies are typically very poor. A Hartree-Fock wavefunction is a well-controlled approximation to the many-body wavefunction, and for this reason Hartree-

Fock continues to be widely used: it is often predictably accurate or inaccurate, and therefore useful for determining qualitative information such as trends in a structural parameter with system size.

Almost all post Hartree-Fock methods share the combined limitations of a poor scaling with system size and a strong basis set dependence. In practice, post Hartree-Fock methods typically scale with the fourth or higher power of the number of basis states included in the calculation, limiting their application to small systems. The basis states depend on the original basis set used in their numeric expansion, and it is commonly found that the use of improved methods requires an improved basis set, further increasing the cost of calculation. Configuration Interaction (CI) and Coupled-Cluster (CC) based methods effectively transform the electron-correlation problem into a basis set problem, where the basis set is the set of molecular orbitals derived from a Hartree-Fock (or similar) calculations.

2.3 Density Function Theory

Density Function Theory (DFT) is a powerful method of calculation and has become an important research tool for chemists, physicists and materials scientists [34]. The foundation of using DFT in computational chemistry was the introduction of electron orbitals by Kohn and Sham (KS). The basic idea in the KS formalism is the splitting of kinetic energy functional into two parts, one of which can be calculated exactly, and a small correction term [19].

Assume a Hamilton operator of the following form with $0 \le \lambda \le 1$.

$$H_\lambda = T + V_{ext}(\lambda) + \lambda V_{ee} \qquad 2.5$$

Where V_{ext} operator is equal to V_{ne} for $\lambda = 1$, for intermediate λ values, however, it is assumed that the external potential $V_{ext}(\lambda)$ is adjusted so that the same density is obtained for both $\lambda = 1$ (the real system) and $\lambda = 0$ (a hypothetical system with non-interacting electron). For the $\lambda = 0$ case the exact solution to the Schrödinger equation is given as Slater determinant composed of molecular orbitals, ϕ_i for which the exact kinetic energy functional is given as

$$T_s = \sum_{i=1}^{N} \left\langle \phi_i \left| -\frac{1}{2}\nabla^2 \right| \phi_i \right\rangle \qquad 2.6$$

Where subscript s is for the kinetic energy calculated from a Slater determinant.

The key to KS theory is thus the calculation of the kinetic energy under the assumption of non-interacting electron (in the same of HF orbitals in wave mechanics describe non-interacting electrons). In reality, the electrons are interacting and this equation doesn't provide the total kinetic energy. However, just as HF theory provides ~ 99% of the correct answer, the difference between the exact kinetic energy and that calculated by assuming non-interacting orbitals is small. The remaining kinetic energy is absorbed into an exchange-correlation term, and a general DFT energy expression can be written as

$$E_{DFT}[\rho] = T_s[\rho] + E_{ne}[\rho] + J[\rho] + E_{xc}[\rho] \qquad 2.7$$

By equating E_{DFT} to the exact energy, this expression may be taken as the definition of E_{xc}, it is the part which remains after subtraction of the non-interacting kinetic energy, and the E_{ne} and J potential energy terms.

$$E_{xc}[\rho] = (T[\rho] - T_s[\rho]) + (E_{ee}[\rho] - J[\rho]) \qquad 2.8$$

The first parenthesis in the Eq. 2.8 is for the kinetic correlation energy, while the second contains both exchange and potential correlation energy [19].

The strength of DFT is that only the total density needs to be considered. In order to calculate the kinetic energy with sufficient accuracy, however, orbitals have to be reintroduced. However, DFT has a computational cost which is similar to HF theory, with the possibility of providing more accurate (exact, in principle) results [19].

2.4 Basis Sets

Most methods require a basis set to be specified. For the transition metals, the suitable basis sets are based on Effective Core Potential (ECP) methods. ECP was the pioneer work of Hellmann and Gombas around 1935 [20]. For system involving elements from the third row or higher in the periodic table, there is a large number of core electrons which in general are unimportant in a chemical sense. However, it is necessary to use a large number of basis functions to expand the corresponding orbitals, otherwise the valence orbitals will not be properly described (due to a poor description of the electron-electron repulsion). In the lower half of the periodic table, relativistic effects complicate the case. The two branches of ECP approaches are: the model potential (MP) and the pseudopotential (PP) techniques. The main focus is on those ECP methods which proved

to be successful in atomic and molecular relativistic electronic structure calculations during the past decade [19,20].

The advantage of ECP is the presenting of all core electrons of an element. This is in the strength of semi-empirical methods; the core electrons are modeled by a suitable function, and only the valence electrons are treated explicitly. In many cases, this gives quite good results at a fraction of the cost of a calculation involving all electrons. Part of the relativistic effects may also be taken care of especially the scalar effects without having to perform the full relativistic calculation. ECP methods have also been designed for second row elements, although the saving is only insignificant relative to all-electrons calculation [19,20].

There are four major steps in designing ECP basis sets type. First, a good quality all-electron wave function is generated for atom. This will typically be a numerical HF or Dirac-Hartree-Fock, calculation. The valence orbitals are then replaced by a set of node less pseudo-orbitals. The regular valence orbitals will have a series of radial nodes in order to make them orthogonal to the core orbitals, and the pseudo-orbitals are designed so that they behave correctly in the outer part, but do not have a nodal structure in the core region. The core electrons are then changed by a potential so that the solution of the Schrödinger (or Dirac) equation produces valence orbitals matching the pseudo-orbitals. Since relativistic effects are mainly important for the core electrons, this potential effectively includes relativity. The potential will be different for each angular momentum, and will normally be obtained in a tabulated form. In the final step, this numerical potential is fitted to a suitable set of analytical functions, normally a set of Gaussian functions [19].

$$U_{ECP}(r) = \sum_i a_i r^{n_i} e^{-\alpha_i r^2} \qquad 2.9$$

The parameters a_i, n_i and α_i depend on the angular momentum (s, p, d, etc) and are determined by least squares fit. Typically, between two and seven Gaussian functions are used in the fit. Many Gaussian functions improve the fit and consequently the resulting orbitals with increased computational time.

For transition metals, it is clear that the outer (n+1)s, (n+1)p and (n)d orbitals represent the valence space. While the full-core potentials give reasonable geometries, it has been found that the energies are not always acceptable. Better results can be obtained by also including the orbitals in the next lower shell in the valence space, although at an increase in the execution time [19].

The gain by using ECPs is the largest for atoms in the lower part of the periodic table, especially those where relativistic effects are important. Since fully relativistic results are limited, the performance of ECPs is somewhat difficult to be evaluated by comparison with other calculations, but they often reproduce the known experimental results, thereby justifying the approach. Table 2.1 contains a list of the commonly used ECP-basis sets [21,22] and their notation.

2.5 Vibrational Frequency Calculations

Within the framework of quantum mechanics, the pure vibrational spectra of a molecule can be approximated by assuming the nuclei perform only simple harmonic motions. The potential energy of these motions is approximated by a second-order Taylor expansion around the stationary geometry [19].

Table 2.1: commonly used ECP basis sets [35]

Type	Specification
CEP-4G	Stevens/Basch/Krauss ECP minimal basis function.
CEP-31G	Stevens/Basch/Krauss ECP split valence basis function.
CEP-121G	Stevens/Basch/Krauss ECP triple-split basis function.
LanL2MB	This basis set consists of STO-3G on first row and Los Alamos ECP plus MBS on Na-Bi.
LanL2DZ	Dunning/Huzinaga valence double-zeta (D95V) on first row, Los Alamos ECP plus DZ on Na-Bi.
SDD	D95V up to Ar and Stuttgart/Dresden ECPs on the remainder of the periodic table.
SDDAll	Selects Stuttgart potentials for $Z > 2$
DGDZVP	basis sets used in *DGauss*
UGBS	The universal Gaussian basis set of de Castro, Jorge and coworkers

$$V(x) \cong V(x_0) + \left(\frac{dV}{dx}\right)^t (x - x_0) + \frac{1}{2}(x - x_0)^t \left(\frac{d^2V}{dx^2}\right)(x - x_0) \qquad 2.10$$

The energy for the expansion point, $V(x_0)$ may be chosen as zero, and the first derivative is zero since x_0 is a stationary point, i.e.

$$V(\Delta x) = \frac{1}{2}\Delta x^t F \Delta x \qquad 2.11$$

Where F is a $3N \times 3N$ (N being the number of atoms in the molecule) matrix containing the second derivatives of the energy with respect to the coordinates (the force constant matrix). The nuclear Schrödinger equation for an N-atom system then becomes

$$\left\{-\sum_{i=1}^{3N} \frac{1}{2m_i}\frac{\partial^2}{\partial x_i^2} + \frac{1}{2}\Delta x^t F \Delta x\right\}\Psi = E\Psi \qquad 2.12$$

It is first transformed to mass-dependent coordinates by a G-matrix containing the inverse square root of atomic masses (it atomic not nuclear, masses are used, this is in line with the Born-oppenheimer approximation)

$$\begin{aligned} y_i &= \sqrt{m_i}\Delta x_i \\ \frac{\partial^2}{\partial y_i^2} &= \frac{1}{m_i}\frac{\partial^2}{\partial x_i^2} \\ G_{ij} &= \frac{1}{\sqrt{m_i m_{\cdot i}}} \end{aligned} \qquad 2.13$$

$$\left\{-\sum_{i=1}^{3N} \frac{1}{2}\frac{\partial^2}{\partial y_i^2} + \frac{1}{2}y^t (FG) y\right\}\Psi = E\Psi \qquad 2.14$$

A unitary transformation is then introduced which diagonatizes the FG-matrix, yielding eigenvalues ε_i and eigenvectors q_i. The kinetic energy operator is still diagonal in these coordinates [19].

$$
\begin{aligned}
& q = Uy \\
& \left\{ -\sum_{i=1}^{3N} \frac{1}{2} \frac{\partial^2}{\partial q_i^2} + \frac{1}{2} q^t (U(FG)U^t) q \right\} \Psi = E\Psi \\
& -\sum_{i=1}^{3N} \left\{ \frac{1}{2} \frac{\partial^2}{\partial q_i^2} + \frac{1}{2} \varepsilon_i q_i^2 \right\} \Psi = E\Psi \\
& \sum_{i=1}^{3N} \{h_i\} \Psi = E\Psi
\end{aligned}
\qquad 2.15
$$

In the q-coordinate system, the vibrational normal coordinates, the 3N-dimensional Schrödinger equation can be separated into 3N one-dimensional Schrödinger equation, which are in the form of a standard harmonic oscillator. The eigenvectors of the FG matrix are the (mass-weighted) vibrational normal coordinates, and the eignvalues ε_i are related to the vibrational frequencies [19].

$$
\nu_i = \frac{1}{2\pi} \sqrt{\varepsilon_i} \qquad 2.16
$$

2.6 Transition State Calculations

To locate minima of functions is easy. On the other hand, to find first-order saddle point, which is transition states (TS), it is much more difficult. There are no general methods that are guaranteed to work. Many different strategies have been proposed, the majority of which can be divided into two general categories, those based on interpolation between two minima, and those using only local information.

Although, there are many different methods for locating TS, here the description is limited to those mainly used for the current calculations. This method is the quadratic synchronous transit. The Linear Synchronous Transit (LST) and Quadratic Synchronous Transit (QST) methods are classified as transition state methods which are based on interpolation between reactant and product structures [19,35].

LST method forms the geometry difference vector between the reactant and product and then locates the highest energy structure along this line. The assumption is that all variables change the rate along the reaction path. Generally, this is not a good approximation and only in simple systems, LST leads to a reasonable estimation of TS. However, QST method approximates the reaction path by forming a parabola instead of a straight line in the LST (Figure 2.1). After the maximum on the LST is found, the QST is generated by minimizing the energy in the directions perpendicular to the LST path. The QST path may then be searched for the optimized energy [19].

2.7 Intrinsic Reaction Coordinate Methods

The important points for discussing path of a chemical reaction are minima, corresponding to reactant and product, and saddle points, corresponding to transition structures. Once the TS has been found, it should be verified that it indeed connects the desired minima [19,35-37]. At the TS, the vibrational normal mode gives negative (imaginary) frequency and an inspection of the corresponding atomic motions can strongly indicate the correct TS. A clear proof, however, requires a determination of the Minimum Energy Path (MEP) from the TS to the connecting minima. If the MEP is located in mass-weight coordinates, it is called the intrinsic reaction coordinate (IRC).

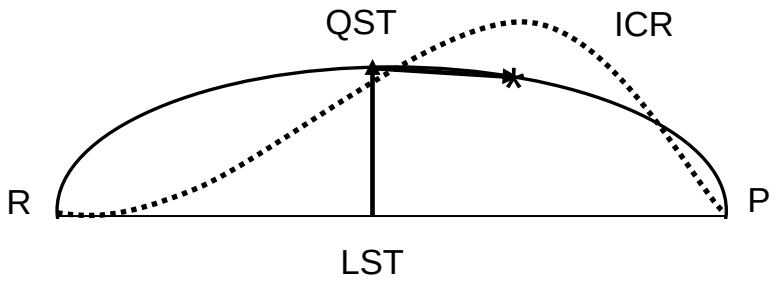

Figure 2.1: LST and QST methods. (∗) indicates the energy maxima and (•) the minima.

The IRC path is of special importance in connection with studies of reaction dynamics, since the nuclei usually will stay close to the IRC, and a model for the reaction surface may be constructed by expanding the energy to second order for example, around points on the IRC.

The IRC path is defined by the differential equation.

$$\frac{dx}{ds} = -\frac{g}{|g|} = v \tag{2.17}$$

Here x is the (mass-weighted) coordinates, s is the path length and v is the (negative) normalized gradient. Determining the IRC requires solving the equation. Starting from geometry slightly displaced from the TS along with normal coordinate for the imaginary frequency [19].

CHAPTER THREE

METHODS OF CALCULATIONS

Homogenous catalysis is a challenging problem to be addressed computationally using quantum mechanical calculations [24]. The modeling of organmetallic complexes with molecular mechanics or semi-empirical methods has many problems [19,23,38,39]. For example, representing suitable equations for each energy terms and calculating correct parameters is the main problem [19, 38]. Ab initio model is capable to overcome most of these problems since no parameters are needed [38]. However, it is a very time consuming methodology [19,38,40].

The current calculations were carried out using personal computer, which is another challenge to use microcomputers for such complicated type of calculation and achieve comparable results to those obtained by either workstation or super computers. The hardware specifications of the used computer were Pentium 4 possessor of 2.4 gaga-byte and 1.0 gaga byte as cash memory of RAM.

Five programs were tested to select the suitable one for the studied reaction system, HyperChem 5 [41], Cambridge Software (CS Chem3D Pro) [42], Titan [43], Gaussian 98W [44], Gaussian 03W [45]. GaussView 03 [46] was used visualize the Gaussian input-output results. The comparison between these programs is based on the calculations of ground states, transition states, and vibrational modes. Geometrical parameterizations, relative energies and the execution time are also considered. The following summarize on

the most general characteristics of these programs in the case of transition metal calculations.

3.1 Molecular Modeling Software

3.1.1 HyperChem 5

HyperChem software is produced by Hypercube, Inc. It is a flexible molecular modeler and editor and a powerful computational package. It offers many types of molecular and quantum mechanics calculations. It also includes the following functions [41]:

- Drawing molecules from atoms and converting them to three-dimensional(3D) models
- Constructing proteins and nucleic acids from standard residues
- Using molecules from other sources; for example, Brookhaven Protein Data Bank (PDB) files
- Rearranging molecules by rotating and translating them
- Changing display conditions, including stereo viewing, rendering models, and structural labels
- Setting up and directing chemical calculations, including molecular dynamics, by various molecular mechanical or ab initio or semi-empirical quantum mechanics methods
- Determination of isotope effects in vibrational analysis calculations for semi-empirical and ab initio SCF methods
- Graphing the results of chemical calculations

- Solvating molecules in a periodic box

The HyperChem program provides high-quality graphic interface, geometry optimization of ground state structures and excellent presentation of vibrational vectors. On the other hand, its transition states calculations are limited and its computational time is costly. Unfortunately, it does not include density function calculations.

3.1.2 CS-Chem3D Pro

CS Chem3D Pro is a program of CS-ChemOffice provided by Cambridge Soft Corporation. It is an application specifically designed to aid scientists in modeling chemicals. It combines powerful building, analysis and computational tools with a friendly and powerful graphical interface [42].

The CS Chem3D Pro provides computational tools based on molecular mechanics for optimizing models, conformational searching, molecular dynamics, and calculating single point energies for molecules. The semi-empirical methods available in Chem3D and CS MOPAC methods can be successfully applied to:

- Systems containing up to 120 heavy atoms and 300 total atoms (in CS MOPAC for Windows) or 60 heavy atoms and 120 total atoms (in CS MOPAC for Macintosh).
- Organic, organometallics, and small oligomers (peptide, nucleotide, saccharide).
- Gas phase or implicit solvent environment.
- Ground, transition, and excited states.

Ab initio methods (available through the Gaussian interface) can be successfully applied to:

- Systems containing up to 30 atoms.
- Organic, organometallics, and molecular fragments (catalytic components of an enzyme).
- Gas or implicit solvent environment.
- Study ground, transition, and excited states (certain methods).

Semi-empirical and density function methods in CS Chem3D Pro are also utilized through the Gaussian program [42].

The CS Chem3D Pro program affords acceptable ground state optimization. Conversely, number of computed transition states calculations is limited and it takes long computational time.

3.1.3 Titan

Titan is a collaboration program between Wavefunction Inc., maker of Spartan, and Schrödinger Inc., maker of Jaguar, and combines the computational power of the latter with the flexibility and ease of use of the former [43]. This program provides different computational models, which are molecular mechanics force field, semi-empirical molecular orbital, Hartree-Fock molecular orbital, density functional and Moller-Plesset (LMP2) models with regard to the calculation of equilibrium and transition-state geometries, conformations and reaction energetic [43].

Titan incorporates two different force fields, SYBYL, developed at Tripos, Inc., and MMFF94, developed at Merck Pharmaceuticals. The MNDO, AM1 and PM3 semi-empirical models are also offered. Three different types of density functional models are available. These are SVWN (Slater, Vosko, Wilk, Nusair), the BP (Becke, Perdew), BLYP (Becke, Lee, Yang, Parr) models and B3LYP where the "3" is the number of parameters [47-49]. The LMP2 model incorporated into Titan is a formulation of MP2 in which the Hartree-Fock orbitals are localized prior to calculation of the MP2 energy.

The Titan program affords good ground state optimization, flexible use with graphical interface and reasonable execution time. In contrast, it has some limitation in transition states calculations for the studied system.

3.1.4 Gaussian 98W

Gaussian 98W [44] is a powerful program offered by Gaussian, Inc. This program can perform a variety of molecular mechanics, semi-empirical, ab initio molecular orbital (MO), Møller-Plesset and density function calculations. Using Gaussian 98W program, computations can be carried out on systems in the gas phase or in solution, and in their ground state or in an excited state. Thus, it can serve as a powerful tool for exploring areas of chemical interest like substituent effects, reaction mechanisms, potential energy surfaces, and excitation energies. Gaussian 98W is capable of predicting many properties of molecules and reactions, including: Molecular energies and structures, energies and structures of transition states, vibrational frequencies, IR and Raman spectra, thermochemical properties, bond and reaction energies, reaction pathways, molecular orbitals, atomic charges, multipole moments, NMR shielding and magnetic

susceptibilities, vibrational circular dichroism intensities, electron affinities and ionization potentials, polarizabilities and hyper-polarizeabilities, and electrostatic potentials and electron densities [50].

The Gaussian 98W program gives good ground state optimization, many other calculations and reasonable execution time. In contrast, it hasn't a graphical interface. Moreover, this program cannot perform transition state calculations for the studied system.

3.1.5 Gaussian 03W

Gaussian 03W [45] represents the latest development of the previous series of Gaussian programs. It includes new basis sets e.g. the universal Gaussian basis set (UGBS). The Gaussian 03W program affords good ground state optimization in most of the calculation methods, reasonable execution time and it a powerful tool in calculating transition state energies and structures [35].

3.1.6 GaussView 03

GaussView 03 [46] is not integrated with the computational component of Gaussian, but rather is a front-end/back-end processor to aid in the use of Gaussian software [51]. It is a graphical user interface designed to help in the preparation of input for submission to Gaussian and to hence, examine graphically the output that Gaussian.

GaussView 03 provides three main benefits to Gaussian users. First, through its advanced visualization facility, GaussView 03 allows you to rapidly draw even very large molecules, then rotate, translate and zoom in on these molecules through simple mouse

operations. It can also import standard molecule file formats such as PDB files. Second, GaussView 03 makes it easy to set up many types of Gaussian calculations. It makes preparing complex input easy for both routine job types and advanced methods like ONIOM, QST2/QST3 transition structure optimizations, CASSCF calculations, periodic boundary conditions (PBC) calculations, and many more [51].

GaussView 03 can examine the results of Gaussian calculations using a variety of graphical techniques. These includes: optimized molecular structures, molecular orbitals, electron density surfaces from any computed density, electrostatic potential surfaces, surfaces for magnetic properties, atomic charges, animation of the normal modes corresponding to vibrational frequencies, IR, Raman, NMR, VCD and other spectra, animation of geometry optimizations, IRC reaction path following, potential energy surface scans, and ADMP and BOMD trajectories, plots of the total energy and other data from the same jobs types [51].

3.2 The Selection of Programs

The combination of Gaussian 03W and GaussView 03 provides the suitable selection of the programs that can be used especially for the Pd-phosphine system of reaction. This hybrid application of the two programs affords many advantages such as powerful calculations using Gaussian 03W, at suitable methods, of ground and transition states, vibrational frequency and chemical reaction path. Moreover, GaussView 03 graphically offers the preparation of input Gaussian files and the examination the output produces and atomic charges, animation of the normal modes corresponding to vibrational frequencies, animation of geometry optimizations and IRC reaction path following.

3.3 The Selection of the Computational Method

Generally, four methods were examined for the catalytic reaction system. These are universal force field, semi-empirical, Hartree-Fock, and density function methods. Their evaluation depends on the accuracy of output of both ground and transition states geometrical structures and vibrational vectors presentations.

The universal force field method was found to be suitable for providing the initial structure of some of ground states and very fast in execution time. However, it is not suitable for transition states calculations and it has many limitations.

The semi-empirical methods cannot be used for the reaction system. The optimization of ground or transition states as well as other calculations cannot be performed by this method.

The restricted Hartree-Fock calculations were implemented to the system. In some cases, these methods afford relatively good optimized ground and transition states geometries in short execution time using the minimal basis set STO-3G. These geometries were utilized as preliminary input for higher method of calculation. On the other hand, several of the optimized structures had some geometrical problems such as long bond length. Vibrational modes of optimized transition states weren't sometime representative for the proposed reaction path.

Density function method at B3LYP [47-49] level of theory was applied to reaction system. This method provides the best optimized ground and transition states geometries. Moreover, vibrational modes presentation of optimized transition states showed the

optimum proposed reaction path. However, its execution time was lengthy in most of the computed molecules.

3.4 The Selection of the Basis Set

Eleven basis sets were tested. The selection of proper basis set was decided on the bases of the accuracy of optimized geometries, relative energies, execution time and possibility of performing the calculations on personal computer. The test is conducted by calculating the heat of formation of Pd-acetylene π-complex and then compare the obtained results with the reported values of large basis set (BSII) [30,31] was used to calibrate our results. The summary of these results are presented in Figure 3.1.

In general, STO-3G* gives good optimized geometries of π-complex intermediate as well as transition states whereas it does not offer square planer of some intermediates. 3-21G* and DGDZVP provide transition state geometries but it can't correctly optimize the π-complex or the square planer intermediates.

The relative energies of the optimized geometry of π-complex intermediate using CEP-4G, CEP-31G and LanL2MB were comparatively unacceptable. UGBS, UGBS1P, UGBS2P and UGBS3P basis sets generate good results but they can't be utilized using personal computer for the studied reaction system. LanL2DZ and SDD [52-56] basis sets afford fairly optimized geometries and relative energies. The geometrical parameters and relative energy results of SDDAll [52-56] and CEP-121G [57-59] basis sets were in good agreement with those obtained by BSII. The execution time of former basis set was the shortest among others.

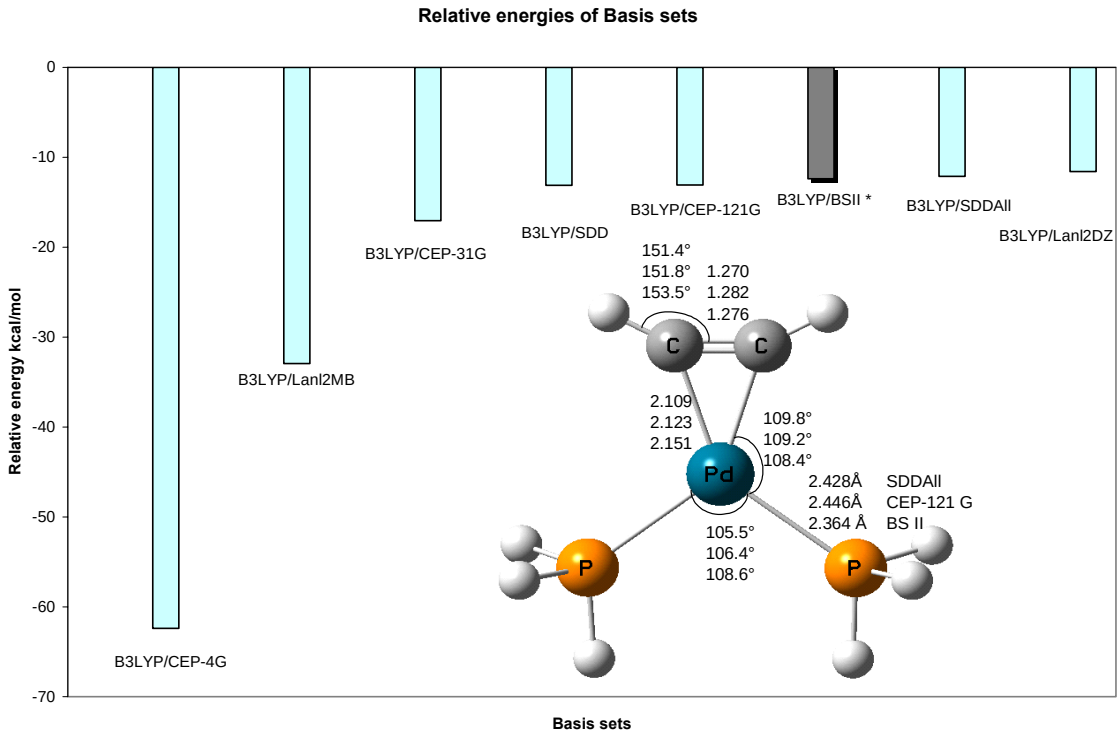

Figure 3.1: Heat of formation and geometrical parameters of Pd-acetylene π-complex coordination using different ECP-basis sets.

The SDDAll-geometrical parameters of the active complex, $Pd(PH_3)_2$ (see Figure3.2), were also found to be the most consistent values to the obtained parameters by more accurate basis set wherein SDD-pseudopotential described the metal and 6-311G* basis was used for all other atoms [60]. The comparison shows that variation of the geometrical parameters from SDDAll to large basis sets never exceed 2%. This reliability, in addition to the shortest execution time using SDDAll basis set, makes it the basis set of choice to carry out the calculations in this study.

A:

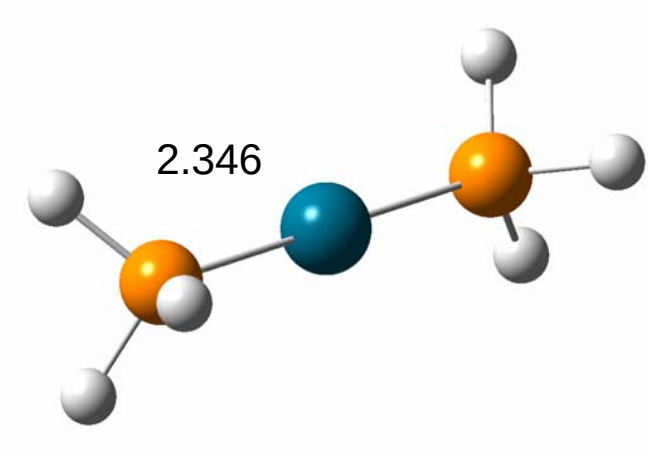

B:

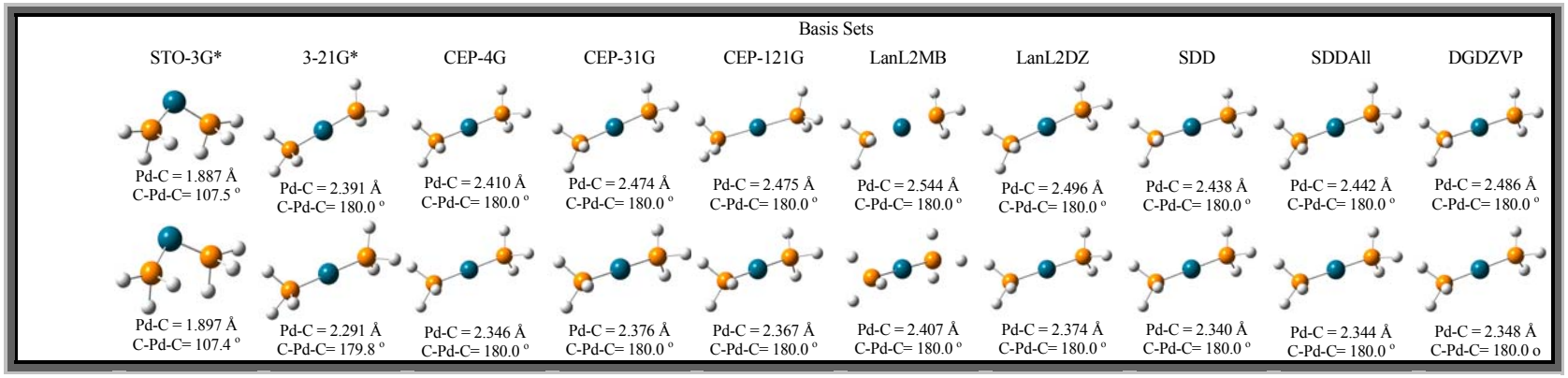

Figure 3.2: Geometrical parameters of the active complex $Pd(PH_3)_2$, A; the reported geometry by the large basis set [30] and B; the obtained geometries under HF and DFT using different basis sets.

CHAPTER FOUR

EXPERIMENTAL SECTION

4.1 Materials

Aniline, alkynes, palladium acetate and phosphine ligand are highly pure commercially available materials and used without further purification. Dry solvents were used in all experiments.

1-heptyne and 2-heptyne were used as alkyne substrates. The utilized phosphine ligands were: 1,3-bis(diphenylphosphino) propane (dppp) and 1,4-bis(diphenylphosphino)butane (dppb). Many solvents were used and they were: dichloromethane, 1,2-dichloroethane, chloroform, tetrahydrofuran (THF), 1,1,1-trichloroethane, carbon tetrachloride, formamide, 3,4-dihydro-2H-parn, dibromomethan and cyclohexane.

4.2 Procedures

4.2.1 The catalytic system (I): $Pd(OAc)_2$/dppp/p-TsOH/CO

A mixture of $Pd(OAc)_2$ (0.02 mmol), 1,3-bis(diphenylphosphino) propane (dppp) (0.04 mmol), p-toluenesulfonic acid (p-TsOH) (0.12), 1-heptyne (2.0 mmol and aniline (2.0 mmol) in 10 ml of THF was placed in the glass liner, equipped with a stirring bar, fitted in 45 ml Parr autoclave. The autoclave was vented three times with CO and then pressurized at room temperature with 100 psi CO. The mixture was stirred and heated for six hours. After cooling, the pressure was released. Then, the reaction mixture was filtered and the

solvent was evaporated. Products were analyzed by Gas chromatography (GC), NMR and FT-IR.

4.2.2 The catalytic system (II): $Pd(OAc)_2$/dppb/CO/H_2

A mixture of $Pd(OAc)_2$ (0.02 mmol), 1,4-bis(diphenylphosphino) butane (dppb) (0.08 mmol), 1- or 2-heptyne (2.0 mmol) and aniline (2.0 mmol) in 10 ml of solvent was placed in the glass liner, equipped with a stirring bar, fitted in 45 ml Parr autoclave. The autoclave was vented three times with CO and then pressurized at room temperature with 300 psi CO and 300 psi H_2. The mixture was stirred and heated for a needed time. After cooling, the pressure was released. Then, the reaction mixture was filtered and the solvent was evaporated. Products were analyzed by Gas chromatography(GC), NMR and FT-IR.

4.3 Experimental Setup

Figure 4.1 shows the experimental setup. All experiments were performed in a fume hood. The autoclave was equipped with pressure gauge and placed in oil bath for heating. The surrounding area is supplied with CO detectors.

4.4 Instruments

Gas chromatography (GC) analyses were performed on HP 6890 plus chromatography. ^{1}H and ^{13}C NMR were record on 500 MHz Jeol 1500 NMR instrument. Chemical shift (δ) were reported in ppm relative to tetramethyl silane (TMS) using $CDCl_3$. Perkin-Elmer 16F PC FT-IR spectrometer was used for IR spectra, which have been reported in wave number (cm^{-1}). Parr stainless autoclave fitted with glass liners were used for high-

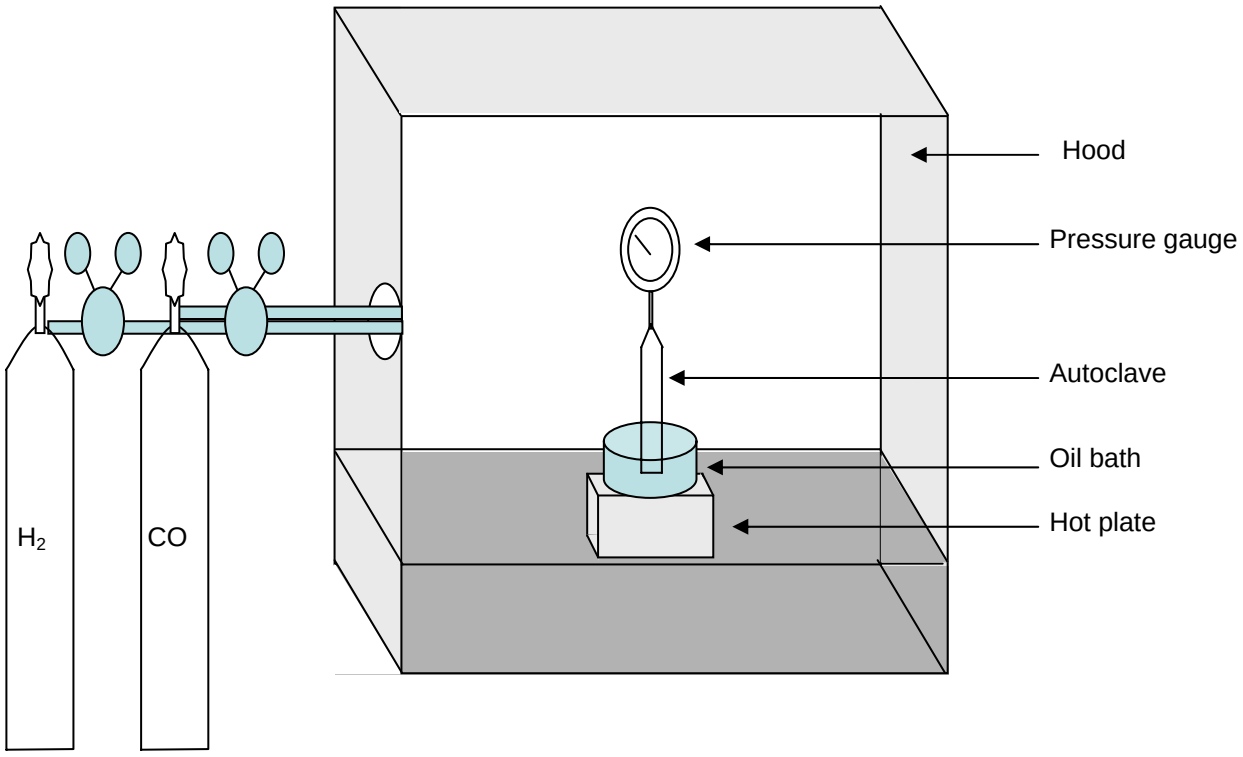

Figure 4.1 a schematic diagram of the experimental set up

pressure reactions. Reduced pressure rotovapor was used to remove the solvent after performing the reaction.

4.5 Spectra and Analytical Data of Some of the Synthesized α,ß-Unsaturated Amides

4.5.1 N-Phenyl-2-pentylpropeneamide

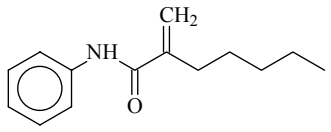

White crystal. m.p.= 59.6°. IR ν (cm^{-1}) KBr: 1656 (CO). ^{1}H NMR δ (ppm) $CDCl_3$: 0.90 (t,3H, *J* = 6.7 Hz, $CH_2C\underline{H}_3$), 1.31 (m, 4H, $CH_2CH_2(C\underline{H}_2)_2CH_3$), 1.59 (m, 2H, $CH_2C\underline{H}_2CH_2CH_2CH_2$), 2.38 (t, 2H, *J* = 7.9 Hz, $C{=}CC\underline{H}_2CH_2$), 5.36 (s, 1H, $C{=}C\underline{H}_2$), 5.68 (s,1H,$C{=}C\underline{H}_2$), 7.08-7.58 (m, 5H, $C_6\underline{H}_5$), 7.74 (s,1H, N<u>H</u>). ^{13}C NMR δ (ppm) $CDCl_3$: 14.03, 22.46, 27.82, 31.46, 32.42, 117.66, 120.05, 124.34, 128.97, 137.92, 146.49, 167.28 (CO).

4.5.2 (E)-N-Phenyl-2-octenamide

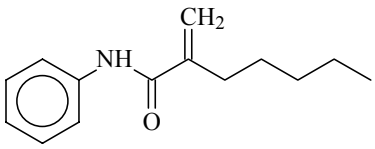

Oil. IR neat ν (cm^{-1}): 1666 (CO). ^{1}H NMR δ (ppm) $CDCl_3$: 0.90 (t,3H, *J* = 6.7 Hz, $CH_2C\underline{H}_3$), 1.31 (m, 4H, $C\underline{H}_2CH_3$), 1.71(m, 4H, $CH_2(C\underline{H}_2)_2CH_2CH_3$), 2.12 (q, $CH{=}CHC\underline{H}_2$), 5.91-5.94 (d, 1H, $CH{=}C\underline{H}$-CO, *J* = 15.25 Hz), 6.92-6.95 (m, 1H, $C\underline{H}{=}CH$-CO), 7.09-7.70 (m, 5H + 1H, C_6H_5 + NH). ^{13}C NMR δ (ppm) $CDCl_3$: 13.81, 22.29, 22.38, 27.80, 31.19, 31.53, 31.99, 34.44, 121.48, 123.72, 129.00, 136.00, 146.75, 164.80 (CO).

CHAPTER FIVE

RESULTS AND DISCUSSIONS

The study will discuss: 1) The validity of two proposed cycles namely, cycle A and cycle B and justify the product distribution of the catalytic formation of the unsaturated amides from alkynes and aniline using Pd-phosphine system. 2) The importance of the decoordination-recoordination of phosphine-ligand (PH_3) of the active Pd-complex at different stages within the catalytic cycle. 3) The influence of type of ligand (mono- or bidentate) on the catalytic process. 4) The regioselectivity of products using different substrate types.

5.1 The Proposed Catalytic Cycles

Recently, many research teams carried out ab initio and density function calculations to shed more light on Pd-catalytic cycles [30-33]. Two different approaches were proposed for these cycles. Jaket et al, [32] suggested that the insertion of palladium into alkynyl carbon-fluorine bonds should proceed via oxidative addition reaction across the carbon-halogen bond. On the other hand, Cui et al studies [30-31] on thioboration or diboration of alkyne using Pd-catalyst reveal that no oxidative addition takes place at the first step of the speculated mechanism while acetylene coordinates to the active catalyst (PdL_2).

Based on the above mentioned, two mechanistic approaches were theoretically investigated to model the catalytic formation of the unsaturated amides (Scheme 5.1). The first approach is initiated with the insertion of palladium into alkynyl carbon-

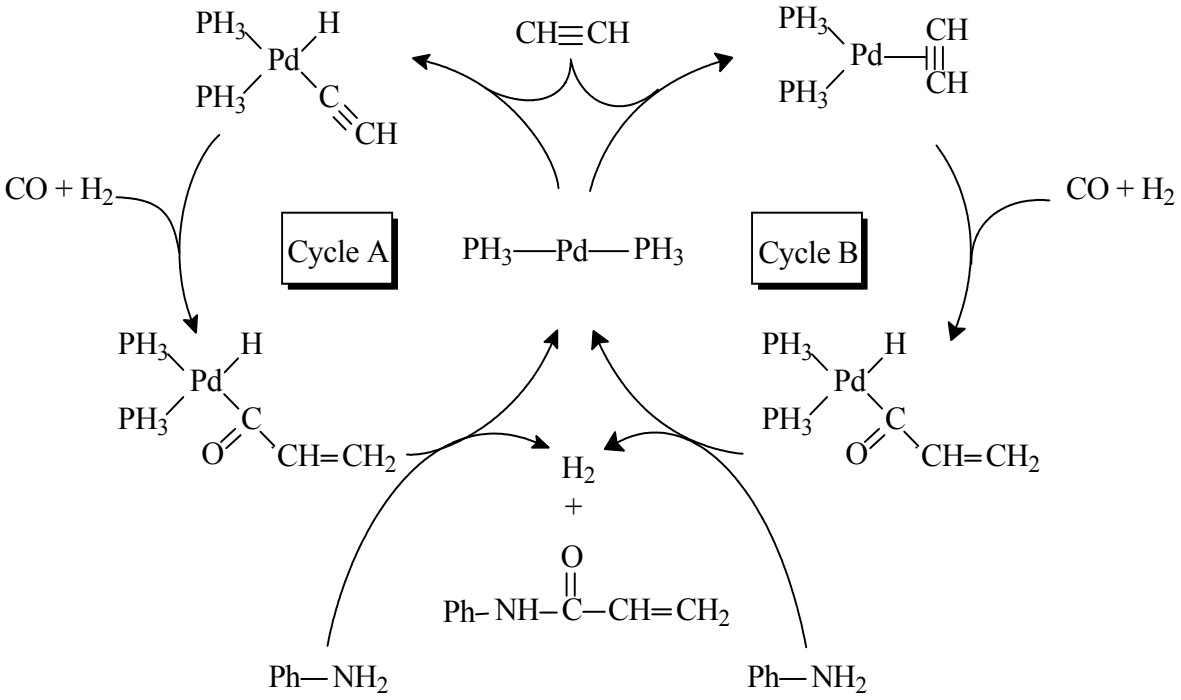

Scheme 5.1: Proposed catalytic cycles of unsaturated amide formation via oxidative addition (A) or π-coordination (B) route.

hydrogen bonds and it is called oxidative addition route (cycle A). The other one is started with acetylene coordination to the active catalyst (PdL_2) to form π-complex and it is named π-coordination route (cycle B).

Unlike the earlier computational modeling on other Pd-catalytic cycles [30-33], the consideration of decoordination/recoordination of a phosphine ligand (PH_3) of the active Pd-complex within the catalytic cycle plays an important role and provides two non-similar paths for each cycle. The proposed molecular systems within theses paths are based either on published X-ray structures [25,26] theoretical results of similar systems [30-33] or the stability of the derived intermediates that trace the reaction path.

5.1.1 Cycle A: The Oxidative Addition Route

Five steps represent this catalytic cycle: (I) oxidative-addition of alkyne, (II) substitution reaction of phosphine ligand by carbon monoxide, (III) migratory insertion of CO ligand into $Pd-CCH$ bond, (IV) hydrogenation of propiolyl group and (V) reductive-elimination to produce unsaturated amides and to regenerate the active Pd(0)-catalyst. Moreover, the possibility of a phosphine ligand (PH_3) in the active Pd-complex to decoordinate/recoordinate at different stages within the catalytic cycle was found to play an important role and supports two non-similar paths (path A and A') of the same cycle. Scheme 5.2 is a schematic diagram of these proposed paths and their five main steps. In both paths, the decoordination of phospine ligand in step II is accompanied by the coordination of CO group. Starting from step III, two paths are expected on the base of the possibility of recoordination of phosphine ligand where PH_3 recoordinates in this step in path A', while in path A it is delayed until the step-V.

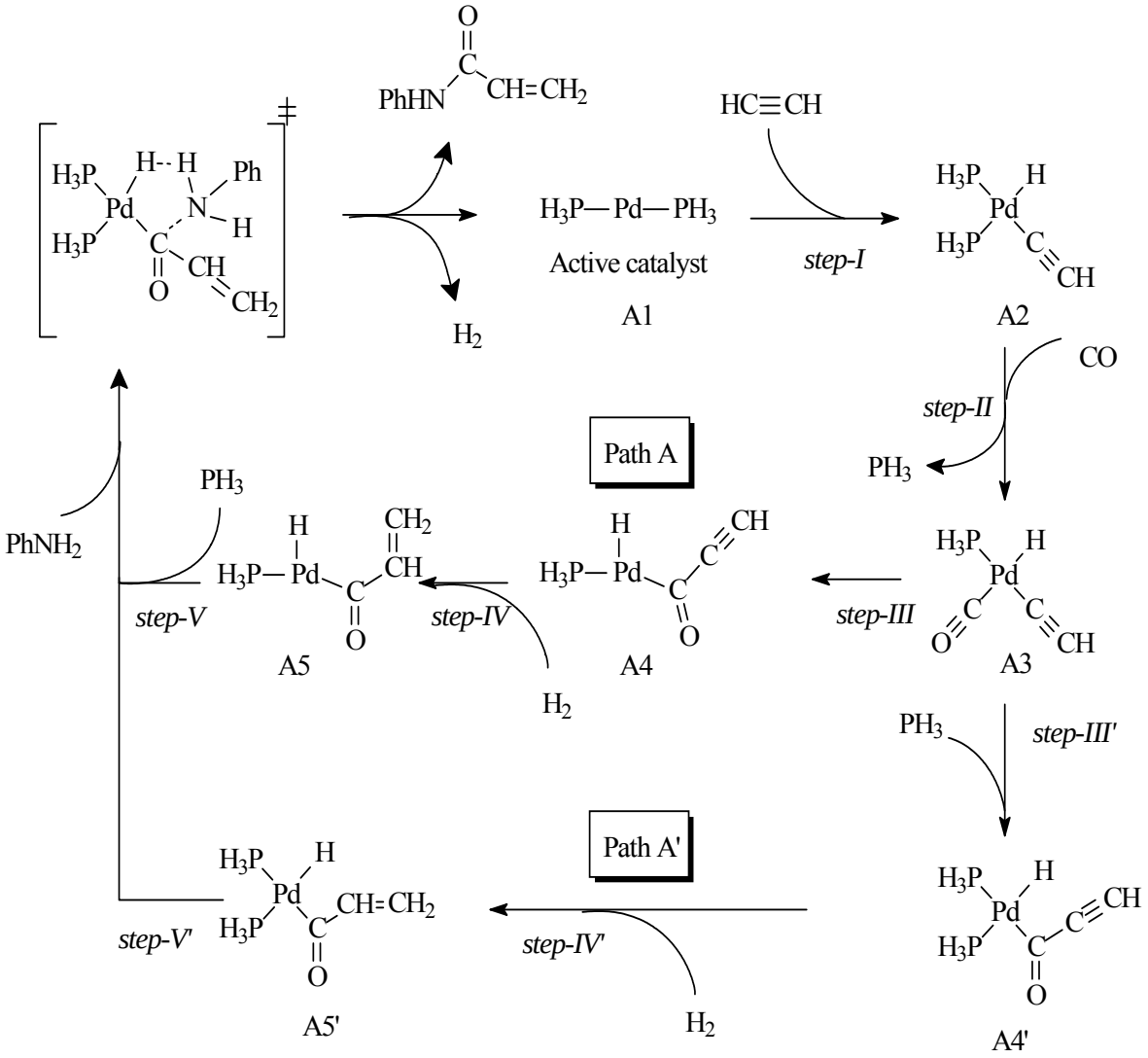

Scheme 5.2: Catalytic cycle of oxidative-addition route (cycle A) includes two paths (A and A') as the result of PH_3-coordination/decoordination possibility.

5.1.2 Cycle B: The π-Coordination Route

The characteristic of cycle B is the first step, which is π-coordination interaction of alkyne with palladium active complex. Similar to cycle A, five steps represent this catalytic cycle: (I) π-coordination of alkyne, (II) substitution reaction of a phosphine ligand by carbon monoxide, (III) oxidative-addition process via alkyne-group migration to the adjacent carbon atom of the coordinated-CO on the Pd-system. (IV) Hydrogenation of the bonded oxo-propynyl group ($-CO-C\equiv CH$) associated with the opening of four-membered metallocyclic intermediate then (V) reductive-elimination to produce unsaturated amides and regenerate the active Pd(0)-catalyst.

Parallel to cycle A, the possibility of a phosphine ligand (PH_3) in the active Pd-complex decoordination-recoordination affords non-similar paths of cycle B. Scheme 5.3 shows the proposed paths and their five main steps. In step-II, a decoordination of phospine ligand facilitates the coordination of CO group. A possibility of recoordination of phosphine ligand takes place in step-III of path B' while it recoordinates later in step-V for path B.

5.2 The Computational Results

Modeling and analyses are needed to test the validity of the proposed cycles and their mechanisms. The proposed mechanistic steps of the cycles are therefore studied computationally by the Density Function Theory (DFT). This study includes ground, transition states and their intrinsic reaction coordinate (IRC) for all the proposed steps

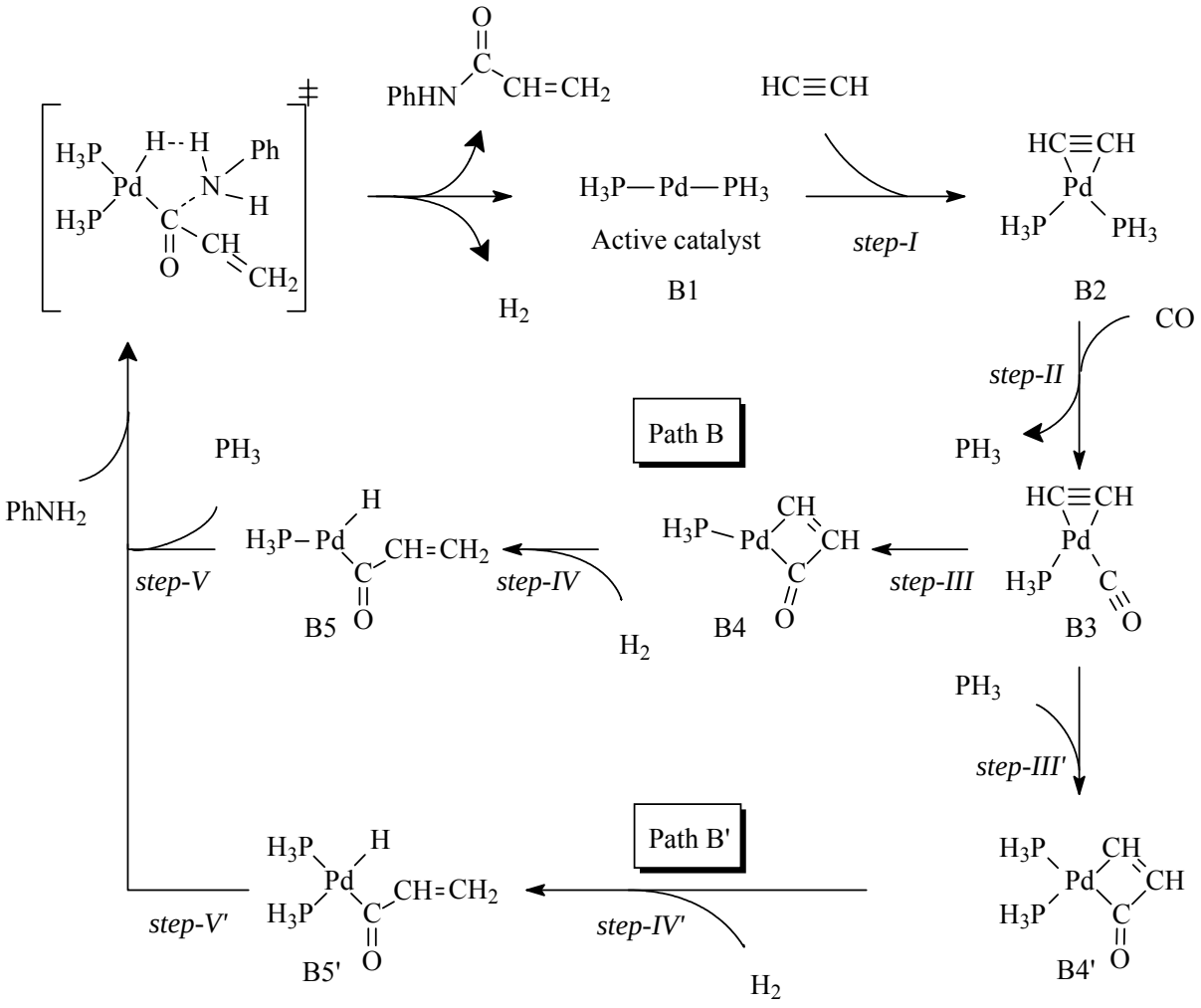

Scheme 5.3: Catalytic cycle of π-coordination route (cycle B) including the effect of PH_3-coordination/decoordination possibility in two paths (B and B').

within the cycles. Mono-dentate and bidentate ligands (phosphine group) were used to model the reaction.

5.2.1 The Mono-dentate Ligand

For the study of the mom-dentate ligand used in the investigated reaction system, acetylene and PH_3 were computed in place of substituted alkynes and aryl phosphine ligands, respectively, to simplify the calculations. In this part, both proposed cycles will be discussed in detail.

5.2.1.1 Oxidative-Addition Route

The potential energy profiles of this cycle (paths A and A') are illustrated in Figure 5.1. Table 5.1 reports the geometrical parameters of the optimized molecular geometry of reactants. The optimized molecular geometries of the products are listed in Table 5.3.

5.2.1.1.1 Path A of The Oxidative Addition Route

In path A, The recoordination of phosphine ligand takes place at the reductive-elimination step. The optimized geometrical parameters of path A in cycle A are recorded in Table 5.2. The following is a detailed discussion on the molecular properties and potential energy surfaces associated with the various steps of the path A of the catalytic cycle A.

Step-I is the oxidative-addition of palladium-phosphine $[Pd(PH_3)_2]$ active catalyst into $H-C$ bond of the alkyne-system. The oxidation state of $[Pd(PH_3)_2]$ is changed from Pd(0) to Pd(II) in the first intermediate A2. This increase in oxidation state needs a promotion energy to change the electronic configuration of Pd from d^{10} to s^1d^9 [30,31]

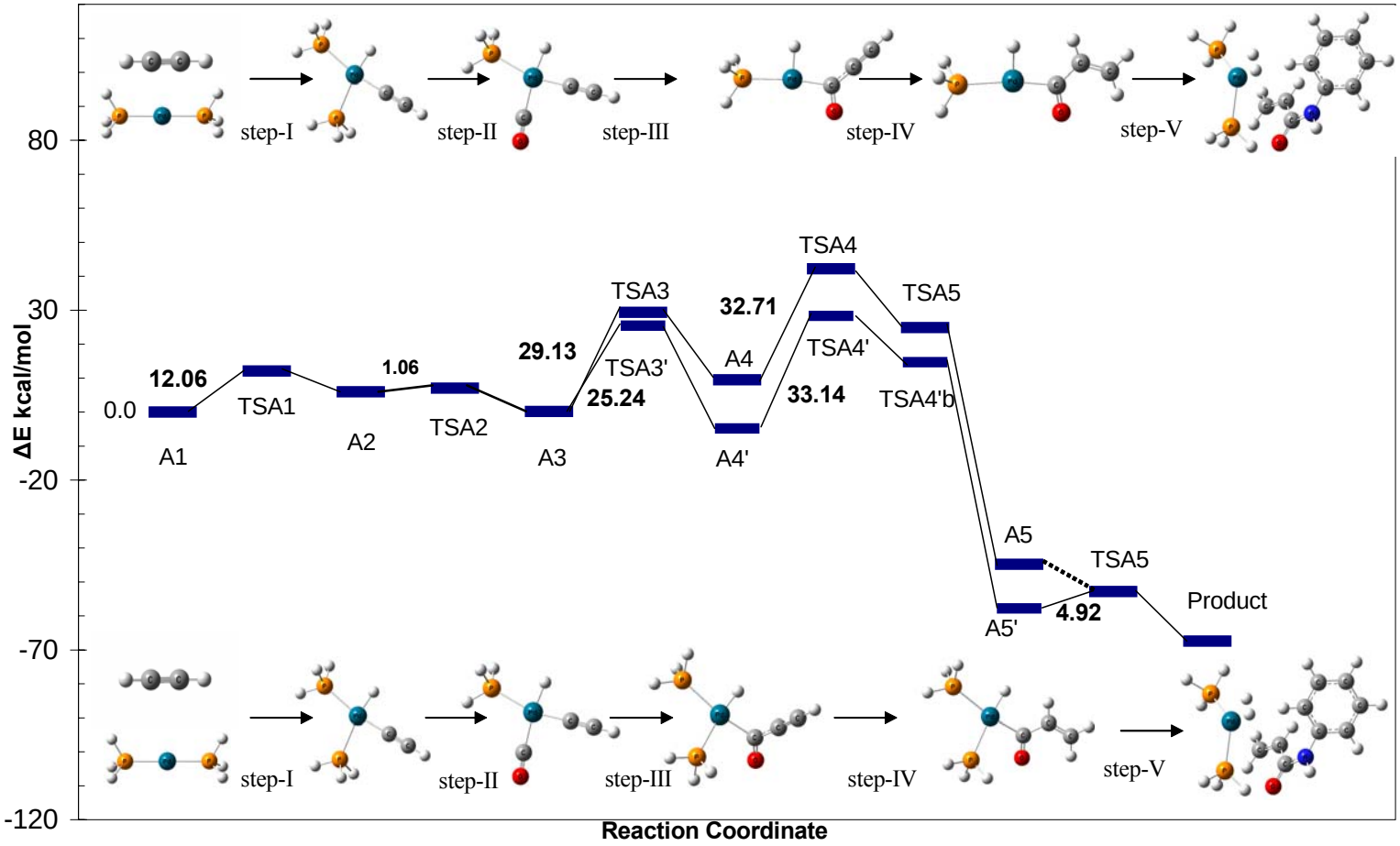

Figure 5.1: Potential energy profiles of cycle A. Optimized structural formulas and relative activation energy above the diagram are of path A while those below it are of path A'.

Table 5.1 The geometrical parameters of the optimized molecular geometry of reactants.

Reactants Molecule	Optimized Structural Parameters							
	#	Type	BL-C	BL	BA-C	BA	DA-C	DA
Active complex  (HF=-144.58105 au)	1	Pd						
	2	P	1	2.34446				
	3	H	2	1.44528	1	120.5949		
	4	H	2	1.445279	1	120.6024	3	120.003
	5	H	2	1.445256	1	120.5951	3	-119.996
	6	P	1	2.344462	2	179.9932	4	18.31535
	7	H	6	1.445279	1	120.602	2	-18.3155
	8	H	6	1.44528	1	120.595	2	101.6872
	9	H	6	1.445255	1	120.5954	2	-138.316
Acetylene 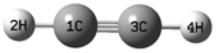 (HF=-12.4482529 au)	1	C						
	2	H	1	1.064425				
	3	C	1	1.212784	2	180		
	4	H	3	1.064425	1	180	2	0
Carbon monoxide 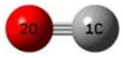 (HF=-21.6600769 au)	1	C						
	2	O	1	1.15217002				
Hydrogen 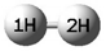 (HF=-1.1744164 au)	1	H						
	2	H	1	0.74347811				
Aniline 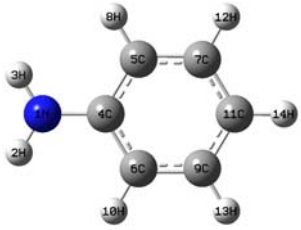 (HF=-48.1304177 au)	1	N						
	2	H	1	1.004622				
	3	H	1	1.004622	2	118.1403		
	4	C	1	1.38671	2	120.9298	3	179.9788
	5	C	4	1.411811	1	120.7187	2	179.9898
	6	C	4	1.411811	1	120.7187	5	-179.958
	7	C	5	1.396546	4	120.4072	1	-179.977
	8	H	5	1.08661	4	119.4962	1	0.019522
	9	C	6	1.396546	4	120.4072	1	179.9772
	10	H	6	1.08661	4	119.4962	1	-0.01952
	11	C	7	1.401026	5	120.8958	4	0.008808
	12	H	7	1.085719	5	119.1469	4	-179.999
	13	H	9	1.085719	6	119.1469	4	179.9988
	14	H	11	1.084275	7	120.5842	5	179.9968

[a] bond length connection (BL-C)
[b] bond length (BL) in (Å)
[c] atoms angle connection (AA-C)
[d] atoms angle (AA) in (degree)
[e] dihedral angle connection (DA-C)
[f] dihedral angle (DA)

Table 5.2: Relative energies (ΔE) and optimized molecular geometries of stationary points of paths A within the oxidative-addition catalytic route (Cycle A)

Path A		
Stationary points	Optimized geometry (Å and degree)	ΔE [a] (ν_{Im})[b]
A1		0.0[c]
TSA1	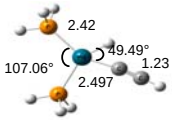	12.06 (-792 .1 i)
A2	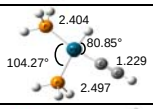	5.93
TSA2	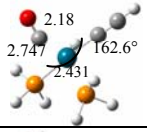	6.99 (-289.86 i)
A3	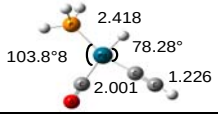	0.18
TSA3	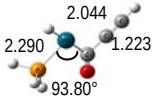	29.31 (-19.6 i)
A4	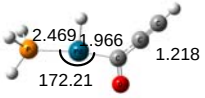	9.48
$TSA4_a$	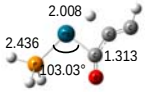	42.18 (-921.1 i)
$TSA4_b$	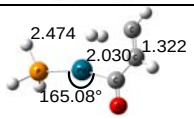	24.84 (-1217.1 i)
A5	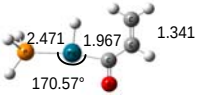	-44.86
TSA5	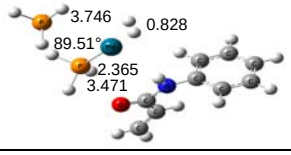	-52.87 (-20.4 i)[d]

[a] Relative energy to the total heat of formation of acetylene and $Pd(PH_3)_2$ in kcal/mol
[b] Imaginary frequency in cm^{-1}
[c] The total heat of formation of acetylene and $Pd(PH_3)_2$ in hartree-fock is -157.02933610 a u
[d] More than an imaginary frequency were observed, the listed value is for the one that present the movement of atoms according to the reaction path.

Table 5.3 The geometrical parameters of the optimized molecular geometry of products.

Product	Optimized Structural Parameters							
Molecule	Atom #	Atom Type	BL-C[a]	BL[b]	AA-C[c]	AA[d]	DA-C[e]	DA[f]
Amide 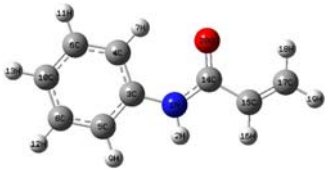 (HF=-82.3462551 au)	1	N						
	2	H	1	1.01155				
	3	C	1	1.418517	2	114.6812		
	4	C	3	1.406997	1	123.3074	2	179.9971
	5	C	3	1.408708	1	117.0057	4	-179.999
	6	C	4	1.399488	3	119.1707	1	-180
	7	H	4	1.079439	3	119.4816	1	-0.0042
	8	C	5	1.395302	3	120.3764	1	-179.999
	9	H	5	1.087214	3	119.7632	1	0.002942
	10	C	8	1.400678	5	120.1961	3	-0.00157
	11	H	6	1.084912	4	118.797	3	179.9989
	12	H	8	1.08489	5	119.5212	3	-179.999
	13	H	10	1.084435	8	120.2959	5	179.9997
	14	C	1	1.381307	3	129.1391	5	179.9799
	15	C	14	1.487375	1	113.8442	3	-179.986
	16	H	15	1.088029	14	117.9115	1	-0.02808
	17	C	15	1.33899	14	121.4521	1	179.974
	18	H	17	1.084896	15	120.3609	14	-0.00399
	19	H	17	1.084208	15	121.6707	14	179.9988
	20	O	14	1.256289	1	123.4475	3	0.01403

[a] bond length connection (BL-C)
[b] bond length (BL) in (Å)
[c] atoms angle connection (AA-C)
[d] atoms angle (AA) in (degree)
[e] dihedral angle connection (DA-C)
[f] dihedral angle (DA)

which permits palladium active catalyst to form two new bonds. One bond is formed with hydrogen atom and the other bond is formed with carbon atom of the acetylene. The process takes place via a three-centered molecular structure of palladium, carbon, and hydrogen atom of acetylene (TSA1). The energy barrier of this process is +12.06 kcal/mol relative to reactants (A1). This activation energy can be explained in terms of the needed promotion energy.

The IR-vector displacements of its imaginary vibration in Figure 5.2 confirm the H-atom migration from the moiety of the acetylenic-carbon to the palladium. Pd(II)-complex intermediate "A2" will be produced as a result of this step, which is +5.93 kcal/mol relative to reactants. The active catalyst A1 is linear whereas the intermediate "A2" has a square planar geometry with the (P-Pd-P) angle value of 104.27°. This angle in the transition state TSA1 (107.05°) is in between A1 and A2. The angle (H-Pd-C) in TSA1 is 49.49° while it becomes larger in the intermediate A2 (80.86°). The bond length of the "Pd-P" in A2, which is cis to the acetylenyl group, is slightly elongated than the other one. This elongation can be related to the bulkiness effect of the neighbor acetynyl group.

Step-II represents a substitution reaction of a coordinated PH_3-group in A2 by a CO-group via backside attack to produce the intermediate A3, which is more stable than A2 by about 5.75 kcal/mol and has a square planar arrangement (Figure 5.1). This step is characterized by a very small energy barrier of about +1.06 kcal/mol relative to A2. The IR-vector displacement of the imaginary vibrational mode of step-II transition state (TSA2) indicates that this substitution can be classified as associative mechanism. Its modeling in Figure 5.3 shows that the attack does not occur via axial

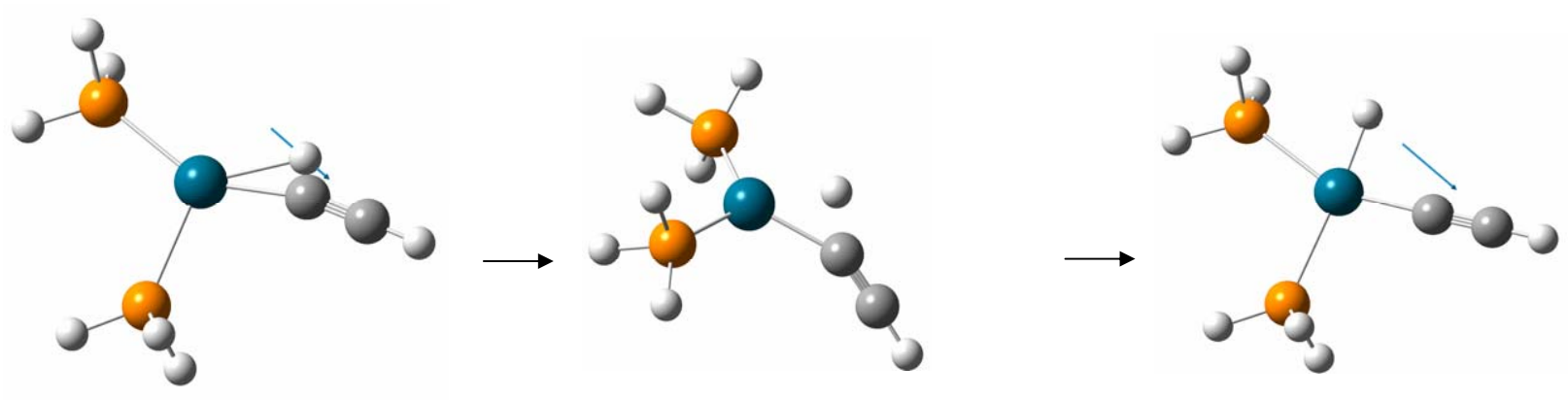

TSA1-A TSA1-B TSA1-C

Figure 5.2: H-atom migration from the moiety of the acetylenic-carbon (TSA1-A) to the palladium-atom side (TSA1-C) using IR-vector displacement motions of the imaginary vibrational mode of transition state (TSA1). TSA1-B is the molecular geometry at the IRC-maximum.

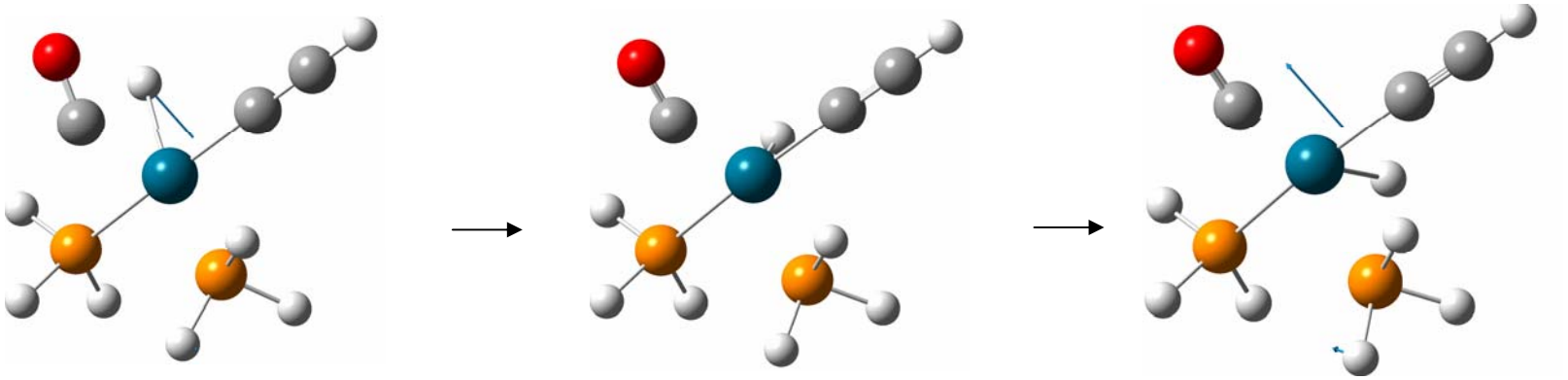

TSA2-A TSA2-B TSA2-C

Figure 5.3: The backside-CO substitution of the coordinated PH_3-group using the IR-vector displacement of the imaginary vibrational mode of TSA2. The illustrations in TSA2-A and TSA2-C show the Hydrogen-vibration due to the approach of CO-group toward palladium-atom and then the go-away of the PH_3-group. TSA2-B is the molecular geometry at the IRC-maximum.

positions similar to the generally held explanation of carbon-center SN2 [61]. The well known extended-octet nature of Pd-metal system can account on this non-axial attack that is supported by the bond angle of the axial groups, which approach the linearity (162.6^{o}). At the same time, the bond length of a phosphine-leaving group increases from 2.431 to 2.747 Å (Table 5.1). Step-III is the migratory insertion of CO-ligand into $Pd-CCH$ bond. According to the modeling output in Figure 5.1, in path A, this step requires about +29.13 kcal/mol to activate A3 to TSA3. The CO-group migratory insertion takes place via a three-center arrangement including C(CO)-C(acetynyl)-Pd in TSA3. In Figure 5.4, the vibrational vector displacements of the imaginary frequency of TSA3 show that the acetynyl group moving apart from Pd atom. This movement is also confirmed by the increasing of the $Pd-CCH$ bond length which is needed to break this bond and to insert the CO group and by increasing of the P-Pd-CO angle from 103.88° in intermediate A3 to 172.21° in intermediate A4 which is the product of this step.

A4 is less stable than A3 by about 9.30 kcal/mol. Moreover, this intermediate (A4) has the highest ground state energy among all other intermediates in the whole cycle. Thus, the formation of A4 is unfavorable.

Step-IV is the hydrogenation of the alkynyl side of the propiolyl group ($-CO-C\equiv CH$). It also consists of two successive transition states (Figure 5.5), namely, four-centered and six-centered metallocyclic systems ($TSA4_a$ and $TSA4_b$, respectively). No intermediate can be located between these two transition states. According to the modeling outputs in Figure 5.1, this step has the highest activation energy of about 32.71 kcal/mole.

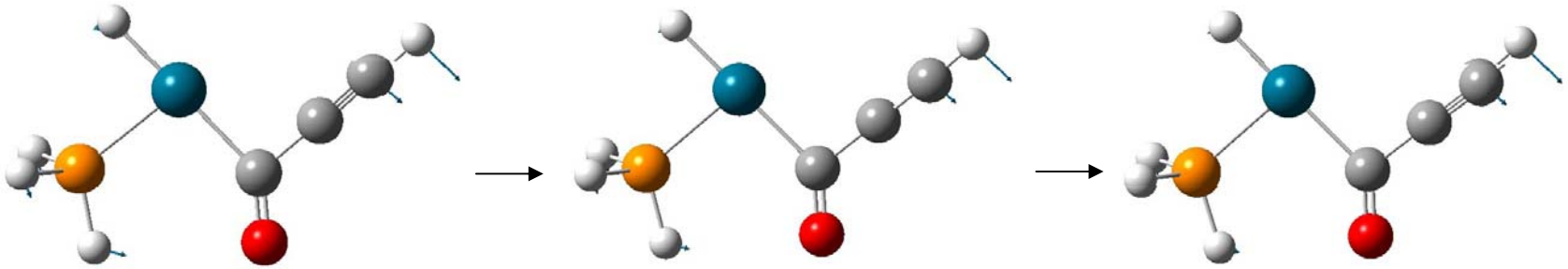

TSA3-A TSA3-B TSA3-C

Figure 5.4: The CO-group migratory insertion takes place via a three-center arrangement including C(CO)-C(acetynyl)-Pd in TSA3. The illustrations in TSA3-A and TSA3-C show the acetynyl group vibration. TSA3-B is the molecular geometry at the IRC-maximum.

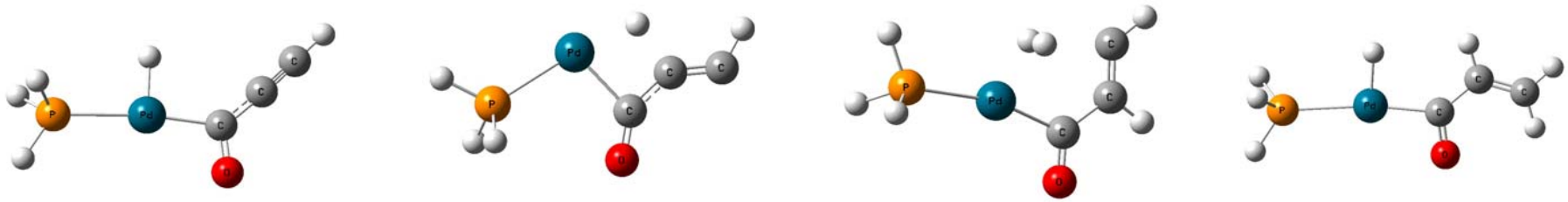

A4 $_{a}$TSA4 $_{b}$TSA4 A5

Figure 5.5: Transition states associated with the hydrogenation-step in path A. $TSA4_a$ and $TSA4_b$ are the four-centered and the six-centered metalocyclic transition states, respectively.

In the $TSA4_a$, the hydrogen atom migrates from palladium atom (reaction center) to the α-carbon via a four-centered metallocyclic system of hydrogen, palladium, carbon (of carbonyl group) and α-carbon. This hydrogen migration is essential to make a vacant site on the palladium reaction center and to complete this step. The change in geometry of intermediate A4 facilitates the hydrogen atom movement. Table 5.1 presents the changes of the P-Pd-CO angle from 172.21° in A4 to 103.03° in $TSA4_a$.

In the $TSA4_b$, the addition of hydrogen molecule takes place where one hydrogen atom is added to the palladium atom and the other hydrogen atom is added to ß-carbon atom. This addition proceeds through a six-centered metallocyclic system of palladium atom, three carbon, and two hydrogen atoms. The P-Pd-CO angle changes from 103.03° in $TSA4_a$ to 165.08° in $TSA4_b$ (Table 5.1). The $TSA4_b$ is lower in energy than $TSA4_a$ by about 17.34 kcal/mol. The product of this step (intermediate A5) is the most stable intermediate in the cycle. Thus, the process of formation of A5 has the highest exothermic reaction where the drop in energy is about 69.70 kcal/mol.

Step-V is the reductive elimination process to produce unsaturated amide, hydrogen molecule, and the active catalyst (PdL_2). The computed models of this step is presented in Figure 5.6 that indicate the aniline approaching toward the acrylyl- side of Pd-complex is assisted by the expelling of a trans-PH_3-group (TSA5) while the hydrogen atom on Pd-complex goes away together with another one from aniline molecule. These models also show that the complete disintegration of the unsaturated amide and hydrogen molecule is then supported by the recoordination of the expelled PH_3-group via backside attack to reactivate PdL_2-complex at a bond length of about 2.43 Å (product in Figure 5.6).

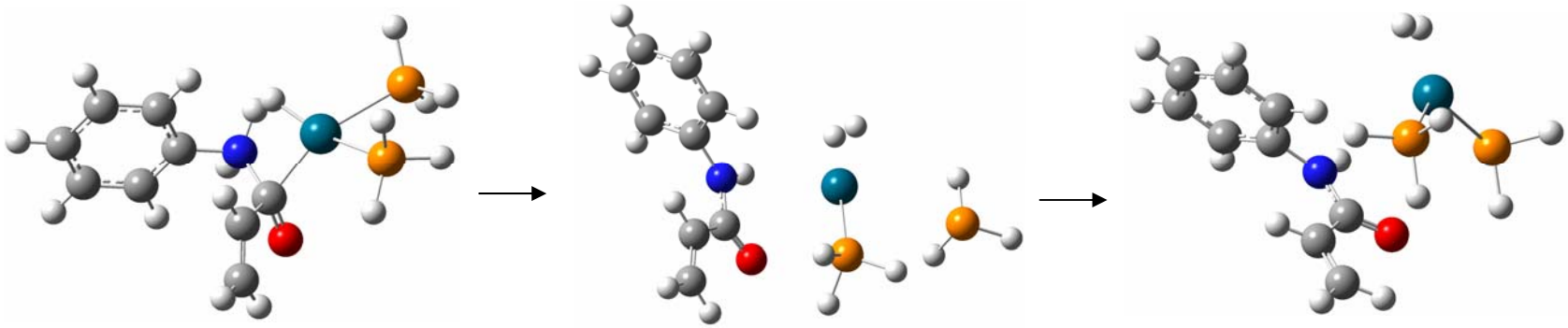

Aniline-acrylyl-Pd TSA5 product

Figure 5.6: Five-centered metalocyclic presentation of aniline-acrylyl-Pd complex interaction in step-V. TSA5 is the predicted transition state associated with this interaction while "product" is the disintegrated unsaturated amide, hydrogen gas, and reactivated of Pd-phsophine complex.

5.2.1.1.2 Path A' of The Oxidative Addition Route

The main difference between the two paths (A and A') is the possibility of decoordination-recoordination of PH_3-ligand in path A' that was totally omitted by most of the earlier modeling studies of similar systems [24-26, 30-33]. They only considered the recoordination of PH_3-ligand around catalyst's reactivation step [30-33]. The potential energy profiles of this cycle (paths A and A') are illustrated in Figure 5.1. The geometrical parameters of the optimized molecular geometries of path A' in cycle A are recorded in Table 5.4. The following is a discussion on the molecular properties and potential energy surfaces associated with the various steps of the path A' of the catalytic cycle A.

Step-I and Step-II are the same as path A in cycle A and they are discussed there.

Step-III is the migratory insertion of CO-ligand into $Pd-CCH$ bond. The modeling outputs in Figure 5.1 show the activation energy of the transition state (TSA3') is +25.24 kcal/mol. The consideration of recoordination of the previously expelled PH_3-group via path A' has many advantages. For example, reduction of the activation energy from TSA3 in path A to TSA3' is about 3.89 kcal/mole, and stability of the produced intermediate A4' compared to A4 is about 14.48 kcal/mole. Moreover, it will maintain a consistent molecular geometry, namely square planar of intermediates and trigonal bipyramidal of transition states and a single oxidation state of Pd-system (except the initial step of the active complex) over the process. The vibrational vector displacement presentations of the imaginary frequency of TSA3' in Figure 5.7 confirms the associative mechanistic

Table 5.4: Relative energies (ΔE) and optimized molecular geometries of stationary points of paths A' within the oxidative-addition catalytic route (Cycle A)

Path A'		
Stationary points	Optimized geometry (Å and degree)	ΔE [a] (ν_{Im})[b]
A1	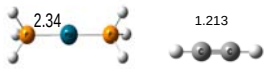	0.0[c]
TSA1	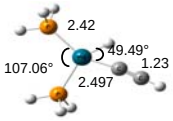	12.06 (-792 .1 i)
A2	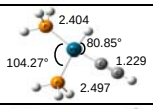	5.93
TSA2	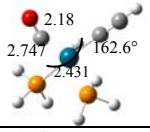	6.99 (-289.86 i)
A3	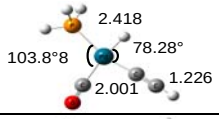	0.18
TSA3'	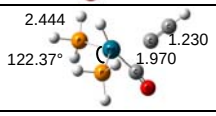	25.42 (-373.63 i)
A4'	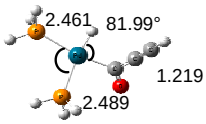	-4.82
TSA4'$_a$	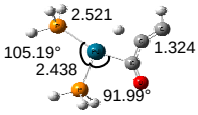	28.31 (-859.6i)
TSA4'$_b$	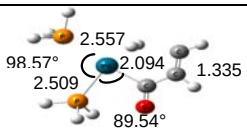	14.69 (-1321.2 i)
A5'	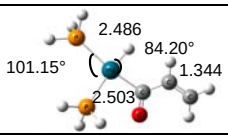	-57.81A5'
TSA5	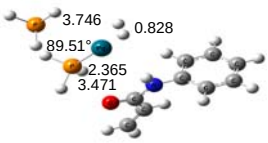	-52.87 (-20.4 i)[d]

[a] Relative energy to the total heat of formation of acetylene and $Pd(PH_3)_2$ in kcal/mol
[b] Imaginary frequency in cm^{-1}
[c] The total heat of formation of acetylene and $Pd(PH_3)_2$ in hartree-fock is -157.02933610 a u
[d] More than an imaginary frequency were observed, the listed value is for the one that present the movement of atoms according to the reaction path.

feature of this step. It also shows that the recoordination process of the PH_3-group is associated with the CO-group insertion via a three-center arrangement including C(CO)-C(acetynyl)-Pd, which includes bond shortening of Pd-CO from 2.00 to 1.97 Å while Pd-C(acetynyl) bond is getting longer (from 1.98 Å in A3 to 2.23 Å in TSA3').

Step-IV is the hydrogenation of the alkynyl side of the propiolyl group ($-CO-C\equiv CH$). According to the modeling outputs in Figure 5.1, this step presents the highest activation energy within the cycle. It also consists of two successive transition states (Figure 5.8), namely, four-centered and six-centered metallocyclic systems (TSA4'$_a$ and TSA4'$_b$, respectively). The initial activation energy of this step is not affected by the absence or the presence of the coordinated PH_3-group in A4 or A4' where the activation energies of TSA4 and TSA4'$_a$ are almost the same (32.7 and 33.13 kcal/mole, respectively). On the other hand, the close examination of the geometrical properties of TSA4'$_b$ transition state indicates the PH_3-groups decoordination/recoordination oscillation effect, where the bond length changed from 2.46 (A4') to 2.50 (TSA4'$_a$) to 2.55 (TSA4'$_b$) and then back to 2.48 (A5'). For that, the hydrogenation step is facilitated. Its consideration is also

Step-V presents the reductive elimination process to produce the unsaturated amide, hydrogen molecule and the active catalyst (PdL_2). This step is similar to step-V in path A.

5.2.1.2 Cycle B: the π-Coordination Route

The first step which is the interaction of alkyne and palladium active complex via π-coordination system is the main distinction characteristic of cycle B. Similar to cycle A, the inclusion of decoordination/recoordination of a phosphine ligand (PH_3) at different

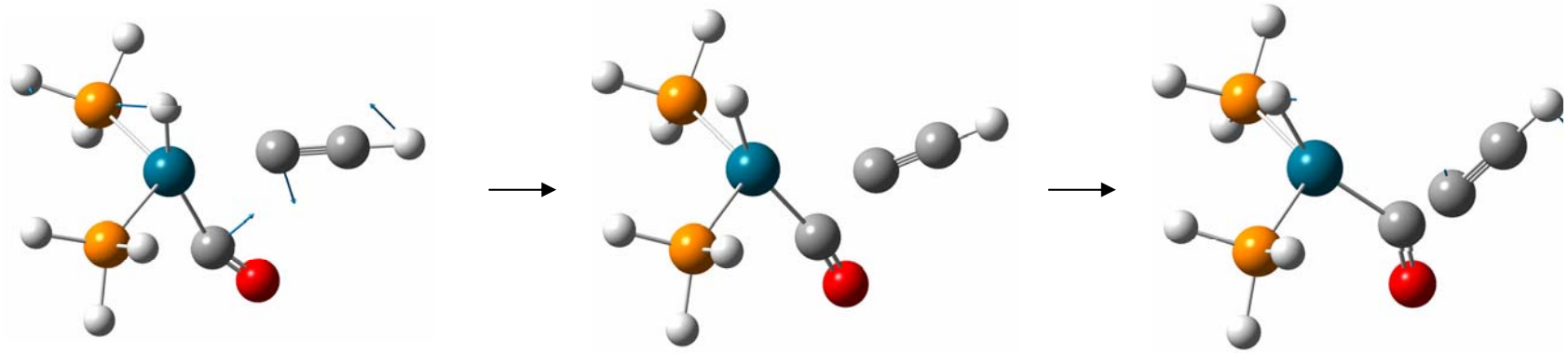

TSA3'-A TSA3'-B TSA3'-C

Figure 5.7: CO-group insertion into the acetynlyl-Pd bond using IR-vector displacement of the imaginary vibrational mode of TSA3'. TSA3'-A to TSA3'-C is the movement of the coordinated CO-group toward the bonded acetynyl. TSA3'-B is the molecular geometry at the IRC-maximum.

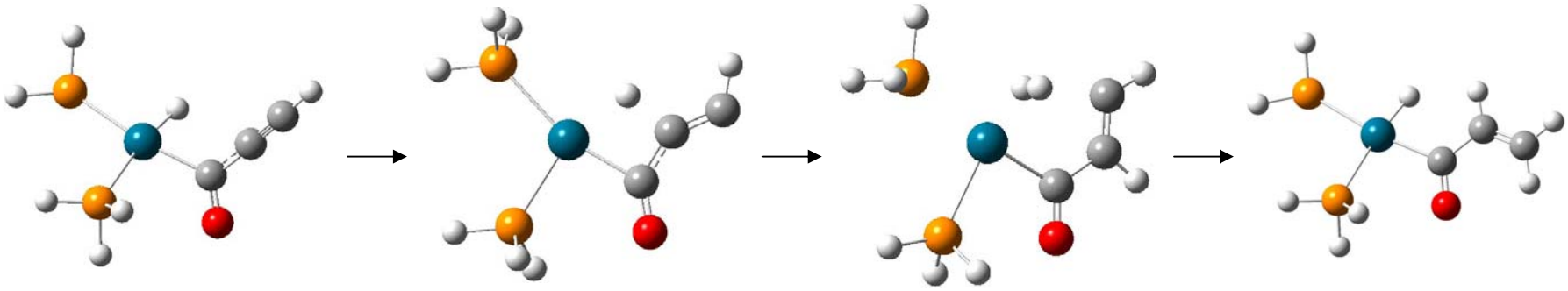

A4' TSA4'$_a$ TSA4'$_b$ A5'

Figure 5.8: Transition states associated with the hydrogenation-step in cycle A'. TSA4'$_a$ and TSA4'$_b$ are the four-centered and the six-centered metalocyclic transition states, respectively.

stages within the catalytic cycle will produce two paths of the cycle B, namely, path B and B'. The potential energy profiles of this cycle (paths B and B') are illustrated in Figure 5.9. The optimized geometrical parameters of reactants are reported in Table 5.1 and of the products are listed in Table 5.3.

5.2.1.2.1 Path B of π-Coordination Route

In path B, The recoordination of phosphine ligand takes place at the reductive-elimination step. Table 5.5 reports the optimized geometrical parameters, transition states, imaginary frequency, and their relative energies of path B compared to reactants-B1. The following is a discussion on the molecular properties and potential energy surfaces of various steps of this path.

Step-I involves π-coordination of alkyne to the active catalyst $Pd(PH_3)_2$. The coordination energy, as mentioned above, agrees well with the reported value using BSII-Basis Set [30,31] and is found to be -12.14 kcal/mol. The π-coordination takes place via transition state TSB1 and its formation needs very low activation energy of about +2.72 kcal/mol (Figure 5.9). The estimated geometry of this transition state is similar to a reported one of Pd-olefin complex using Molecular Mechanics (MM3*) [25,26] that uses X-ray structural parameters to parameterize the used model.

A square planar Pd(0)-π-complex intermediate B2 is the product of step-I that is thermodynamically more stable than the reactants (B1) by about -12.14 kJ/mol. The $-C \equiv C-$ bond length of the intermediate B2 is 1.270 Å and is almost similar to the one in isolated acetylene (1.213Å). Thus, confirms that only the π-coordination occurs

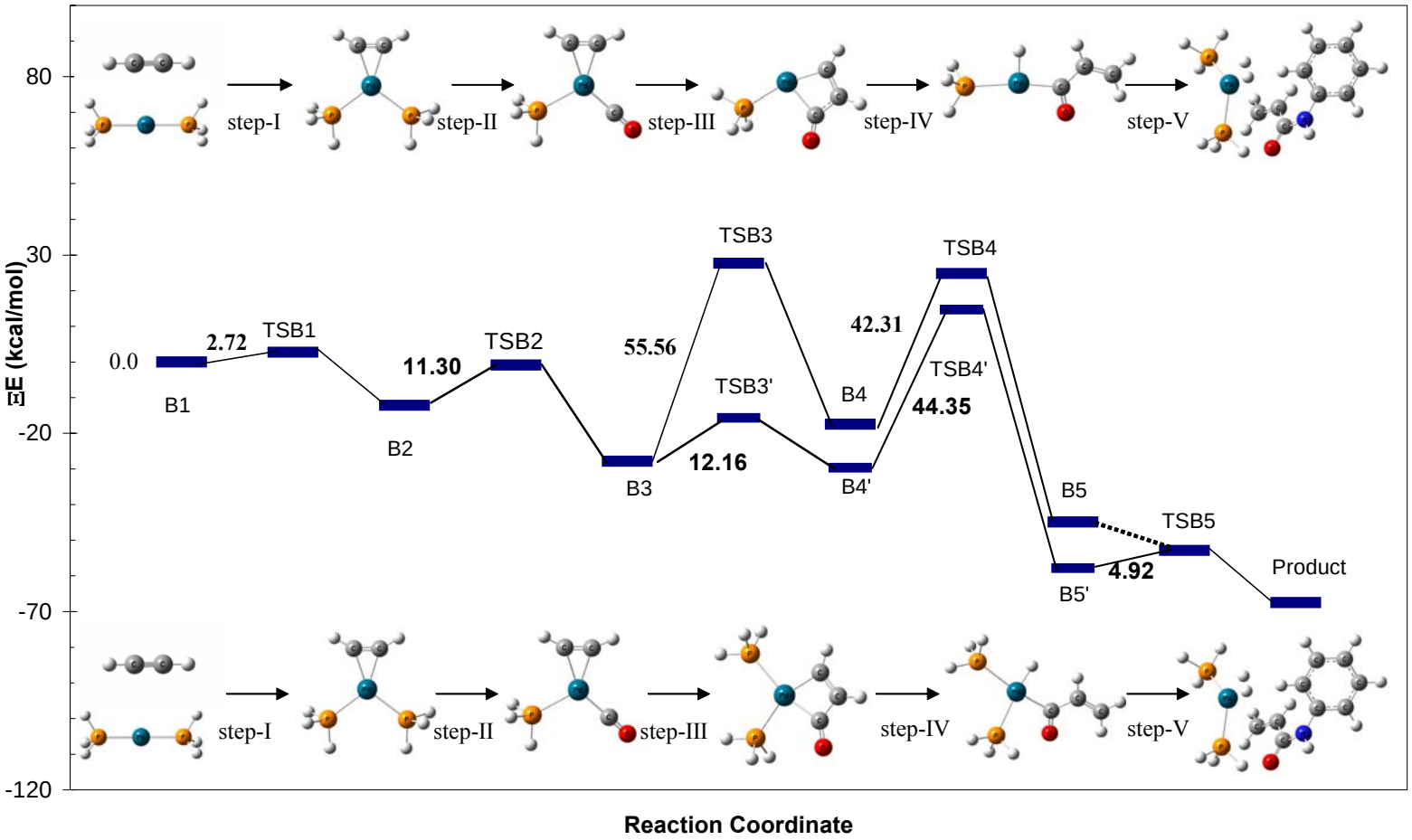

Figure 5.9: Potential energy profiles of cycle B. Optimized structural formulas and relative energies above the diagram are of path B while those below it are of path B'.

Table5.5: Relative energies (ΔE) and optimized molecular geometries of stationary points of paths B of the π-coordination catalytic route (Cycle B)

Stationary points	Optimized geometry (Å and degree)	ΔE [a] (ν_{Im})[b]
B1		0.0[c]
TSB1	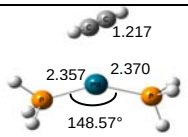	2.72 (-79.07 i)
B2	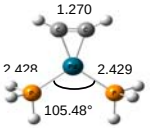	-12.14
TSB2	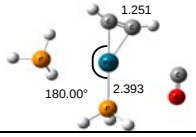	-0.85 (-65.58 i)[d]
B3	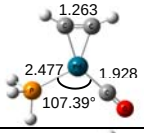	-27.85
TSB3	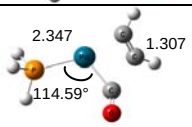	27.71 (-612.23 i)
B4	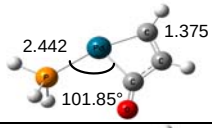	-17.46
TSB4	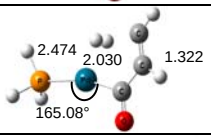	24.84 (-1217.1 i)
B5	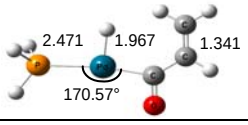	-44.86
TSB5	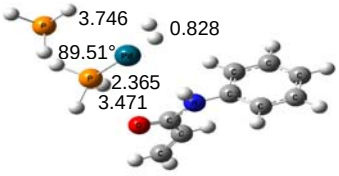	-52.87 (-20.4 i)[d]

[a] Relative energy to the total heat of formation of acetylene and $Pd(PH_3)_2$ in kcal/mol
[b] Imaginary frequency in cm^{-1}
[c] The total heat of formation of acetylene and $Pd(PH_3)_2$ in hartree-fock is -157.02933610 a u
[d] More than an imaginary frequency were observed, the listed value is for the one that present the movement of atoms according to the reaction path.

without any oxidative addition process. The low activation energy and the stability of B2-formation compared to A2-formation in cycle A verify the general believe that the initial step of Pd(0)-catalytic systems of unsaturated hydrocarbons is the formation of π-complex system (B2). In addition, the observed Pd-P and C-C bonds lengthening as well as the P-Pd-P and H-C-C angle closing from the IR-vector displacement motion of its imaginary vibrational mode in Figure 5.10 confirms the π-coordination process.

In step-II, CO-substitution reaction, a backside attack of associative mechanism is observed in this cycle too and is presented in Figure 5.11. Although the produced square planar Pd(0)-π-complex with CO-coordinated intermediate (B3) is more stable than B2 by about 15.71 kcal/mol, its energy of activation is high (about 11.30 kcal/mol in Figure 5.9) compared to the corresponding step in cycle A (about 1.06 kcal/mol).

The oxidative-addition of step-III proceeds via alkyne-group migration to the adjacent carbon atom of coordinated-CO-Pd-system. This migration process is clear from the IR-vectors presentation of the imaginary frequency of TSB3 vibrational modes in Figure 5.12. As indicated in Figure 5.9, this step needs about 55.56 kcal/mol as activation energy that presents the highest activation energy in the catalytic process. The product of the step is the four-membered metallocyclic intermediate B4 which is less stabile than intermediate B3 by about 10.39 kcal/mol. Therefore, the formation of B4 is thermodynamically and kinetically difficult.

Step-IV is the addition of hydrogen to the four-membered metallocyclic intermediate B4. The hydrogen addition needs the opining of the four-membered metallocyclic intermediate B4 then, the hydrogen is added as follows: one atom moves to palladium

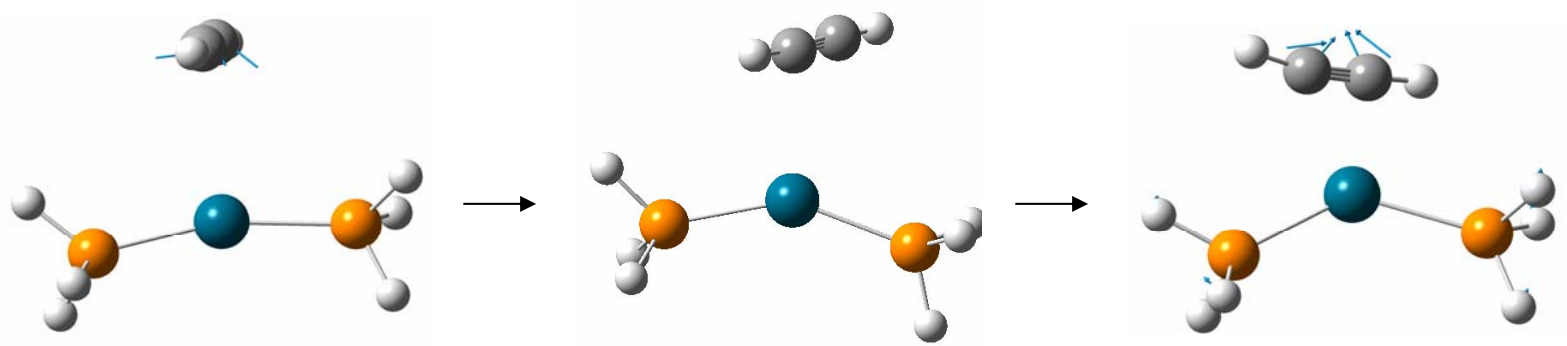

TSB1-A TSB1-B TSB1-C

Figure 5.10: π-Complex transition state (TSB1-B). TSB1-A and TSB1-C are the maximum IR-vector displacement motions of the imaginary vibrational mode of transition state (TSB1).

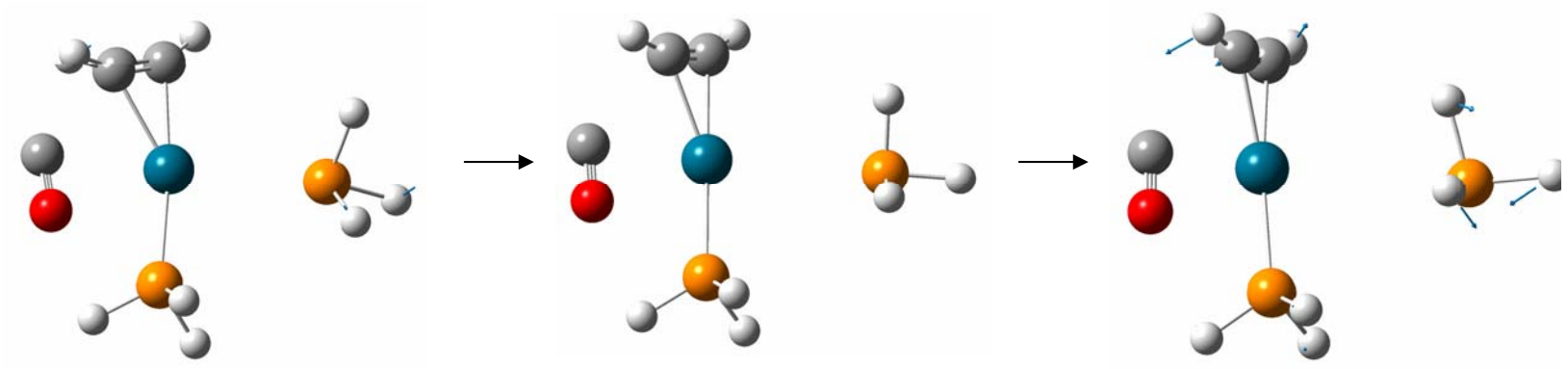

TSB2-A TSB2-B TSB2-C

Figure 5.11: Backside-CO substitution of the coordinated PH_3-group using the IR-vector displacement of the imaginary vibrational mode of TSB2. The illustrations in TSB2-A and TSB2-C of the maximum displacement of the substituted groups. TSB2-B is the molecular geometry at the IRC-maximum.

atom while the other migrates to ß-carbon atom. This step proceeds via six-centered transition state (TSB4). The activation energy of TSB4 requires 42.31 kcal/mol that is higher energy than the corresponding one in cycle A. The vibrational frequency modes of TSB4 are presented in Figure 5.13.

Step-V is the reductive-elimination process that is similar to the proposed one in cycle A.

5.2.1.2.2 Path B' of π-Coordination Route

The main difference between the two paths (B and B') is the possibility of decoordination-recoordination of PH_3-ligand in path B'. The potential energy profiles of this cycle (paths B and B') are illustrated in Figure 5.9. Table 5.6 records the optimized geometrical parameters of path B' in cycle B. The following is a discussion of steps of the path B' in cycle B. it includes the molecular properties and potential energy surfaces.

Step-I and Step-II are explained in path B in this cycle.

Step-III is the oxidative-addition process which occurs via the migration π-coordinated alkyne group to the adjacent carbon atom of coordinated-CO-Pd-system. This migration process is confirmed by the IR-vectors presentation of the imaginary frequency of TSB3' vibrational modes (Figure 5.14). Similar to cycle A, two paths (B or B′) are proposed at this step where the expelled PH_3-ligand in the previous step recoordinates. The absence of PH_3-ligand will direct the cycle to path B while its inclusion will execute the cycle via path B′. The potential energy profile in Figure 5.8 shows that the recoordination of the PH_3-ligand via the backside attack produces an oxidative-addition adduct namely, four-

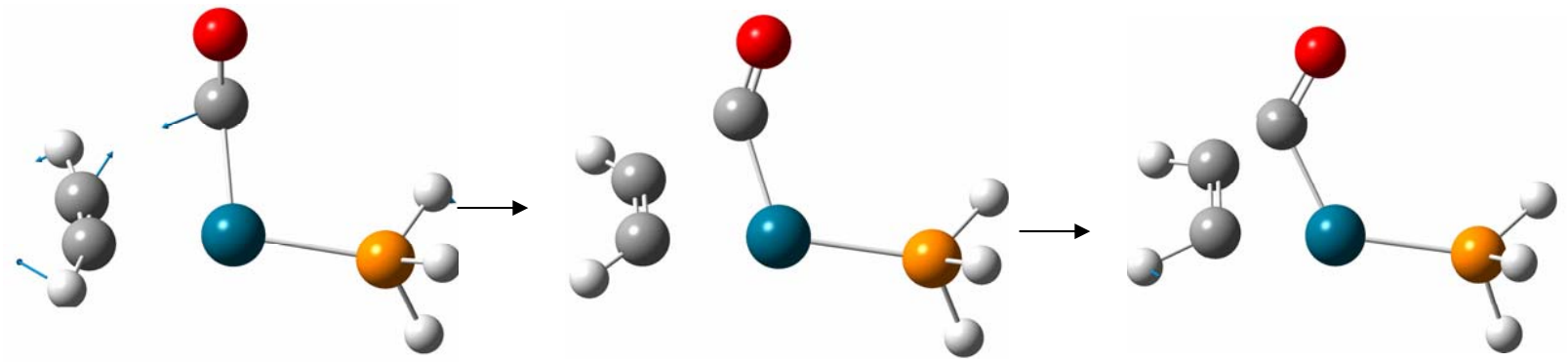

TSB3-A TSB3-B TSB3-C

Figure5.12: Alkyne-group migration transition state (TSB3-B). TSB3-A and TSB3-C are the maximum IR-vector displacement motions of the migration of coordinated alkyne and formation of oxidative-addition as four-membered cycle.

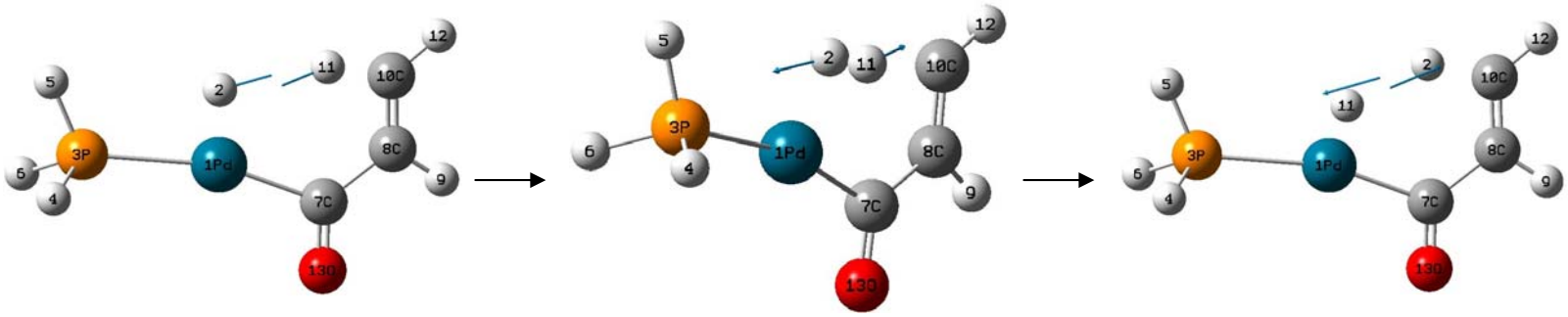

TSB4-A TSB4-B TSB4-C

Figure5.13: Transition state (TSB3-B). TSB3-A and TSB3-C are the maximum IR-vector displacement motions of two hydrogen atoms.

membered metallocyclic intermediate (B4′). It is kinetically more favorable than the formation of B4. The presence of this backside attack reduces the activation energy of the production of oxidative-addition adduct from 55.56 kcal/mol to 12.16 kcal/mol. This fact and the 12.20 kJ/mol stabilization of B4′ compared to B4 add another support the importance of the recoordinated PH_3-ligand via associative mechanism over the process. Step-IV is the addition of hydrogen associated with the opening of the four-membered metallocyclic intermediate B4'. The activation of this step requires higher energy than the corresponding one in cycle A. It also represents the highest energetic step in this cycle. Figure 5.8 shows that the steps IV and IV' in paths B and B' are almost of the same activation energy (42.3 kcal/mol and 44.37 kcal/mol, respectively). These results agree with the previous proposal in cycle A that the PH_3-ligand recoordination within the TSB4' has no influence on its energy barrier. However, the consideration of PH_3-ligand recoordination increases the stability of the intermediate B5' by about 12.96 kcal/mol more than B5. The IR-vector displacements of imaginary vibrational modes of TSB4' present the hydrogen addition process (Figure 5.15). Step-V is the reductive-elimination process that is similar to the proposed one in the cycle A.

The results of cycle A (path A') and cycle B (path B') in Figure 5.16 show that path B' is thermodynamically more stable than cycle A'. However, both cycles have a comparable activation energy in the five proposed steps except the hydrogenation (Step-IV), where path-A' in cycle A is kinetically more favorable.

Table5.6: Relative energies (ΔE) and optimized molecular geometries of stationary points of paths B ' of the π-coordination catalytic route (Cycle B)

Stationary points	Optimized geometry (Å and degree)	ΔE [a] (ν_{Im})[b]
B1		0.0[c]
TSB1	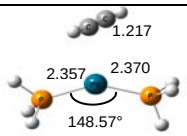	2.72 (-79.07 i)
B2	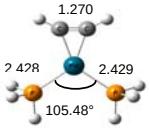	-12.14
TSB2	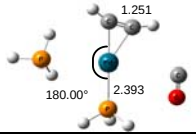	-0.85 (-65.58 i)[d]
B3	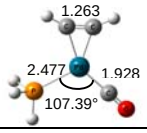	-27.85
TSB3'	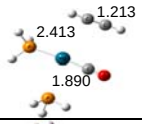	-15.69 (-41.19 i)
B4'	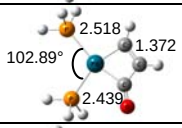	-29.66
TSB4'	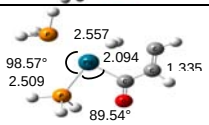	14.69 (-1321.2 i)
B5'	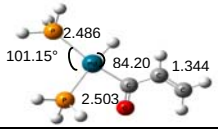	-57.81
TSB5	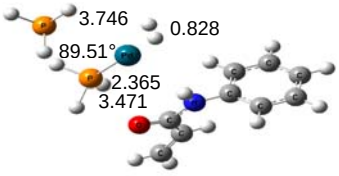	-52.87 (-20.4 i)[d]

[a] Relative energy to the total heat of formation of acetylene and $Pd(PH_3)_2$ in kcal/mol
[b] Imaginary frequency in cm^{-1}
[c] The total heat of formation of acetylene and $Pd(PH_3)_2$ in hartree-fock is -157.02933610 a u
[d] More than an imaginary frequency were observed, the listed value is for the one that present the movement of atoms according to the reaction path.

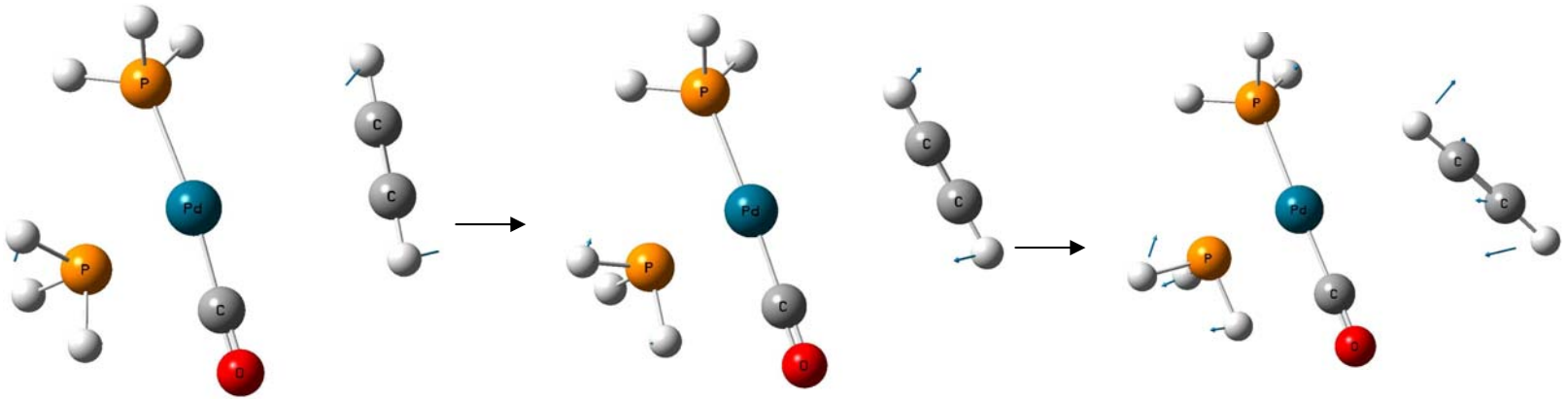

TSB3-A' TSB3-B' TSB3-C'

Figure5.14: Alkyne-group migration transition state (TSB3-B'). TSB3-A' and TSB3-C' are the maximum IR-vector displacement motions of the migration of coordinated alkyne and formation of oxidative-addition as four-membered cycle.

5.2.2 The bidentate ligand

To study of the effect of a bidentate ligand, acetylene and $H_3P(CH_2)_4PH_3$ were computed in place of substituted alkynes and aryl phosphine ligands, respectively, to simplify the calculations of the investigated reaction system. In this part, both proposed cycles will be discussed.

5.2.2.1 Cycle A: Oxidative-Addition Route

The potential energy profiles of this cycle (paths A and A') are illustrated in Figure 5.17. Tables 5.7 and 5.3 report the optimized geometrical parameters of reactants and product respectively.

From the discussion of cycle A, the importance of the phosphine ligand oscillation and the computed results of the bi-dentate ligand, only path A' of cycle A will be considered.

5.2.2.1.1 Path A' of Oxidative Addition Route

As mentioned in cycle A of the mono-dentate ligand, the main difference between the two paths (A and A') is the possibility of decoordination-recoordination of PH_3-ligand in path A'. The optimized molecular geometries of path A' in cycle A are recorded in Table 5.8.

A comparison between the energy profiles of path A' in mono-dentate ligand (Figure 5.1) and path A' in bi-dentate ligand (Figure 5.17) shows that all of the proposed stationary points (ground and transition states) of path A' in bi-dentate ligand are thermodynamically more stable than the corresponding ones in mono-dentate ligand. In addition, kinetically,

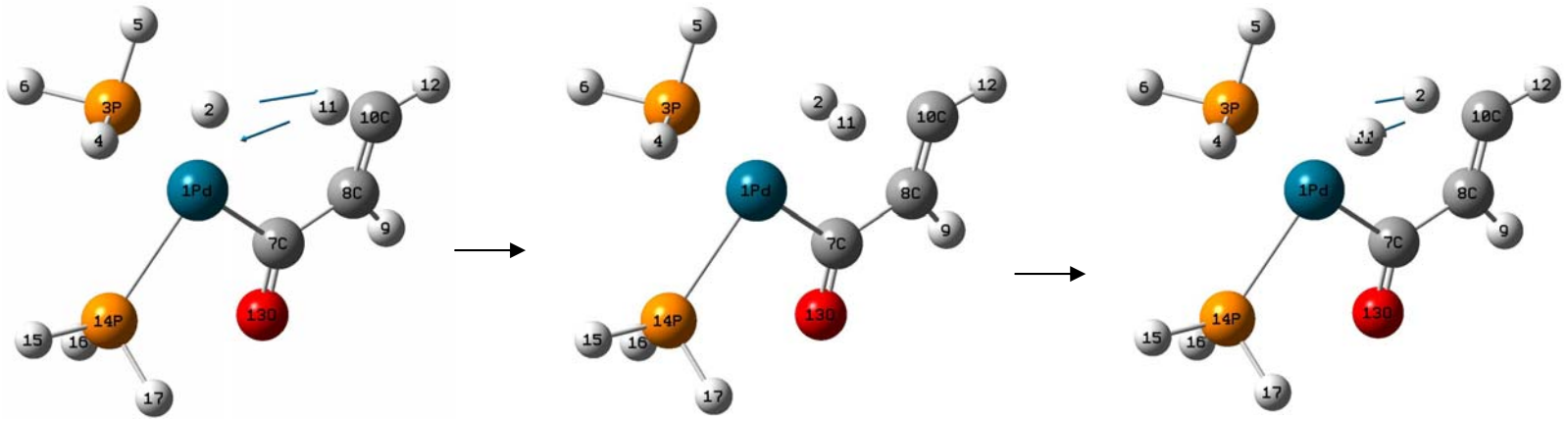

TSB3-A' TSB3-B' TSB3-C'

Figure5.15: Transition state (TSB4-B') of Hydrogen addition. TSB4-A' and TSB4-C' are the maximum IR-vector displacement motions of two hydrogen atoms.

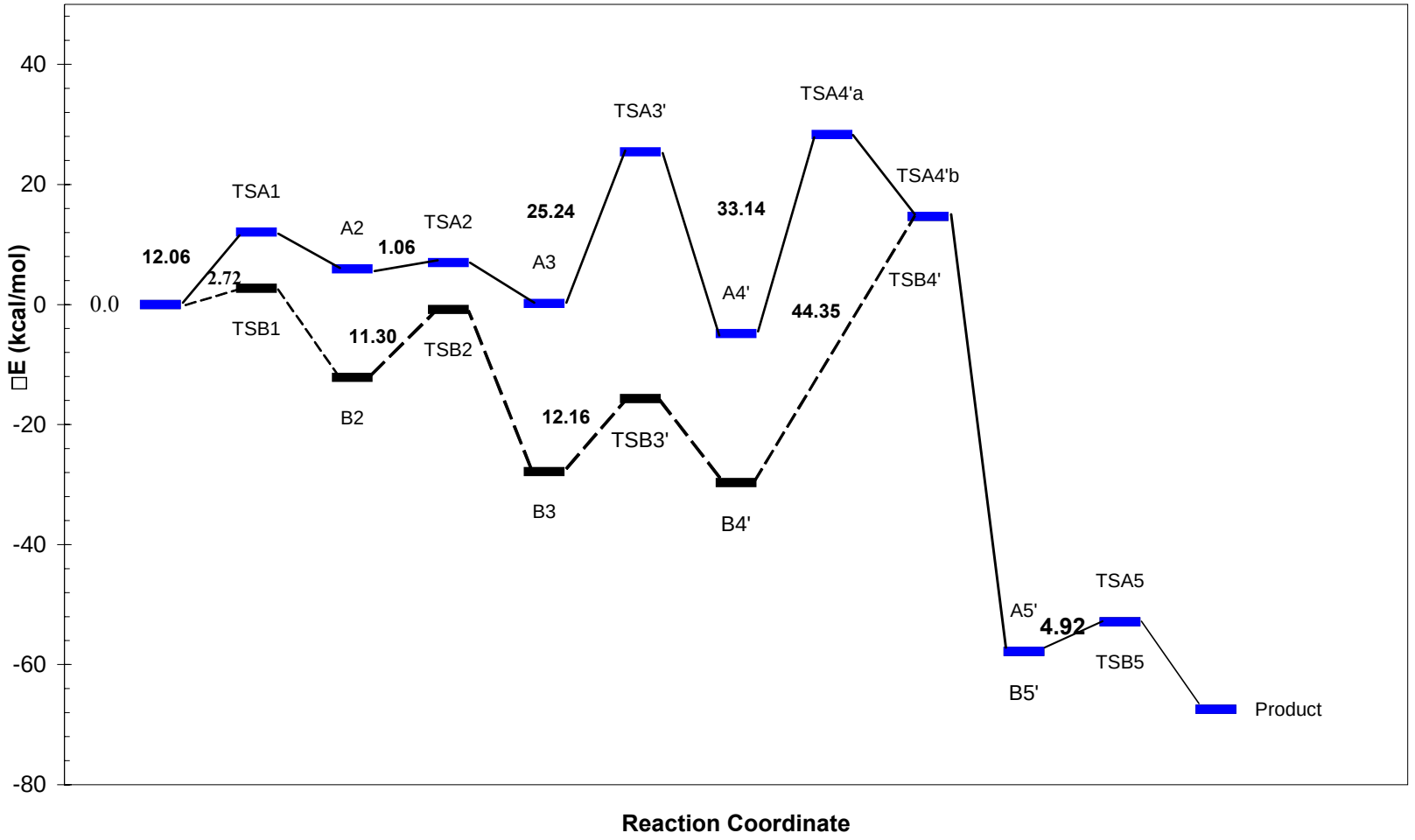

Figure 5.16: Potential energy profiles of mono-dentate ligand for path A' and B' relative to reactants total energy. Upper section of the diagram is of path A' while the lower one is of path B'.

some of the activation energies are lowered. For example, the energy barrier of oxidative addition (step-I) reduces from 12.06 kcal/mol in mono-dentate to 3.55 kcal/mol in bi-dentate ligand. For step-II, there is no significant change in energy barrier. However, the activation energy for step-III in mono-dentate is lower by about 6.67 kcal/mol. The energy barrier of the hydrogenation process (step-IV) is almost the same for both types of ligands. The transition state of step-V is hard to be optimized for the black system of bi-dentate ligand due to hardware limitations.

5.2.2.1.2 Path B' of Π-coordination route

In cycle B, the possibility of decoordination-recoordination of PH_3-ligand is considered for path B'. The potential energy profiles of this cycle (paths B and B') are illustrated in Figure 5.20. Table 5.9 shows the optimized molecular geometries, transition states, imaginary frequency, and their relative energies of path B' compared to reactants-B1.

A comparison between the energy profiles of path B' in mono-dentate ligand (Figure 5.8) and path B' in bi-dentate ligand (Figure 5.20) shows that all of the proposed stationary points (ground and transition states) of path B' in bi-dentate ligand are thermodynamically more stable than the corresponding ones in mono-dentate ligand. On the other hand, some changes are observed in activation energies.

The results of cycle A (path A') and cycle B (path B') of bi-dentate ligand (Figure 5.21) show that path B' is thermodynamically more stable than path A'. However, the activation energies of step-III and step-IV in path B' are higher than the parallel ones in path A'.

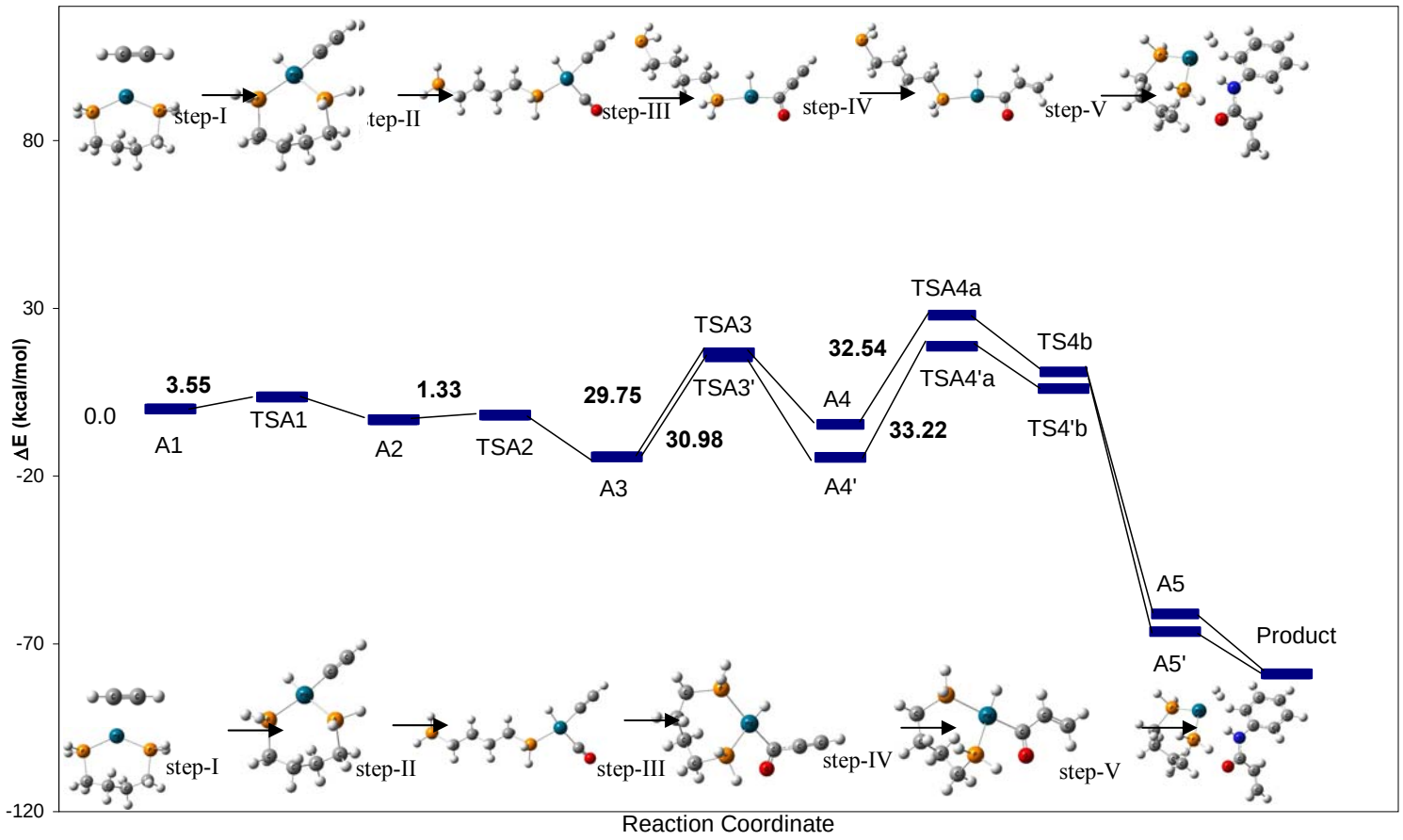

Figure 5.17: Potential energy profiles of cycle A (bi-dentate ligand). Optimized structural formulas and relative activation energy above the diagram are of path A while those below it are of path A'.

Table 5.7 The optimized geometrical parameters of reactant.

Reactants Molecule	Optimized Structural Parameters							
	#	Type	BL-C	BL	BA-C	BA	DA-C	DA
Active complex 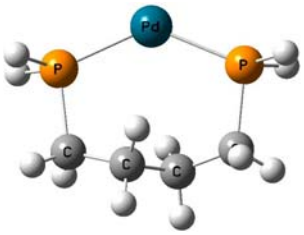 (HF= -170.8455822au)	1	Pd						
	2	P	1	2.353944				
	3	H	2	1.451279	1	121.3825		
	4	H	2	1.451532	1	129.0528	3	129.9285
	5	P	1	2.35394	2	132.458	4	-116.272
	6	H	5	1.451274	1	121.3801	2	113.7363
	7	H	5	1.45154	1	129.0585	2	-116.33
	8	C	2	1.957915	1	107.679	5	1.627945
	9	H	8	1.093379	2	107.5758	1	141.9407
	10	H	8	1.094904	2	107.0288	1	-102.435
	11	C	8	1.543675	2	111.4604	1	19.29335
	12	H	11	1.097647	8	108.8588	2	38.65204
	13	H	11	1.098892	8	108.9469	2	154.306
	14	C	5	1.957933	1	107.6774	2	1.570589
	15	H	14	1.094904	5	107.0277	1	-102.405
	16	H	14	1.093378	5	107.5754	1	141.9702
	17	C	11	1.552105	8	113.9199	2	-83.7199
	18	H	17	1.097646	11	109.3965	8	24.55001
	19	H	17	1.098891	11	109.0373	8	-91.4495

[a] bond length connection (BL-C)
[b] bond length (BL) in (Å)
[c] atoms angle connection (AA-C)
[d] atoms angle (AA) in (degree)
[e] dihedral angle connection (DA-C)
[f] dihedral angle (DA)

Table 5.8: Relative energies (ΔE) and optimized molecular geometries of stationary points of path A' within the oxidative-addition catalytic route (Cycle A) for bi-dentate ligand

Path A'		
Stationary points	Optimized geometry (Å and degree)	ΔE [a] (ν_{Im})[b]
A1	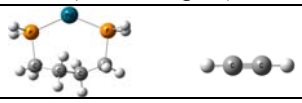	[c]0.0
TSA1		3.55 (-781 .3 i)
A2		-3.24
TSA2		-1.92 (-272.2 i)
A3	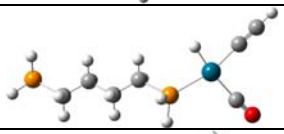	-14.27
TSA3'	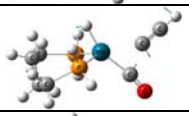	(15.47) (-367.01 i)
A4'	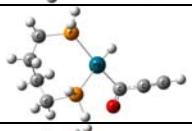	-4.60
TSA4'$_a$	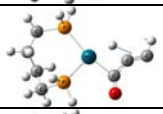	27.94 (-867.25 i)
TSA4'$_b$	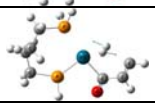	11.02 (-1286.12i)
A5'		-66.34
Activated complex (Prior to product)	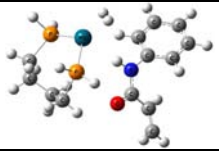	-78.96

[a] Relative energy to the total heat of formation of acetylene and Pd PH_3 $(CH_2)_4$ PH_3 in kcal/mol
[b] Imaginary frequency in cm^{-1}
[c] The total heat of formation of acetylene and Pd PH_3 $(CH_2)_4$ PH_3 in Hartree-Fock is -170.8455822 a u

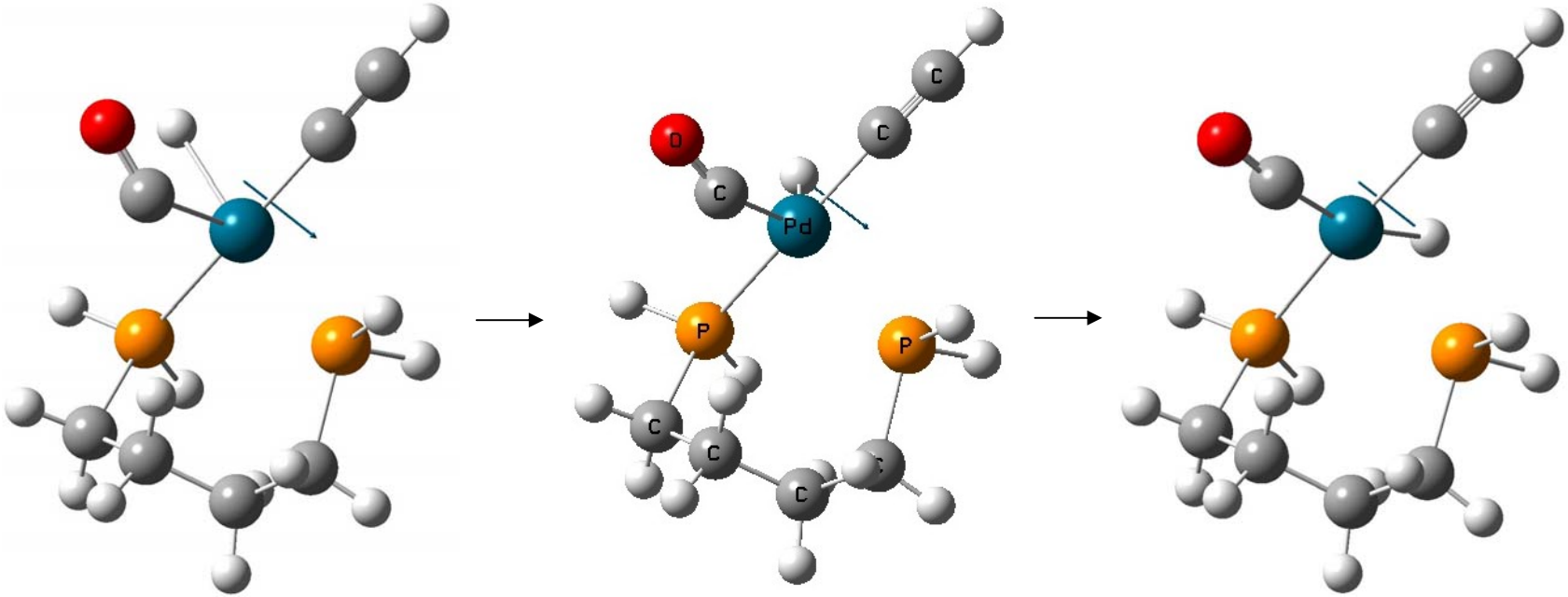

TSA2-A TSA2-B TSA2-C

Figure 5.18: The backside-CO substitution of the coordinated PH_3-group using the IR-vector displacement of the imaginary vibrational mode of TSA2. The illustrations in TSA2-A and TSA2-C show the Hydrogen-vibration due to the approach of CO-group toward palladium-atom and then the go-away of the PH_3-group. TSA2-B is the molecular geometry at the IRC-maximum.

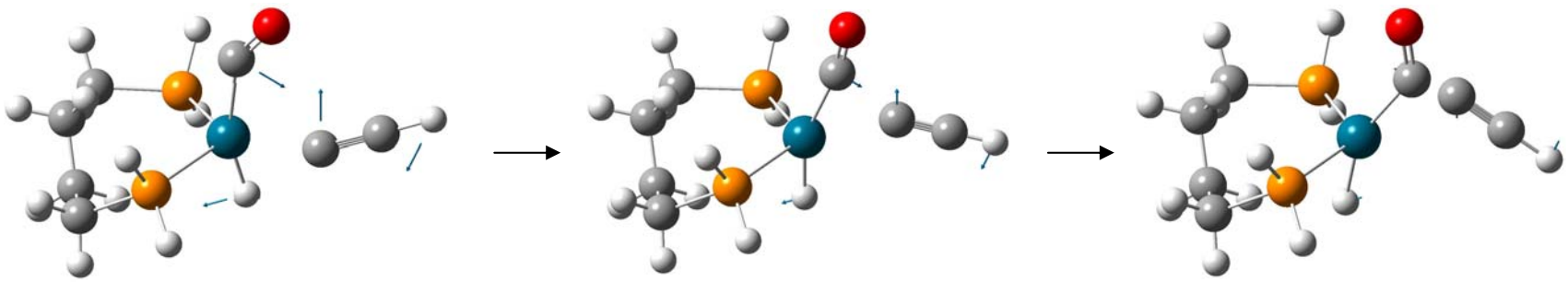

TSA3'-A TSA3'-B TSA3'-C

Figure 5.19: CO-group insertion into the acetynlyl-Pd bond using IR-vector displacement of the imaginary vibrational mode of TSA3'. TSA3'-A to TSA3'-C is the movement of the coordinated CO-group toward the bonded acetynyl. TSA3'-B is the molecular geometry at the IRC-maximum.

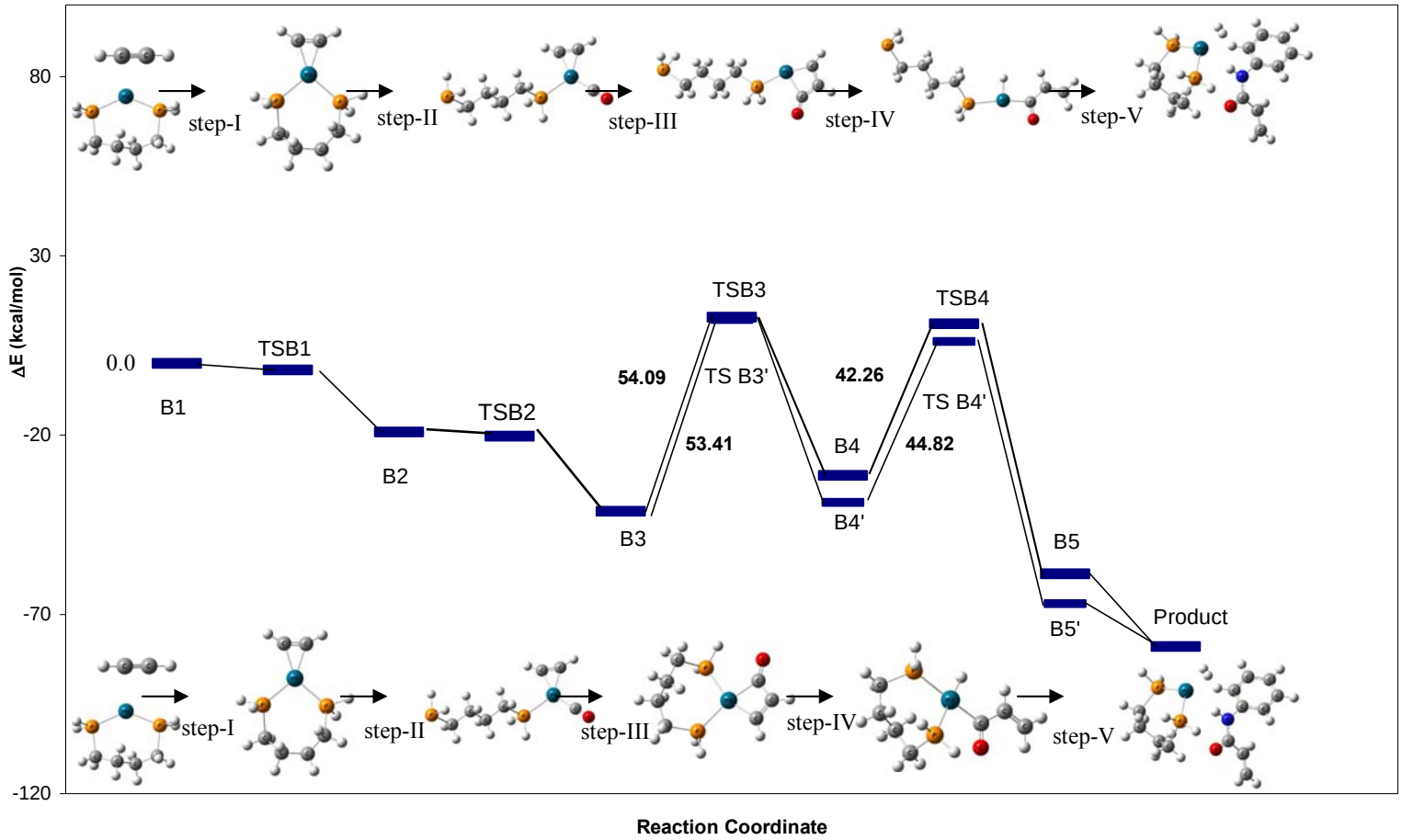

Figure 5.20: Potential energy profiles of cycle B (bi-dentate ligand). Optimized structural formulas and relative energies above the diagram are of path B while those below are of path B'.

Table 5.9: Relative energies (ΔE) and optimized molecular geometries of stationary points of path B ' of the π-coordination catalytic route (Cycle B)

Stationary points	Optimized geometry	ΔE [a] (ν_{Im})[b]
B1	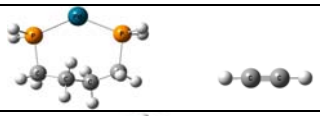	[c]0.0
TSB1	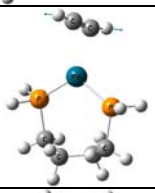	-1.85 (-111.81i)
B2		-19.23
TSB2	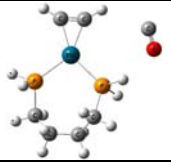	-20.34 (-6.10 i)
B3	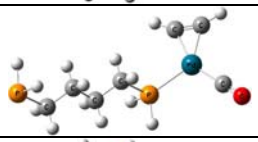	-41.27
TSB3'	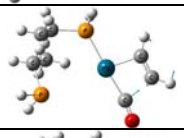	12.82 (-721.81 i)
B4'	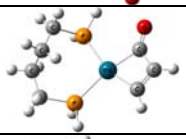	-38.76
TSB4'	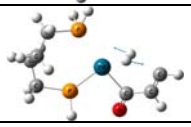	6.05 (-1286.12i)
B5'		-66.34
Activated complex (Prior to product)	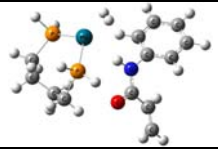	-78.96

[a] Relative energy to the total heat of formation of acetylene and Pd PH_3 $(CH_2)_4$ PH_3 in kcal/mol
[b] Imaginary frequency in cm^{-1}
[c] The total heat of formation of acetylene and Pd PH_3 $(CH_2)_4$ PH_3 in Hartree-Fock is -170.8455822 a u

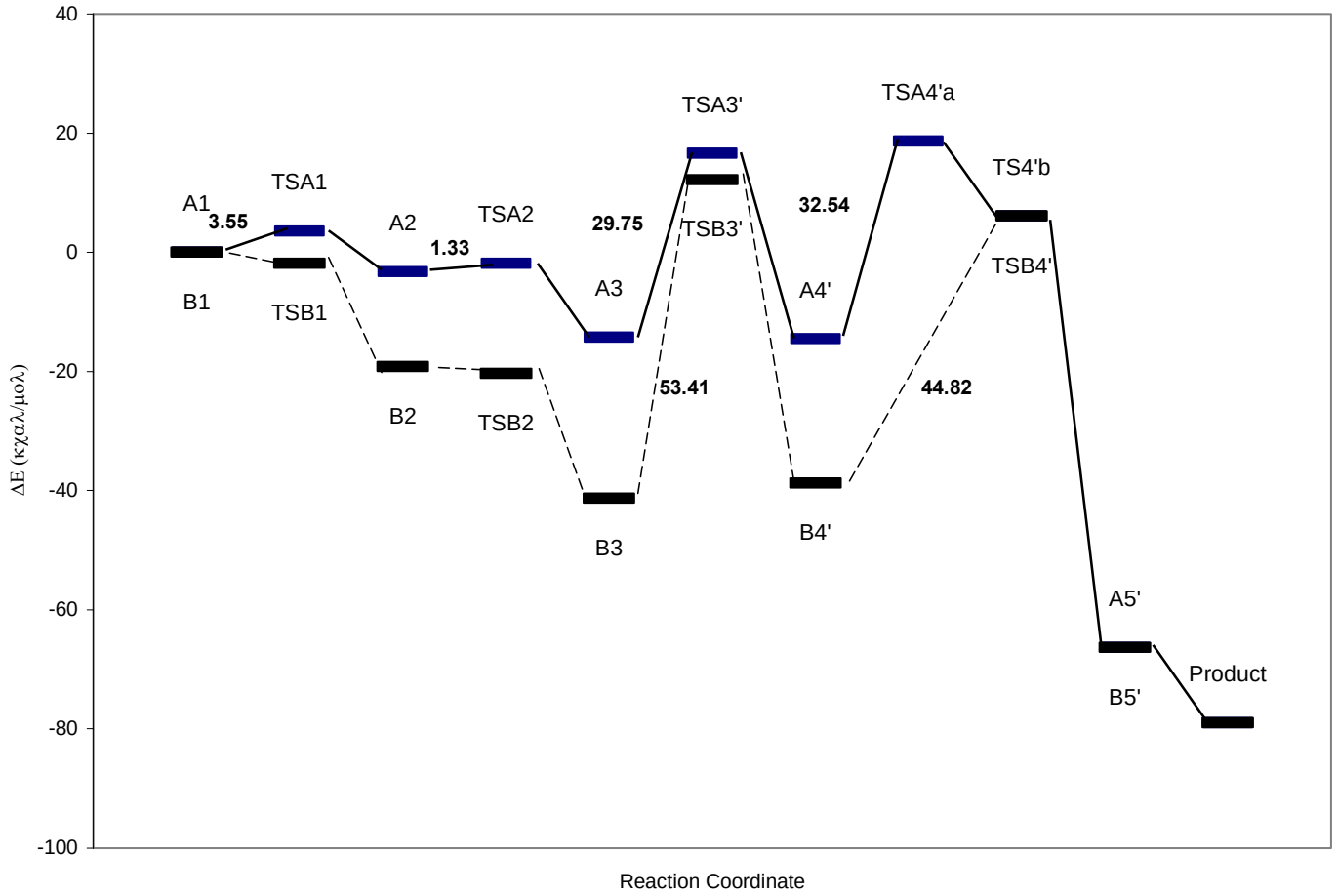

Figure 5.21: Potential energy profiles of bi-dentate ligand for path A' and B' relative to reactants total energy. Upper section of the diagram is of path A' while the lower one is of path B'.

5.3 The Experimental Results

In addition to the recently reported results of the formation of unsaturated amides using palladium catalyst [29], series of experiments were performed to verify the proposed catalytic cycle. The catalytic system, composed of $Pd(OAc)_2$/1,4-bis(diphenylphosphino)butane (dppb)/ CO/H_2 in CH_2Cl_2 as a solvent, was used in the reaction. The speculated cycles were examined by varying the type of substrate. The rate determining step was tested with different hydrogen partial pressure, and amount of aniline.

The analysis of the reaction mixture of different substrates shows a low yield of amides with 2-heptyne (32%) compared to 1-heptyne (90%) after 16 hours of the reaction.

The variation of the hydrogen partial pressure as well as the aniline amount with 1-heptyne shows same distribution of the unsaturated amides (80% is of trans-α,ß-unsaturated amide and 20% of gem-α,ß-unsaturated amide) as proposed earlier [29].

5.3.1 The Test of the Proposed Cycles

The computational studies of the proposed cycles A and B of the reaction of carbonylative addition of acetylene with aniline explain the experimental results obtained from the carbonylative addition of 1-heptyne and aniline. The high yield of Trans unsaturated amide from 1-heptyne as a substrate indicates that the catalytic carbonylation reaction of 1-heptyne proceeds via oxidative-addition route. In Figure 5.21, this conclusion was validated by the observed low activation energies of the cycle A compared to cycle B. The activation energies of step-III and step-IV in path B' are higher than the

corresponding ones in path A'. Therefore, the formation of trans unsaturated amide of 1-heptyne as a major product compared to gem can be explained by a low activation energy of oxidative-addition route (path A') compared to π-coordination route (path B').

Moreover, the low yield of amides with 2-heptyne (32%) compared to 1-heptyne (90%) after 16 hours of the reaction indicates that the oxidative-addition route (path A') is the major path while π-coordination route (path B') is the minor.

5.3.2 The Examination of the Rate Determining Step

The variation of the partial hydrogen pressure from 100 to 500 psi (with fixed CO pressure at 300 psi) shows a linear dependence of the yield of amides. On the other hand, further increase in the hydrogen partial pressure (more than 500 psi) maintains the total yield of the reaction (Figure 5.22).The observed linear dependence of the total yield of the amides with the variation of partial hydrogen pressure indicates that the hydrogenation reaction (step-IV) is the most probably rate determining step of the cycle. That is also consistent with the proposed oxidative-addition cycle which is the main reaction route.

5.3.3 The Independence of Aniline Concentration

Several experiments were performed with increasing of aniline amount from (2-5 mmol). It is observed that the total yield does not affected by the variation of aniline concentration (Figure 5.23). This observation validates the computational results for the proposed cycles where the aniline doesn't play a significant role in the reaction rate. In addition, aniline interaction is considered as a fast step (reductive-elimination step).

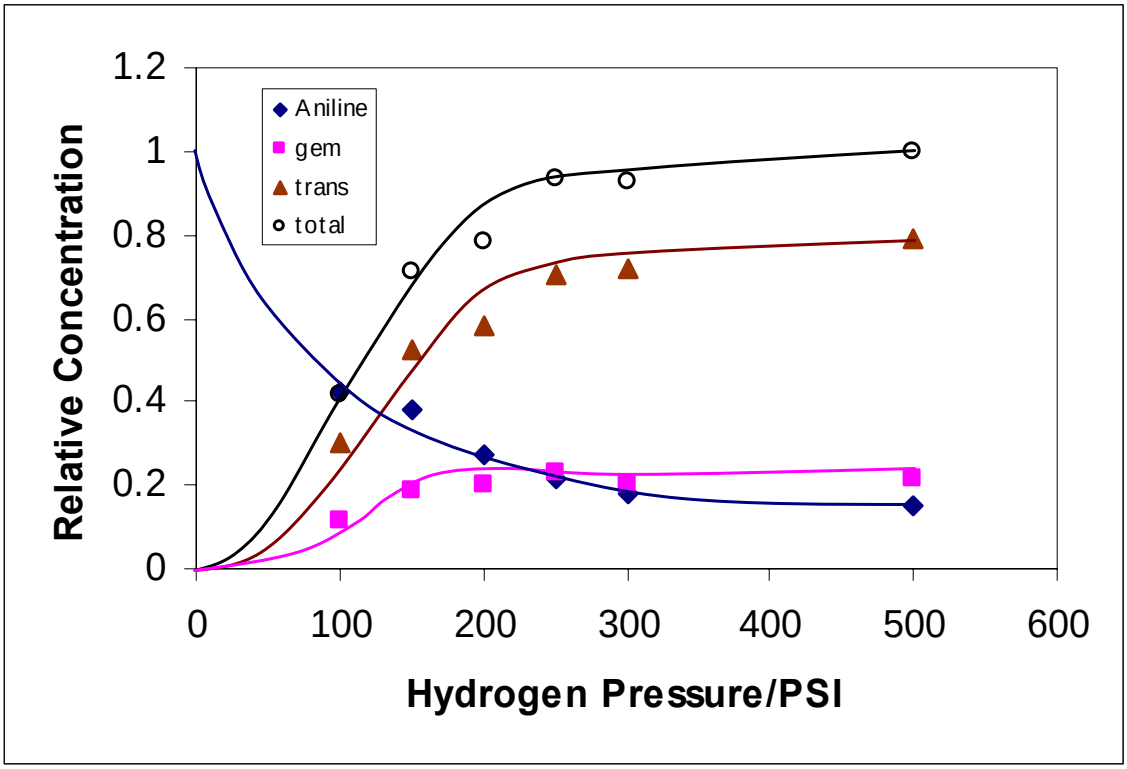

Figure 5.22: Relative concentration changes as a function of hydrogen partial gas pressure

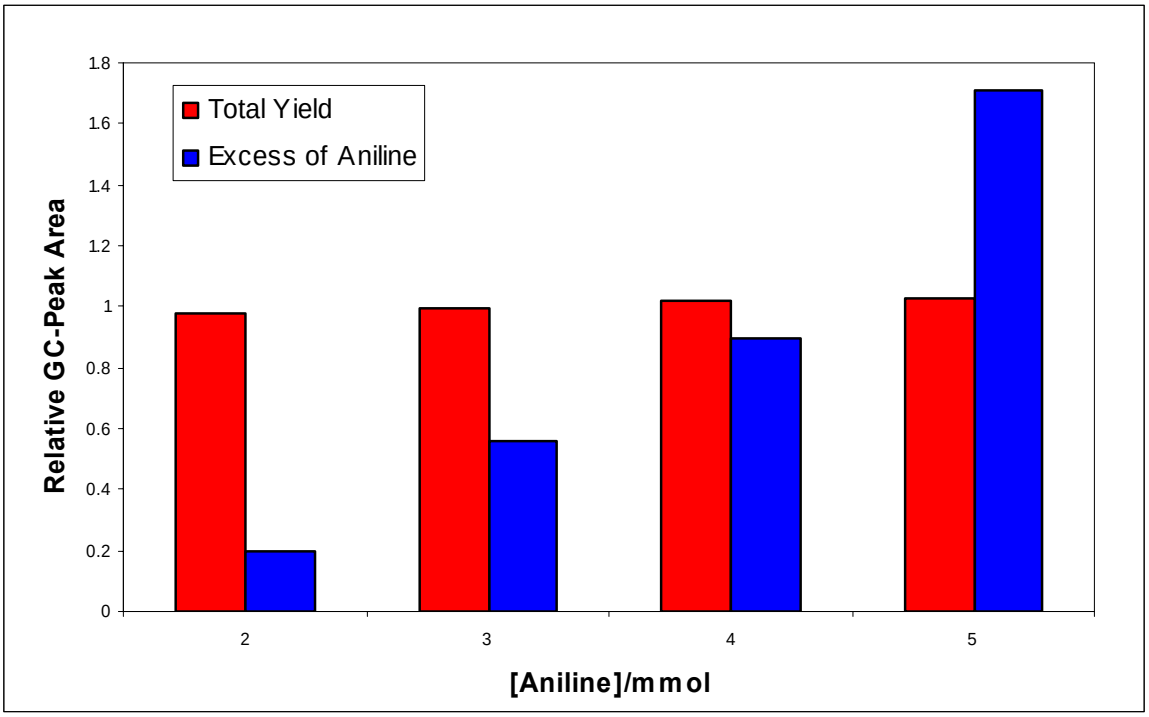

Figure 5.23: Relative concentration changes as a function of aniline concentration.

CHAPTER SIX

CONCLUSION

The density function method at B3LYP was adopted for the palladium systems to test different effective core potential (ECP) basis sets that are available in Gaussian-03 (GW-03) program under MS-Windows. The test includes calculations of geometrical parameters and heat of formation of Pd-acetylene π-complex. The predicted molecular geometries and the relative heat of formation using SDDAll and CEP-121G basis sets are in good agreement with those obtained by the large basis set (BSII). Furthermore, the SDDAll-geometrical parameters of the active complex, $Pd(PH_3)_2$, were found to be the most consistent values with the obtained parameters by accurate basis set calculations, wherein SDD-pseudopotential described the metal and 6-311G* basis that was used for all the other atoms. The results show that variation of the geometrical parameters from SDDAll to large basis sets, never exceed 2%. This reliability, in addition to the short execution time of the SDDAll basis set, makes it the basis set of choice to carry out mechanistic studies of the investigated system. The basis set was further tested with transition state calculations using quadratic synchronous transit (QST2) approach and vibrational frequency calculations of transition states to confirm the imaginary mode of vibration for each transition state. Moreover, intrinsic reaction coordinate (IRC) calculations were implemented on the obtained transition state geometries to examine the reaction path leading down from these transition states.

Two catalytic cycles are proposed for the studied reaction system. These cycles include the most probable mechanistic paths based on oxidative-addition and π-coordination

route. The computed results show that an oxidative-addition mechanism with phosphine ligand coordination/decoordination (path A') is the major pathway of the process using syngas (CO/H_2) and terminal alkyne. Five-steps are proposed to present this catalytic cycle: (I) oxidative-addition of alkyne, (II) substitution reaction of a phosphine ligand by carbon monoxide, (III) migratory insertion of CO ligand into Pd-acetynyl bond accompanied with recoordination of the phosphine ligand, (IV) hydrogenation of propiolyl group and (V) reductive-elimination to produce an unsaturated amide and to regenerate the active Pd(0)-complex. The reaction profile, except step-(I), proceeds via associative mechanism facilitated by a PH_3-ligand. These results indicate that the hydrogenation process (step-IV) is the most probable rate-determining step of the cycle.

A comparison between stationary points of intermediates and transition states in the proposed mechanisms indicates that paths A' and B' are generally more stable than the path A and path B respectively. Thus, the coordination/decoordination of PH_3-ligand facilitates the catalytic process. It also indicates that associative mechanism is the nature of the proposed cycle. The computed results also show a linear correlation between the proposed mechanisms and the region-selectivity where oxidative-addition initiates the process and gives only trans-isomer while π-coordination produces mainly the gem-isomer.

The main difference between mono- and bidentate ligand is the non-linearity of the active complex which facilitates the coordination of the substrate. Thus, this is confirmed by the observed low activation energy of the step-I and step-II in the case of bidentate ligand for both cycles (figure 5.22). Therefore, the coordination process of the bidentate is more

favorable than the mono-dentate ligand. The complexes of bidentate ligand stabilize all stationary points (ground and transition states) of the studied system. Whereas, the activation energies of CO migration (step-III) and/or hydrogenation (step-IV) aren't affected in the cycle A. On the other hand, in the case of cycle B', the bidentate ligand adds extra energy and makes it less favorable comparing to cycle A, since alkyne migration (step-III) needs almost four times the activation energy of the mono-dentate ligand in cycle B'. These results confirm the proposed model of this mechanism to proceed mainly via oxidative addition route.

Several experiments were performed to test the proposed model mechanism and its rate-determining step. The proposed cycles were experimentally tested by using 1-hetyne and 2-heptyne as substrates. The high yield of Trans unsaturated amide from 1-heptyne comparing to 2-heptyne indicates that the catalytic carbonylation reaction of 1-heptyne proceeds probably via an oxidative-addition route. The variations of the partial pressure of hydrogen gas indicate that the hydrogenation reaction (step-IV) is the most likely rate-determining step of the catalytic process. At the experimental conditions, the yield is independent of the aniline concentration. This fact can be explained by the spontaneous reaction of the reductive-elimination step-V of the proposed cycle as shown in the computed results.

APPENDIX

Appendix A- (Mono-dentate ligand)
Reactants

Table A1: The optimized geometrical parameters of reactants (mono-dentate ligand) using B3LYP/SDDAll level.

Structure of Reactants	Optimized Geometrical Parameters							
	#	Type	BL-C	BL	BA-C	BA	DA-C	DA
Active complex 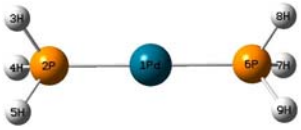 (HF=-144.58105 au)	1	Pd						
	2	P	1	2.34446				
	3	H	2	1.44528	1	120.5949		
	4	H	2	1.445279	1	120.6024	3	120.003
	5	H	2	1.445256	1	120.5951	3	-119.996
	6	P	1	2.344462	2	179.9932	4	18.31535
	7	H	6	1.445279	1	120.602	2	-18.3155
	8	H	6	1.44528	1	120.595	2	101.6872
	9	H	6	1.445255	1	120.5954	2	-138.316
Acetylene 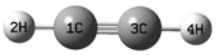 (HF=-12.4482529 au)	1	C						
	2	H	1	1.064425				
	3	C	1	1.212784	2	180		
	4	H	3	1.064425	1	180	2	0
Carbon monoxide 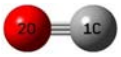 (HF=-21.6600769 au)	1	C						
	2	O	1	1.15217002				
Molecular Hydrogen 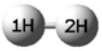 (HF=-1.1744164 au)	1	H						
	2	H	1	0.74347811				
Aniline 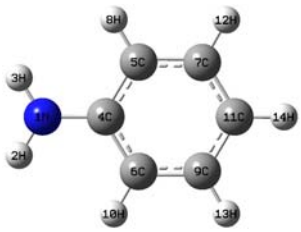 (HF=-48.1304177 au)	1	N						
	2	H	1	1.004622				
	3	H	1	1.004622	2	118.1403		
	4	C	1	1.38671	2	120.9298	3	179.9788
	5	C	4	1.411811	1	120.7187	2	179.9898
	6	C	4	1.411811	1	120.7187	5	-179.958
	7	C	5	1.396546	4	120.4072	1	-179.977
	8	H	5	1.08661	4	119.4962	1	0.019522
	9	C	6	1.396546	4	120.4072	1	179.9772
	10	H	6	1.08661	4	119.4962	1	-0.01952
	11	C	7	1.401026	5	120.8958	4	0.008808
	12	H	7	1.085719	5	119.1469	4	-179.999
	13	H	9	1.085719	6	119.1469	4	179.9988
	14	H	11	1.084275	7	120.5842	5	179.9968

[a] bond length connection, [b] bond length in (Å),[c] atoms angle connection, [d] atoms angle in (degree), [e] dihedral angle connection, and [f] dihedral angle

Appendix A-(Mono-dentate ligand)

Cycle A

Table A2: The optimized geometrical parameters of intermediates in cycle A (path A) using B3LYP/SDDAll level.

Structure of Intermediates	Optimized Geometrical Parameters							
	#	Type	BL-C	BL	BA-C	BA	DA-C	DA
A2 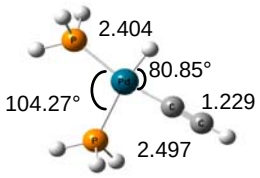 (HF=-157.0198825 au)	1	Pd						
	2	H	1	1.553594				
	3	C	1	1.977494	2	80.85921		
	4	C	3	1.229312	1	178.0645	2	-179.958
	5	H	4	1.065075	3	179.0975	1	-179.941
	6	P	1	2.496621	3	88.10566	4	0.040002
	7	H	6	1.438327	1	114.2578	3	-55.8253
	8	H	6	1.438331	1	114.2584	3	55.82546
	9	H	6	1.448162	1	129.5785	3	179.9997
	10	P	1	2.403766	3	167.624	4	179.9488
	11	H	10	1.44419	1	124.3791	3	-179.947
	12	H	10	1.439229	1	117.2514	3	-57.8839
	13	H	10	1.439223	1	117.2562	3	57.98602
A3 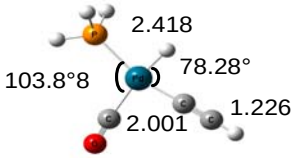 HF=-170.3866174 au)(	1	Pd						
	2	H	1	1.569164				
	3	C	1	1.983529	2	78.27978		
	4	C	3	1.226395	1	178.5669	2	179.1
	5	H	4	1.064983	3	179.9687	1	158.5268
	6	P	1	2.418301	3	163.5963	4	179.0652
	7	H	6	1.439943	1	123.6229	3	-179.961
	8	H	6	1.436344	1	116.6358	3	-57.9563
	9	H	6	1.43635	1	116.6677	3	57.99793
	10	C	1	2.00125	3	92.52166	4	-0.92323
	11	O	10	1.156405	1	173.8157	3	-0.52626
A4 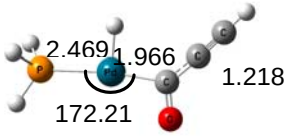 (HF=-170.3717841 au)	1	Pd						
	2	P	1	2.468639				
	3	H	2	1.439506	1	116.6435		
	4	H	2	1.443808	1	125.4056	3	122.5274
	5	H	2	1.439506	1	116.6557	4	122.5417
	6	H	1	1.552237	2	94.74349	5	-57.4719
	7	C	1	1.965659	2	172.2148	5	122.5784
	8	C	7	1.423731	1	132.8192	2	179.9479
	9	C	7	2.64053	1	131.5036	2	179.9579
	10	H	7	3.704574	1	130.9775	2	179.9581
	11	O	7	1.260851	1	103.019	2	-0.04988
A5 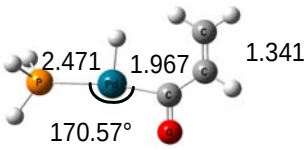 (HF=-171.6365568 au)	1	Pd						
	2	C	1	1.966836				
	3	O	2	1.258091	1	100.8167		
	4	H	1	1.560731	2	93.96995	3	-179.996
	5	P	1	2.471051	2	170.5727	3	0.116613
	6	H	5	1.44045	1	116.825	2	122.5645
	7	H	5	1.444724	1	125.7008	2	-0.01015
	8	H	5	1.440473	1	116.8397	2	-122.602
	9	C	2	1.468693	1	136.6471	5	-179.881
	10	C	9	1.341241	2	122.7403	1	-0.00807
	11	H	10	1.084657	9	121.6199	2	-179.997
	12	H	10	1.086022	9	120.5756	2	0.001434
	13	H	9	1.088143	2	115.6289	1	179.9948

[a] bond length connection, [b] bond length in (Å),[c] atoms angle connection, [d] atoms angle in (degree), [e] dihedral angle connection, and [f] dihedral angle

Table A3: The optimized geometrical parameters of transition states in cycle A (path A) using B3LYP/SDDAll level.

Structure of Transition States	Optimized Geometrical Parameters							
	#	Type	BL-C	BL	BA-C	BA	DA-C	DA
TSA1 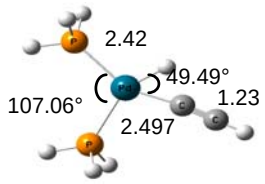 (HF=-157.0101215 au)	1	Pd						
	2	H	1	1.603004				
	3	P	1	2.496593	2	149.6435		
	4	H	3	1.450381	1	131.061	2	179.9943
	5	H	3	1.442915	1	114.7344	2	55.44306
	6	P	1	2.422632	3	107.059	5	-124.559
	7	H	6	1.447109	1	124.998	3	0.015868
	8	H	6	1.442785	1	118.1106	3	122.0502
	9	C	1	1.996886	6	152.7919	3	-179.998
	10	C	9	1.230118	1	173.2142	6	179.9839
	11	H	10	1.065037	9	179.073	1	0.062292
	12	H	3	1.442916	1	114.734	9	-55.4583
	13	H	6	1.442786	1	118.1122	9	57.98164
TSA2 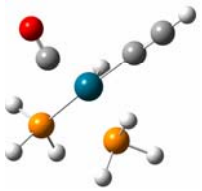 HF=-178.6782707 au)(	1	Pd						
	2	P	1	2.431293				
	3	H	2	1.441682	1	122.3724		
	4	H	2	1.438073	1	118.3453	3	121.8385
	5	H	2	1.438346	1	117.5666	4	117.269
	6	C	1	2.18	2	98.7582	4	68.62881
	7	O	6	1.164031	1	142.5032	2	-101.102
	8	H	1	3.505993	6	80.92501	7	137.9827
	9	P	1	2.746864	6	95.28465	7	155.7574
	10	H	9	1.444158	1	112.0394	6	-156.829
	11	H	9	1.454018	1	138.418	6	74.40526
	12	C	1	1.980668	6	94.8824	7	68.09747
	13	C	12	1.227347	1	178.2209	6	80.82639
	14	H	13	1.064933	12	179.3715	1	-69.5345
	15	H	1	1.549786	12	76.13925	13	-156.504
TSA3 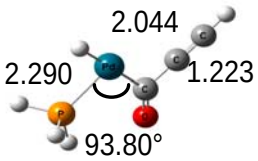 (HF=-170.3376303 au)	1	Pd						
	2	H	1	1.656519				
	3	P	1	2.289902	2	86.2009		
	4	H	3	1.433644	1	117.2046	2	57.71237
	5	H	3	1.438072	1	116.985	2	178.5148
	6	H	3	1.433863	1	116.9726	2	-60.9872
	7	C	1	2.629696	3	127.1555	6	118.4421
	8	C	7	1.22313	1	129.3861	3	-178.759
	9	H	8	1.065663	7	177.7889	1	4.461494
	10	C	7	1.45412	1	50.61293	3	1.066953
	11	O	10	1.243034	7	125.6274	1	179.8565
$TSA4_a$ 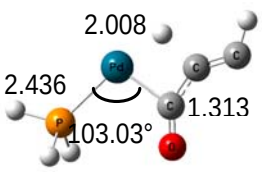	1	Pd						
	2	H	1	1.733834				
	3	P	1	2.436205	2	172.039		
	4	H	3	1.440102	1	122.7045	2	177.2029
	5	H	3	1.437022	1	117.1159	2	-60.9961
	6	H	3	1.436954	1	116.9166	2	55.60369
	7	C	1	2.007896	3	103.0326	6	58.16098
	8	C	7	1.392084	1	91.87878	3	-179.94

(HF=-170.3196633 au)	9	C	8	1.313389	7	142.6211	1	-179.31
	10	H	9	1.089483	8	124.2275	7	179.5409
	11	O	7	1.21993	1	125.8511	3	0.108122
TSA4$_b$ 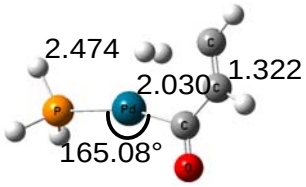 (HF=-171.5217115 au)	1	Pd						
	2	H	1	1.830297				
	3	P	1	2.474077	2	117.1272		
	4	H	3	1.441989	1	120.0343	2	-134.536
	5	H	3	1.441198	1	119.9578	2	-14.5301
	6	H	3	1.44199	1	120.0399	2	105.4808
	7	C	1	2.02964	3	165.079	5	-179.891
	8	C	7	1.520069	1	122.1353	3	179.9904
	9	H	8	1.088696	7	110.0346	1	-179.997
	10	C	8	1.322307	7	123.9269	1	0.001545
	11	H	10	2.087537	8	92.15746	7	11.37868
	12	H	10	1.08764	8	126.4333	7	-179.999
	13	O	7	1.229237	1	111.3917	3	-0.00743
TSA5 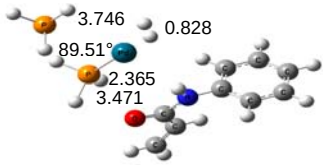 (HF=-228.0785029 au)	1	Pd						
	2	C	1	3.471408				
	3	C	2	1.487211	1	102.6882		
	4	O	2	1.259385	1	81.99644	3	-121.742
	5	C	3	1.33985	2	121.0923	1	-94.6379
	6	H	5	1.084634	3	121.4566	2	-179.129
	7	H	3	1.084125	2	117.9618	1	86.41079
	8	P	1	2.364908	2	94.94024	4	-71.9157
	9	H	8	1.441635	1	119.099	2	153.6923
	10	H	8	1.444563	1	123.1143	2	-84.3591
	11	H	8	1.443131	1	118.0614	2	36.41381
	12	H	5	1.085072	3	120.6222	2	0.388542
	13	H	1	1.761989	8	152.8456	4	-179.569
	14	H	2	2.015004	1	80.87502	8	-165.839
	15	N	2	1.380469	1	86.58618	8	167.1641
	16	H	15	3.27799	2	99.26901	1	6.93294
	17	H	1	3.945409	8	90.00157	4	-81.7107
	18	P	1	3.745633	8	89.51143	4	-103.311
	19	H	18	1.454697	1	86.80682	8	-175.053
	20	H	18	1.462631	1	178.498	8	-50.7636
	21	C	15	1.440971	2	128.1301	1	-98.9919
	22	C	21	1.402409	15	119.4892	2	-106.549
	23	C	21	1.403157	15	120.4434	2	74.99198
	24	C	22	1.399596	21	119.9195	15	-178.28
	25	H	22	1.084589	21	119.2484	15	1.880283
	26	C	23	1.399561	21	119.7889	15	178.8414
	27	H	23	1.085721	21	119.146	15	-1.01271
	28	C	24	1.400439	22	120.1172	21	-0.51277
	29	H	24	1.08472	22	119.7525	21	179.8495
	30	H	26	1.084791	23	119.6329	21	179.8511
	31	H	28	1.084702	24	120.0439	22	-179.792

[a] bond length connection, [b] bond length in (Å),[c] atoms angle connection, [d] atoms angle in (degree), [e] dihedral angle connection, and [f] dihedral angle

Table A4: The optimized geometrical parameters of intermediates and transition states in cycle A (path A') using B3LYP/SDDAll level.

Structure of Intermediates and Transition States	Optimized geometrical Parameters							
	#	Type	BL-C	BL	BA-C	BA	DA-C	DA
TSA3' 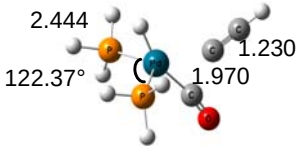 (HF=-178.648906 au)	1	Pd						
	2	P	1	2.44369				
	3	H	2	1.441494	1	117.5622		
	4	H	2	1.441788	1	118.3536	3	116.1734
	5	H	2	1.444997	1	123.9354	3	-121.505
	6	C	1	2.224896	2	118.6335	5	-78.5326
	7	C	6	1.229537	1	151.9107	2	-93.69
	8	H	6	3.097344	1	29.81464	2	-93.5739
	9	H	7	1.066112	6	179.3995	1	179.9328
	10	C	1	1.970493	6	50.59913	7	179.9386
	11	O	10	1.195064	1	168.9314	6	179.4576
	12	H	1	3.464335	10	86.7923	11	-57.2624
	13	P	1	2.443673	10	105.192	11	-65.7978
	14	H	13	1.441482	1	117.5529	10	-96.1361
	15	H	13	1.441802	1	118.3682	10	147.6843
A4' 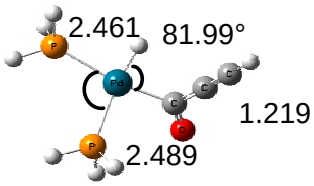 HF=-178.6970982 au)(	1	Pd						
	2	P	1	2.461089				
	3	H	2	1.440257	1	115.8205		
	4	H	2	1.448318	1	127.961	3	123.4682
	5	H	2	1.440487	1	115.6943	3	-113.178
	6	H	1	1.58196	2	85.9944	5	-58.747
	7	C	1	2.0227	2	167.887	5	-66.0156
	8	C	7	1.443603	1	117.8066	2	70.37702
	9	C	8	1.218688	7	177.425	1	14.4147
	10	H	9	1.064193	8	179.5098	7	-73.5363
	11	O	7	1.254953	1	121.1548	2	-113.374
	12	P	1	2.489238	7	89.5074	11	56.75006
	13	H	12	1.438404	1	113.3306	7	-66.8195
	14	H	12	1.439725	1	118.2232	7	46.65143
	15	H	12	1.444016	1	126.6757	7	172.3956
TSA4'$_a$ 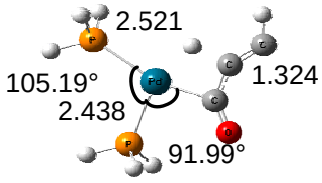 (HF=-178.6442939 au)	1	Pd						
	2	P	1	2.520604				
	3	H	2	1.442382	1	116.6557		
	4	H	2	1.447333	1	127.1327	3	123.0497
	5	H	2	1.442389	1	116.6454	3	-113.913
	6	H	1	1.763599	2	96.41973	5	-57.0597
	7	C	1	2.042869	2	162.8175	5	-57.0084
	8	C	7	1.392027	1	91.38367	2	-0.06656
	9	C	8	1.324451	7	144.0017	1	-179.981
	10	H	9	1.093897	8	121.7222	7	179.9846
	11	O	7	1.235032	1	130.1098	2	179.925
	12	P	1	2.438189	7	91.98986	11	-0.02951
	13	H	12	1.436733	1	114.7514	7	-56.2262
	14	H	12	1.436767	1	114.7849	7	56.52942
	15	H	12	1.443469	1	127.1101	7	-179.838

TSA4'$_b$ 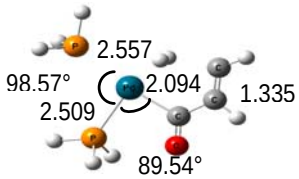 (HF=-179.8404216 au)	1	Pd						
	2	H	1	1.811778				
	3	P	1	2.55702	2	95.11643		
	4	H	3	1.446229	1	120.5423	2	-133.734
	5	H	3	1.444459	1	120.7113	2	-13.4987
	6	H	3	1.446212	1	120.4195	2	106.612
	7	C	1	2.093943	3	171.8901	5	-1.03371
	8	C	7	1.509238	1	118.7811	3	0.748986
	9	H	8	1.090701	7	109.1765	1	179.9925
	10	C	8	1.334915	7	125.8653	1	-0.00786
	11	H	10	2.054105	8	91.52056	7	11.51314
	12	H	10	1.092819	8	121.426	7	-179.999
	13	O	7	1.24048	1	118.4952	3	-179.237
	14	P	1	2.508884	7	89.53896	13	0.176157
	15	H	14	1.448508	1	128.7569	7	179.8661
	16	H	14	1.436721	1	114.3338	7	-56.0892
	17	H	14	1.436693	1	114.3289	7	55.81402
A5' 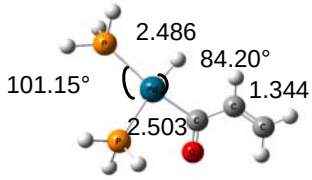 (HF=-179.9559566 au)	1	Pd						
	2	P	1	2.486072				
	3	H	2	1.441509	1	115.3		
	4	H	2	1.449785	1	129.4294	3	123.9412
	5	H	2	1.441621	1	115.3078	3	-112.095
	6	H	1	1.580831	2	85.2915	3	55.50838
	7	C	1	2.025428	2	169.2071	3	42.18627
	8	C	7	1.496371	1	121.7613	2	50.84465
	9	C	8	1.343567	7	122.7612	1	173.2824
	10	O	7	1.255233	1	118.0469	2	-131.241
	11	P	1	2.502593	7	89.31005	10	34.67513
	12	H	11	1.438376	1	114.5373	7	-75.0272
	13	H	11	1.437207	1	116.8929	7	38.47075
	14	H	11	1.446161	1	126.7716	7	163.1687
	15	H	8	1.083795	7	115.6241	1	-6.07714
	16	H	9	1.085257	8	121.004	7	0.669533
	17	H	9	1.085347	8	121.4945	7	-179.608

[a] bond length connection, [b] bond length in (Å),[c] atoms angle connection, [d] atoms angle in (degree), [e] dihedral angle connection, and [f] dihedral angle

Appendix A-(Mono-dentate ligand)
Cycle B

Table A5: The optimized geometrical parameters of intermediates in cycle B (path B) using B3LYP/SDDAll level.

Structure of Intermediates	Optimized Geometrical Parameters							
	#	Type	BL-C[a]	BL[b]	BA-C[c]	BA[d]	DA-C[e]	DA[f]
B2 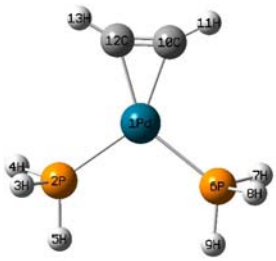 (HF= -157.04869 au)	1	Pd						
	2	P	1	2.428415				
	3	H	2	1.44759	1	119.2343		
	4	H	2	1.447283	1	119.5581	3	116.9876
	5	H	2	1.451449	1	124.4713	3	-121.328
	6	P	1	2.428682	2	105.4789	5	-5.45346
	7	H	6	1.447283	1	119.48	2	126.8581
	8	H	6	1.447559	1	119.218	2	-116.232
	9	H	6	1.451484	1	124.5612	2	5.169401
	10	C	1	2.109136	2	144.837	6	-179.753
	11	H	10	1.073365	1	136.0783	2	179.9056
	12	C	10	1.269687	1	72.48826	2	-0.16858
	13	H	12	1.073365	10	151.4301	1	-179.916
B3 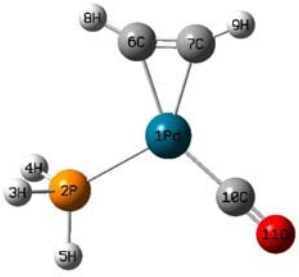 (HF=-170.4312638 au)	1	Pd						
	2	P	1	2.477365				
	3	H	2	1.444104	1	119.4087		
	4	H	2	1.444108	1	119.3878	3	118.1207
	5	H	2	1.443918	1	122.3634	4	120.9282
	6	C	1	2.142399	2	102.8338	4	59.15786
	7	C	6	1.263399	1	72.17094	2	-179.998
	8	H	6	1.072289	1	135.5932	7	-179.989
	9	H	7	1.071347	6	155.1475	1	179.9958
	10	C	1	1.928238	6	149.7784	7	-0.04606
	11	O	10	1.168829	1	179.2873	6	-175.223
B4 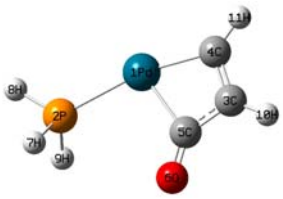 (HF=-170.414714 au)	1	Pd						
	2	P	1	2.442001				
	3	C	1	2.594448	2	135.4898		
	4	C	3	1.375073	1	51.42031	2	179.9916
	5	C	3	1.441979	1	51.77386	4	179.9882
	6	O	5	1.224543	3	138.6397	1	-179.995
	7	H	2	1.438217	1	117.1893	4	58.12691
	8	H	2	1.441614	1	123.4852	4	-179.919
	9	H	2	1.438264	1	117.1627	4	-58.0001
	10	H	3	1.090562	1	176.9667	4	179.9525
	11	H	4	1.08995	3	123.6101	1	180

B5  (HF=-171.6327904 au)	1	Pd						
	2	C	1	1.961056				
	3	O	2	1.257742	1	102.507		
	4	H	1	1.560868	2	92.20649	3	-179.986
	5	P	1	2.481016	2	171.3671	3	-0.01756
	6	H	5	1.440524	1	116.7079	2	122.7041
	7	H	5	1.445007	1	125.9888	2	0.006809
	8	H	5	1.440523	1	116.7047	2	-122.687
	9	C	2	1.476636	1	133.5044	5	-179.994
	11	C	9	1.344206	2	122.7513	1	179.9869
	12	H	10	1.084958	9	121.3967	2	179.9985
	13	H	10	1.085275	9	121.2088	2	-0.00113
[a] bond length connection, [b] bond length in (Å),[c] atoms angle connection, [d] atoms angle in (degree), [e] dihedral angle connection, and [f] dihedral angle								

Table A6: The optimized geometrical parameters of transition states in cycle B (path B) using B3LYP/SDDAll level

Structure of Transition States	Optimized Geometrical Parameters							
	#	Type	BL-C[a]	BL[b]	BA-C[c]	BA[d]	DA-C[e]	DA[f]
TSB1 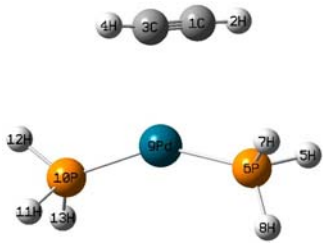 (HF=-157.0250031 au)	1	C						
	2	H	1	1.064125				
	3	C	1	1.217445	2	178.3589		
	4	H	3	1.064345	1	173.7981	2	-173.337
	5	H	1	4.137311	3	108.7587	4	147.5904
	6	P	1	4.036127	3	88.4723	4	149.9502
	7	H	6	1.450014	1	98.92965	3	-79.1174
	8	H	6	1.448387	1	165.5647	3	99.55757
	9	Pd	6	2.369973	1	49.0068	3	42.66678
	10	P	9	2.356605	6	148.5973	1	172.0713
	11	H	10	1.448551	9	120.8086	6	46.81458
	12	H	10	1.454575	9	124.9237	6	169.7832
	13	H	10	1.448281	9	118.2645	6	-70.1221
TSB2  (HF=-178.6907612 au)	1	Pd						
	2	P	1	2.393381				
	3	H	2	1.445059	1	120.9641		
	4	H	2	1.441259	1	121.4236	3	121.5895
	5	H	2	1.443192	1	118.1619	4	119.7237
	6	C	1	2.148678	2	146.012	5	176.9239
	7	C	6	1.250946	1	72.23519	2	-180
	8	H	6	1.071039	1	126.6314	7	179.9315
	9	H	7	1.070364	6	158.1486	1	178.3555
	10	C	1	3.686044	7	102.1248	6	0.301881
	11	O	1	4.042217	6	84.46773	7	179.337
	12	H	2	3.82002	1	67.90834	10	-119.964
	13	P	2	4.1903	1	55.75283	10	-138.426
	14	H	13	1.452024	2	114.4781	1	38.65548
	15	H	13	1.461705	2	145.4163	1	-178.741
TSB3 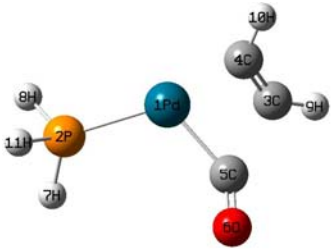 (HF=-170.3427277 au)	1	Pd						
	2	P	1	2.346515				
	3	C	1	2.291909	2	165.5309		
	4	C	3	1.307366	1	72.0097	2	-138.238
	5	C	3	1.859942	1	55.92328	4	140.7701
	6	O	5	1.188988	3	135.686	1	-147.697
	7	H	2	1.441679	1	121.0047	5	-23.2247
	8	H	2	1.440711	1	117.7384	5	-142.981
	9	H	3	1.081369	1	133.5726	5	73.68233
	10	H	4	1.084214	3	128.4137	1	-153.267
	11	H	2	1.440666	1	119.8028	5	98.26168

TSB4 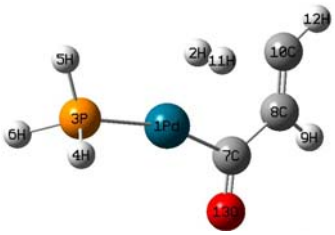 (HF=-171.5217115 au)	1	Pd						
	2	H	1	1.830297				
	3	P	1	2.474077	2	117.1272		
	4	H	3	1.441989	1	120.0343	2	-134.536
	5	H	3	1.441198	1	119.9578	2	-14.5301
	6	H	3	1.44199	1	120.0399	2	105.4808
	7	C	1	2.02964	3	165.079	5	-179.891
	8	C	7	1.520069	1	122.1353	3	179.9904
	9	H	8	1.088696	7	110.0346	1	-179.997
	10	C	8	1.322307	7	123.9269	1	0.001545
	11	H	10	2.087537	8	92.15746	7	11.37868
	12	H	10	1.08764	8	126.4333	7	-179.999
	13	O	7	1.229237	1	111.3917	3	-0.00743
TSB5 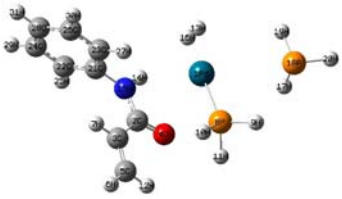 (HF=-228.0785029 au)	1	Pd						
	2	C	1	3.471408				
	3	C	2	1.487211	1	102.6882		
	4	O	2	1.259385	1	81.99644	3	-121.742
	5	C	3	1.33985	2	121.0923	1	-94.6379
	6	H	5	1.084634	3	121.4566	2	-179.129
	7	H	3	1.084125	2	117.9618	1	86.41079
	8	P	1	2.364908	2	94.94024	4	-71.9157
	9	H	8	1.441635	1	119.099	2	153.6923
	10	H	8	1.444563	1	123.1143	2	-84.3591
	11	H	8	1.443131	1	118.0614	2	36.41381
	12	H	5	1.085072	3	120.6222	2	0.388542
	13	H	1	1.761989	8	152.8456	4	-179.569
	14	H	2	2.015004	1	80.87502	8	-165.839
	15	N	2	1.380469	1	86.58618	8	167.1641
	16	H	15	3.27799	2	99.26901	1	6.93294
	17	H	1	3.945409	8	90.00157	4	-81.7107
	18	P	1	3.745633	8	89.51143	4	-103.311
	19	H	18	1.454697	1	86.80682	8	-175.053
	20	H	18	1.462631	1	178.498	8	-50.7636
	21	C	15	1.440971	2	128.1301	1	-98.9919
	22	C	21	1.402409	15	119.4892	2	-106.549
	23	C	21	1.403157	15	120.4434	2	74.99198
	24	C	22	1.399596	21	119.9195	15	-178.28
	25	H	22	1.084589	21	119.2484	15	1.880283
	26	C	23	1.399561	21	119.7889	15	178.8414
	27	H	23	1.085721	21	119.146	15	-1.01271
	28	C	24	1.400439	22	120.1172	21	-0.51277
	29	H	24	1.08472	22	119.7525	21	179.8495
	30	H	26	1.084791	23	119.6329	21	179.8511
	31	H	28	1.084702	24	120.0439	22	-179.792

[a] bond length connection, [b] bond length in (Å),[c] atoms angle connection, [d] atoms angle in (degree), [e] dihedral angle connection, and [f] dihedral angle

Table A7: The optimized geometrical parameters of intermediates in cycle B (path B') using B3LYP/SDDAll level

Structure of Intermediates	Optimized Geometrical Parameters							
	#	Type	BL-C[a]	BL[b]	BA-C[c]	BA[d]	DA-C[e]	DA[f]
B2 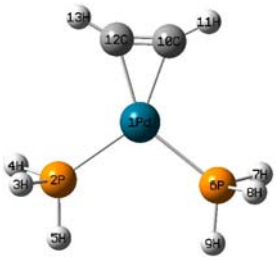 (HF= -157.04869 au)	1	Pd						
	2	P	1	2.428415				
	3	H	2	1.44759	1	119.2343		
	4	H	2	1.447283	1	119.5581	3	116.9876
	5	H	2	1.451449	1	124.4713	3	-121.328
	6	P	1	2.428682	2	105.4789	5	-5.45346
	7	H	6	1.447283	1	119.48	2	126.8581
	8	H	6	1.447559	1	119.218	2	-116.232
	9	H	6	1.451484	1	124.5612	2	5.169401
	10	C	1	2.109136	2	144.837	6	-179.753
	11	H	10	1.073365	1	136.0783	2	179.9056
	12	C	10	1.269687	1	72.48826	2	-0.16858
	13	H	12	1.073365	10	151.4301	1	-179.916
B3 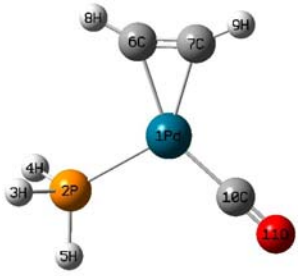 (HF=-170.4312638 au)	1	Pd						
	2	P	1	2.477365				
	3	H	2	1.444104	1	119.4087		
	4	H	2	1.444108	1	119.3878	3	118.1207
	5	H	2	1.443918	1	122.3634	4	120.9282
	6	C	1	2.142399	2	102.8338	4	59.15786
	7	C	6	1.263399	1	72.17094	2	-179.998
	8	H	6	1.072289	1	135.5932	7	-179.989
	9	H	7	1.071347	6	155.1475	1	179.9958
	10	C	1	1.928238	6	149.7784	7	-0.04606
	11	O	10	1.168829	1	179.2873	6	-175.223
B4' 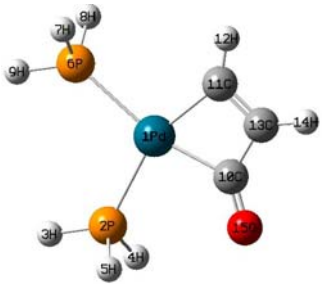 (HF=-178.7366871 au)	1	Pd						
	2	P	1	2.43905				
	3	H	2	1.444254	1	127.957		
	4	H	2	1.437352	1	114.631	3	123.8823
	5	H	2	1.437658	1	114.7453	4	112.2122
	6	P	1	2.51847	2	102.8935	5	-122.595
	7	H	6	1.443666	1	115.6788	2	123.8081
	8	H	6	1.443685	1	115.7152	2	-124.06
	9	H	6	1.449525	1	129.5288	2	-0.10215
	10	C	1	2.058365	2	92.26734	6	179.8957
	11	C	1	2.056691	10	64.54842	2	-179.979
	12	H	11	1.09156	1	137.9487	10	-179.986
	13	C	11	1.37183	1	97.96218	10	0.01307
	14	H	13	1.092593	11	130.8354	1	-179.991
	15	O	10	1.240826	1	131.3255	11	179.9758

B5'

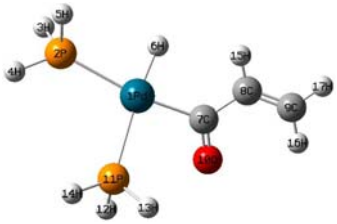

(HF=-179.9559566 au)

1	Pd						
2	P	1	2.486072				
3	H	2	1.441509	1	115.3		
4	H	2	1.449785	1	129.4294	3	123.9412
5	H	2	1.441621	1	115.3078	3	-112.095
6	H	1	1.580831	2	85.2915	3	55.50838
7	C	1	2.025428	2	169.2071	3	42.18627
8	C	7	1.496371	1	121.7613	2	50.84465
9	C	8	1.343567	7	122.7612	1	173.2824
10	O	7	1.255233	1	118.0469	2	-131.241
11	P	1	2.502593	7	89.31005	10	34.67513
12	H	11	1.438376	1	114.5373	7	-75.0272
13	H	11	1.437207	1	116.8929	7	38.47075
14	H	11	1.446161	1	126.7716	7	163.1687
15	H	8	1.083795	7	115.6241	1	-6.07714
16	H	9	1.085257	8	121.004	7	0.669533
17	H	9	1.085347	8	121.4945	7	-179.608

[a] bond length connection, [b] bond length in (Å),[c] atoms angle connection, [d] atoms angle in (degree), [e] dihedral angle connection, and [f] dihedral angle

Table A8: The optimized geometrical parameters of transition states in cycle B (path B') using B3LYP/SDDAll level

Structure of Intermediates	Optimized Geometrical Parameters							
	#	Type	BL-C[a]	BL[b]	BA-C[c]	BA[d]	DA-C[e]	DA[f]
TSB1	1	C						
	2	H	1	1.064125				
	3	C	1	1.217445	2	178.3589		
	4	H	3	1.064345	1	173.7981	2	-173.337
	5	H	1	4.137311	3	108.7587	4	147.5904
	6	P	1	4.036127	3	88.4723	4	149.9502
	7	H	6	1.450014	1	98.92965	3	-79.1174
	8	H	6	1.448387	1	165.5647	3	99.55757
	9	Pd	6	2.369973	1	49.0068	3	42.66678
	10	P	9	2.356605	6	148.5973	1	172.0713
	11	H	10	1.448551	9	120.8086	6	46.81458
	12	H	10	1.454575	9	124.9237	6	169.7832
	13	H	10	1.448281	9	118.2645	6	-70.1221
TSB2	1	Pd						
	2	P	1	2.393381				
	3	H	2	1.445059	1	120.9641		
	4	H	2	1.441259	1	121.4236	3	121.5895
	5	H	2	1.443192	1	118.1619	4	119.7237
	6	C	1	2.148678	2	146.012	5	176.9239
	7	C	6	1.250946	1	72.23519	2	-180
	8	H	6	1.071039	1	126.6314	7	179.9315
	9	H	7	1.070364	6	158.1486	1	178.3555
	10	C	1	3.686044	7	102.1248	6	0.301881
	11	O	1	4.042217	6	84.46773	7	179.337
	12	H	2	3.82002	1	67.90834	10	-119.964
	13	P	2	4.1903	1	55.75283	10	-138.426
	14	H	13	1.452024	2	114.4781	1	38.65548
	15	H	13	1.461705	2	145.4163	1	-178.741
TSB3'	1	Pd						
	2	P	1	3.783252				
	3	H	2	1.458651	1	86.79922		
	4	H	2	1.458352	1	179.6423	3	19.22573
	5	H	2	1.452824	1	84.71054	4	-113.338
	6	C	1	3.451067	2	128.1431	4	-143.114
	7	C	6	1.213292	1	97.40131	2	-79.0483
	8	H	6	1.062322	1	82.59869	2	100.9517
	9	H	7	1.065034	6	177.2	1	-84.6075
	10	C	1	1.889978	6	91.08094	2	96.36869
	11	O	10	1.170483	1	179.7032	6	-8.78474
	12	H	1	3.353333	6	113.0149	2	-76.8217
	13	P	1	2.413474	2	82.09058	4	-57.6244
	14	H	1	3.319259	6	77.78897	2	-62.5424
	15	H	1	3.421576	6	83.486	2	-100.189

(HF=-157.0250031 au)

(HF=-178.6907612 au)

(HF=-178.7144136 au)

TSB4' 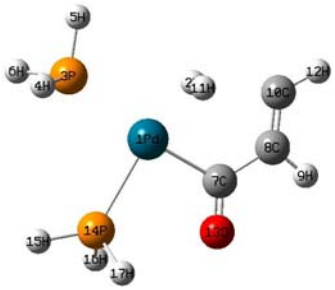 (HF=-179.8404216 au)	1	Pd						
	2	H	1	1.811778				
	3	P	1	2.55702	2	95.11643		
	4	H	3	1.446229	1	120.5423	2	-133.734
	5	H	3	1.444459	1	120.7113	2	-13.4987
	6	H	3	1.446212	1	120.4195	2	106.612
	7	C	1	2.093943	3	171.8901	5	-1.03371
	8	C	7	1.509238	1	118.7811	3	0.748986
	9	H	8	1.090701	7	109.1765	1	179.9925
	10	C	8	1.334915	7	125.8653	1	-0.00786
	11	H	10	2.054105	8	91.52056	7	11.51314
	12	H	10	1.092819	8	121.426	7	-179.999
	13	O	7	1.24048	1	118.4952	3	-179.237
	14	P	1	2.508884	7	89.53896	13	0.176157
	15	H	14	1.448508	1	128.7569	7	179.8661
	16	H	14	1.436721	1	114.3338	7	-56.0892
	17	H	14	1.436693	1	114.3289	7	55.81402
TSB5 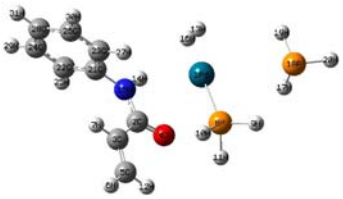 (HF=-228.0785029 au)	1	Pd						
	2	C	1	3.471408				
	3	C	2	1.487211	1	102.6882		
	4	O	2	1.259385	1	81.99644	3	-121.742
	5	C	3	1.33985	2	121.0923	1	-94.6379
	6	H	5	1.084634	3	121.4566	2	-179.129
	7	H	3	1.084125	2	117.9618	1	86.41079
	8	P	1	2.364908	2	94.94024	4	-71.9157
	9	H	8	1.441635	1	119.099	2	153.6923
	10	H	8	1.444563	1	123.1143	2	-84.3591
	11	H	8	1.443131	1	118.0614	2	36.41381
	12	H	5	1.085072	3	120.6222	2	0.388542
	13	H	1	1.761989	8	152.8456	4	-179.569
	14	H	2	2.015004	1	80.87502	8	-165.839
	15	N	2	1.380469	1	86.58618	8	167.1641
	16	H	15	3.27799	2	99.26901	1	6.93294
	17	H	1	3.945409	8	90.00157	4	-81.7107
	18	P	1	3.745633	8	89.51143	4	-103.311
	19	H	18	1.454697	1	86.80682	8	-175.053
	20	H	18	1.462631	1	178.498	8	-50.7636
	21	C	15	1.440971	2	128.1301	1	-98.9919
	22	C	21	1.402409	15	119.4892	2	-106.549
	23	C	21	1.403157	15	120.4434	2	74.99198
	24	C	22	1.399596	21	119.9195	15	-178.28
	25	H	22	1.084589	21	119.2484	15	1.880283
	26	C	23	1.399561	21	119.7889	15	178.8414
	27	H	23	1.085721	21	119.146	15	-1.01271
	28	C	24	1.400439	22	120.1172	21	-0.51277
	29	H	24	1.08472	22	119.7525	21	179.8495
	30	H	26	1.084791	23	119.6329	21	179.8511
	31	H	28	1.084702	24	120.0439	22	-179.792

[a] bond length connection, [b] bond length in (Å),[c] atoms angle connection, [d] atoms angle in (degree), [e] dihedral angle connection, and [f] dihedral angle

Appendix B- (bidentate ligand)
Active catalyst

Table B1: The optimized geometrical parameters of active catalyst (bidentate ligand) using B3LYP/SDDAll level of theory.

Structure of reactant	Optimized Geometrical Parameters							
	#	Type	BL-C[a]	BL[b]	BA-C[c]	BA[d]	DA-C[e]	DA[f]
Active complex 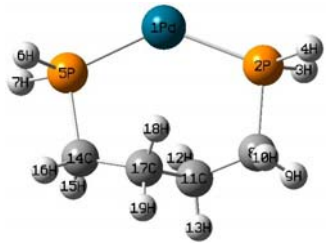 (HF=-170.8455822 au)	1	Pd						
	2	P	1	2.353944				
	3	H	2	1.451279	1	121.3825		
	4	H	2	1.451532	1	129.0528	3	129.9285
	5	P	1	2.35394	2	132.458	4	-116.272
	6	H	5	1.451274	1	121.3801	2	113.7363
	7	H	5	1.45154	1	129.0585	2	-116.33
	8	C	2	1.957915	1	107.679	5	1.627945
	9	H	8	1.093379	2	107.5758	1	141.9407
	10	H	8	1.094904	2	107.0288	1	-102.435
	11	C	8	1.543675	2	111.4604	1	19.29335
	12	H	11	1.097647	8	108.8588	2	38.65204
	13	H	11	1.098892	8	108.9469	2	154.306
	14	C	5	1.957933	1	107.6774	2	1.570589
	15	H	14	1.094904	5	107.0277	1	-102.405
	16	H	14	1.093378	5	107.5754	1	141.9702
	17	C	11	1.552105	8	113.9199	2	-83.7199
	18	H	17	1.097646	11	109.3965	8	24.55001
	19	H	17	1.098891	11	109.0373	8	-91.4495

[a] bond length connection, [b] bond length in (Å),[c] atoms angle connection, [d] atoms angle in (degree), [e] dihedral angle connection, and [f] dihedral angle

Appendix B- (bidentate ligand)
Cycle A

Table B2: The optimized geometrical parameters of bidentate ligand of intermediates in cycle A (path A) using B3LYP/SDDAll level of theory.

Structure of Intermediates	Optimized Geometrical Parameters							
	#	Type	BL-C[a]	BL[b]	BA-C[c]	BA[d]	DA-C[e]	DA[f]
A2 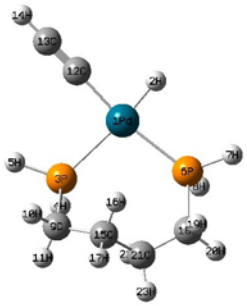 (HF=-183.298992 au)	1	Pd						
	2	H	1	1.555239				
	3	P	1	2.495129	2	172.9087		
	4	H	3	1.446875	1	122.8331	2	143.96
	5	H	3	1.436923	1	116.8462	2	23.70539
	6	P	1	2.406314	3	97.4417	5	-177.747
	7	H	6	1.438376	1	119.0235	3	-171.344
	8	H	6	1.444999	1	115.8156	3	72.79379
	9	C	3	1.940053	1	113.9154	6	64.7975
	10	H	9	1.093778	3	106.0465	1	90.34226
	11	H	9	1.093941	3	109.4813	1	-153.299
	12	C	1	1.977646	6	170.3992	3	176.0132
	13	C	12	1.22981	1	177.9595	6	-171.148
	14	H	13	1.065008	12	178.9914	1	-172.672
	15	C	9	1.538221	3	110.4996	1	-29.1894
	16	H	15	1.097269	9	107.8912	3	56.50547
	17	H	15	1.097483	9	108.6334	3	171.2759
	18	C	6	1.935945	1	121.1307	12	129.0308
	19	H	18	1.094794	6	106.7757	1	-80.173
	20	H	18	1.093497	6	107.5749	1	164.1751
	21	C	18	1.541674	6	111.9243	1	41.14327
	22	H	21	1.099032	18	109.3219	6	48.24786
	23	H	21	1.097155	18	108.3042	6	162.5155
A3  (HF=-204.9766582 au)	1	Pd						
	2	H	1	1.57085				
	3	C	1	1.988025	2	79.07389		
	4	C	3	1.226847	1	178.6874	2	176.3699
	5	H	4	1.064977	3	179.9605	1	179.4794
	6	C	1	1.995293	3	92.57697	4	-3.50781
	7	O	6	1.157054	1	174.5014	3	1.480007
	8	P	1	2.412859	3	163.9831	4	177.3248
	9	H	8	1.439751	1	114.9977	3	-72.1105
	10	H	8	1.442527	1	121.1499	3	170.3749
	11	C	8	1.916042	1	117.5186	3	46.34633
	12	H	11	1.094987	8	105.9871	1	60.6397
	13	H	11	1.09445	8	105.4335	1	-52.7437

	14	C	11	1.5354	8	114.5211	1	-175.959
	15	H	14	1.098423	11	109.8725	8	-58.7591
	16	H	14	1.098436	11	109.7194	8	58.23894
	17	C	14	1.545991	11	111.9703	8	179.7494
	18	H	17	1.097582	14	109.3552	11	58.45462
	19	H	17	1.098322	14	109.0959	11	-57.7237
	20	C	17	1.536885	14	112.2198	11	-179.599
	21	H	20	1.095299	17	110.5399	14	-59.4749
	22	H	20	1.09402	17	111.0232	14	60.36723
	23	P	20	1.952088	17	111.1114	14	-176.69
	24	H	23	1.457674	20	96.52149	17	-167.983
	25	H	23	1.458712	20	96.30986	17	-73.4034
A4  (HF=-204.9612398 au)	1	Pd						
	2	C	1	1.967446				
	3	C	2	1.42456	1	133.1503		
	4	O	2	1.262046	1	102.8945	3	-179.951
	5	C	3	1.217687	2	176.985	1	-0.19086
	6	H	1	1.551818	2	92.98099	4	-179.926
	7	P	1	2.461772	2	171.7321	4	-3.4491
	8	H	7	1.443073	1	116.9083	2	100.5354
	9	H	7	1.445831	1	122.0032	2	-18.5128
	10	C	7	1.920357	1	116.5312	2	-141.159
	11	H	10	1.095073	7	105.6986	1	59.40646
	12	H	10	1.0947	7	105.5235	1	-53.8526
	13	C	10	1.535217	7	114.9893	1	-177.272
	14	H	13	1.098377	10	109.7929	7	-58.4853
	15	H	13	1.098276	10	109.7774	7	58.41917
	16	C	13	1.547209	10	112.029	7	179.9816
	17	H	16	1.098103	13	109.2341	10	-58.1363
	18	H	16	1.098176	13	109.2025	10	57.97065
	19	C	16	1.535395	13	112.381	10	179.9029
	20	H	19	1.095717	16	110.9749	13	-59.4157
	21	H	19	1.095691	16	110.9904	13	59.38359
	22	P	19	1.945951	16	116.1181	13	179.9941
	23	H	22	1.459097	19	96.35718	16	47.25322
	24	H	22	1.459142	19	96.37044	16	-47.0814
	25	H	5	1.064326	3	179.7332	2	2.232179
A5  (HF=-206.2256647 au)	1	Pd						
	2	C	1	1.968409				
	3	C	2	1.469195	1	136.995		
	4	O	2	1.259178	1	100.6826	3	-179.909
	5	C	3	1.341261	2	122.6597	1	-0.04503
	6	H	1	1.560747	2	93.90135	4	-179.96
	7	P	1	2.465047	2	170.0557	4	-3.65221
	8	H	7	1.443969	1	117.2096	2	102.7842
	9	H	7	1.446626	1	122.2901	2	-16.3948
	10	C	7	1.921135	1	116.6119	2	-139.014
	11	H	10	1.095181	7	105.7471	1	59.24423

	12	H	10	1.094856	7	105.4605	1	-53.9438
	13	C	10	1.535092	7	115.1022	1	-177.325
	14	H	13	1.098321	10	109.7794	7	-58.7608
	15	H	13	1.098388	10	109.7531	7	58.08817
	16	C	13	1.547143	10	112.075	7	179.6594
	17	H	16	1.098123	13	109.2197	10	-58.2786
	18	H	16	1.098185	13	109.2324	10	57.81802
	19	C	16	1.535336	13	112.4095	10	179.7599
	20	H	19	1.095712	16	110.9718	13	-59.3397
	21	H	19	1.095723	16	110.9934	13	59.45834
	22	P	19	1.946103	16	116.1174	13	-179.919
	23	H	22	1.459099	19	96.35898	16	47.1146
	24	H	22	1.459157	19	96.37612	16	-47.2171
	25	H	5	1.086051	3	120.5143	2	0.050721
	26	H	5	1.084712	3	121.6633	2	-179.953
	27	H	3	1.08824	2	115.7172	1	179.9925

[a] bond length connection, [b] bond length in (Å),[c] atoms angle connection, [d] atoms angle in (degree), [e] dihedral angle connection, and [f] dihedral angle

Table B3: The optimized geometrical parameters of bidentate ligand of transition states in cycle A (path A) using B3LYP/SDDAll level of theory.

Structure of transition states	Optimized Geometrical Parameters							
	#	Type	BL-C[a]	BL[b]	BA-C[c]	BA[d]	DA-C[e]	DA[f]
TSA1	1	Pd						
	2	H	1	1.608431				
	3	P	1	2.498571	2	153.0298		
	4	H	3	1.443612	1	118.6714	2	23.3145
	5	P	1	2.427496	3	100.2173	4	-159.928
	6	H	5	1.442891	1	121.7769	3	175.6775
	7	C	1	2.001313	5	155.2911	3	179.8675
	8	C	3	4.469434	1	44.94374	7	0.042391
	9	H	8	1.064995	3	141.4036	1	179.7667
	10	H	3	1.447473	1	114.0583	7	-92.7469
	11	H	5	1.446696	1	117.7198	7	113.5206
	12	C	5	1.944081	1	117.2807	7	-126.185
	13	C	12	3.837109	5	87.9107	1	-41.4444
	14	H	12	1.094256	5	105.8784	1	94.13785
	15	H	12	1.094124	5	109.0886	1	-149.899
	16	C	12	1.53698	5	111.0948	1	-25.7102
	17	H	13	1.094967	12	100.7731	5	126.4017
	18	H	13	1.093036	12	139.6103	5	-98.6907
	19	C	13	1.541	12	29.1664	5	-120.195
	20	H	16	1.097501	12	107.9799	5	54.84945
(HF=-183.2881787 au)	21	H	16	1.097934	12	108.6756	5	169.6408
	22	H	19	1.098974	13	109.1168	12	93.05454
	23	H	19	1.097533	13	108.9391	12	-152.224
TSA2	1	Pd						
	2	C	1	2.146762				
	3	O	2	1.165364	1	144.7689		
	4	H	1	3.713889	2	87.13401	3	141.1823
	5	P	1	2.756205	2	98.93027	3	156.7535
	6	H	5	1.446133	1	109.4077	2	-163.573
	7	C	1	1.98593	2	93.91774	3	65.18839
	8	C	7	1.227402	1	178.4397	2	84.93084
	9	H	8	1.064861	7	179.2954	1	-62.2845
	10	H	1	1.553163	7	77.05555	8	-150.318
	11	C	5	1.948951	1	125.7896	7	173.861
	12	C	11	1.541691	5	109.7458	1	20.61
	13	C	12	1.551894	11	112.6763	5	-71.5627
	14	H	12	1.099256	11	108.9819	5	51.35753
	15	H	12	1.097568	11	109.2665	5	166.2312
	16	C	13	1.536675	12	114.9141	11	140.9444
(HF=-204.9569549 au)	17	H	13	1.096795	12	109.5173	11	19.03026
	18	H	13	1.097782	12	109.388	11	-96.8737

	19	P	16	1.939105	13	111.7617	12	-67.7138
	20	H	16	1.094342	13	110.4876	12	174.8178
	21	H	16	1.094221	13	112.2326	12	54.19278
	22	H	19	1.438474	16	100.2682	13	-160.908
	23	H	19	1.439487	16	101.6257	13	99.07084
	24	H	11	1.09499	5	107.3952	1	-99.7108
	25	H	11	1.092817	5	109.3636	1	143.5026
TSA3 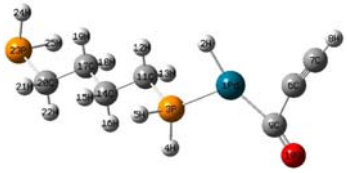 (HF=-204.9292521 au)	1	Pd						
	2	H	1	1.640459				
	3	P	1	2.320551	2	85.81771		
	4	H	3	1.442405	1	120.2011	2	173.4918
	5	H	3	1.438198	1	114.1174	2	-69.3704
	6	C	1	2.215345	3	158.7454	5	111.4098
	7	C	6	1.22666	1	133.4762	3	179.4816
	8	H	7	1.066808	6	179.8874	1	168.0872
	9	C	6	1.623042	1	59.66992	3	-0.77322
	10	O	9	1.211495	6	122.0284	1	179.8406
	11	C	3	1.913028	1	117.6174	9	-130.504
	12	H	11	1.093874	3	105.2067	1	-53.835
	13	H	11	1.094888	3	106.0287	1	59.62682
	14	C	11	1.535582	3	114.2424	1	-177.104
	15	H	14	1.098415	11	109.7897	3	58.2436
	16	H	14	1.098325	11	109.9328	3	-58.8369
	17	C	14	1.547404	11	111.8884	3	179.627
	18	H	17	1.098093	14	109.2306	11	57.83114
	19	H	17	1.097943	14	109.2023	11	-58.2933
	20	C	17	1.535302	14	112.3774	11	179.7447
	21	H	20	1.09571	17	111.0176	14	59.10696
	22	H	20	1.095633	17	110.9968	14	-59.7659
	23	P	20	1.946285	17	116.0161	14	179.6648
	24	H	23	1.459083	20	96.32933	17	-47.7024
	25	H	23	1.45904	20	96.30167	17	46.62351
$TSA4_a$  (HF=-204.9093905 au)	1	Pd						
	2	H	1	1.733217				
	3	P	1	2.432285	2	172.3697		
	4	H	3	1.439406	1	115.1013	2	-54.8124
	5	H	3	1.439528	1	115.228	2	58.33126
	6	C	1	2.004282	3	102.9995	5	57.21882
	7	C	6	1.393471	1	92.10575	3	179.8582
	8	C	7	1.311812	6	142.7215	1	179.9901
	9	H	8	1.089202	7	124.4298	6	-179.993
	10	O	6	1.220458	1	126.1359	3	-0.1516
	11	C	3	1.921097	1	123.0553	6	-179.286
	12	H	11	1.095335	3	106.1201	1	56.83993
	13	H	11	1.095337	3	106.1334	1	-57.0685
	14	C	11	1.536535	3	114.4263	1	179.8798
	15	H	14	1.098156	11	109.7219	3	58.44244
	16	H	14	1.098159	11	109.7195	3	-58.3949

	17	C	14	1.547146	11	112.0553	3	-179.973
	18	H	17	1.098228	14	109.2549	11	58.07518
	19	H	17	1.098233	14	109.2576	11	-58.0808
	20	C	17	1.53538	14	112.3382	11	179.9969
	21	H	20	1.095609	17	110.9921	14	59.41977
	22	H	20	1.095608	17	110.993	14	-59.4034
	23	P	20	1.946178	17	116.032	14	-179.994
	24	H	23	1.459241	20	96.29479	17	47.18699
	25	H	23	1.459227	20	96.28754	17	-47.126
$TSA4_b$  (HF=-206.1107755 au)	1	Pd						
	2	H	1	1.824879				
	3	P	1	2.470986	2	117.9901		
	4	H	3	1.4444	1	117.9865	2	-136.666
	5	H	3	1.444405	1	117.9959	2	107.5145
	6	C	1	2.02912	3	164.1446	4	58.16636
	7	C	6	1.515635	1	122.5522	3	179.9727
	8	H	7	1.088991	6	110.053	1	179.9996
	9	C	7	1.324544	6	124.0104	1	-0.0003
	10	H	1	1.82495	6	77.39856	7	-13.355
	11	O	6	1.22996	1	110.6246	3	-0.02898
	12	C	3	1.924565	1	120.5639	6	-179.751
	13	H	12	1.095235	3	105.7469	1	56.73084
	14	H	12	1.095236	3	105.7432	1	-56.7331
	15	C	12	1.535263	3	114.8722	1	-179.998
	16	H	15	1.098386	12	109.6781	3	-58.3562
	17	H	15	1.098386	12	109.6763	3	58.37598
	18	C	15	1.546849	12	112.1736	3	-179.99
	19	H	18	1.09822	15	109.264	12	-58.0507
	20	H	18	1.098219	15	109.2631	12	58.07254
	21	C	18	1.535394	15	112.4234	12	-179.988
	22	H	21	1.09567	18	111.0161	15	-59.4132
	23	H	21	1.095666	18	111.0168	15	59.45243
	24	P	21	1.9465	18	116.0264	15	-179.976
	25	H	24	1.459152	21	96.30857	18	-47.1445
	26	H	24	1.459133	21	96.30219	18	47.15991
	27	H	9	1.088728	7	125.2998	6	-179.997

[a] bond length connection, [b] bond length in (Å),[c] atoms angle connection, [d] atoms angle in (degree), [e] dihedral angle connection, and [f] dihedral angle

Appendix B- (bidentate ligand)
Cycle A

Table B4: The optimized geometrical parameters of bidentate ligand of intermediates in cycle A (path A') using B3LYP/SDDAll level of theory.

Structure of Intermediates	Optimized Geometrical Parameters							
	#	Type	BL-C[a]	BL[b]	BA-C[c]	BA[d]	DA-C[e]	DA[f]
A2 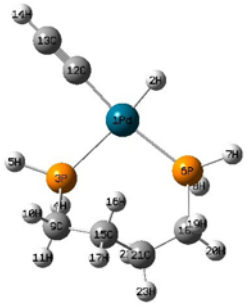 (HF=-183.298992 au)	1	Pd						
	2	H	1	1.555239				
	3	P	1	2.495129	2	172.9087		
	4	H	3	1.446875	1	122.8331	2	143.96
	5	H	3	1.436923	1	116.8462	2	23.70539
	6	P	1	2.406314	3	97.4417	5	-177.747
	7	H	6	1.438376	1	119.0235	3	-171.344
	8	H	6	1.444999	1	115.8156	3	72.79379
	9	C	3	1.940053	1	113.9154	6	64.7975
	10	H	9	1.093778	3	106.0465	1	90.34226
	11	H	9	1.093941	3	109.4813	1	-153.299
	12	C	1	1.977646	6	170.3992	3	176.0132
	13	C	12	1.22981	1	177.9595	6	-171.148
	14	H	13	1.065008	12	178.9914	1	-172.672
	15	C	9	1.538221	3	110.4996	1	-29.1894
	16	H	15	1.097269	9	107.8912	3	56.50547
	17	H	15	1.097483	9	108.6334	3	171.2759
	18	C	6	1.935945	1	121.1307	12	129.0308
	19	H	18	1.094794	6	106.7757	1	-80.173
	20	H	18	1.093497	6	107.5749	1	164.1751
	21	C	18	1.541674	6	111.9243	1	41.14327
	22	H	21	1.099032	18	109.3219	6	48.24786
	23	H	21	1.097155	18	108.3042	6	162.5155
A3  (HF=-204.9766582 au)	1	Pd						
	2	H	1	1.57085				
	3	C	1	1.988025	2	79.07389		
	4	C	3	1.226847	1	178.6874	2	176.3699
	5	H	4	1.064977	3	179.9605	1	179.4794
	6	C	1	1.995293	3	92.57697	4	-3.50781
	7	O	6	1.157054	1	174.5014	3	1.480007
	8	P	1	2.412859	3	163.9831	4	177.3248
	9	H	8	1.439751	1	114.9977	3	-72.1105
	10	H	8	1.442527	1	121.1499	3	170.3749
	11	C	8	1.916042	1	117.5186	3	46.34633
	12	H	11	1.094987	8	105.9871	1	60.6397
	13	H	11	1.09445	8	105.4335	1	-52.7437

	14	C	11	1.5354	8	114.5211	1	-175.959
	15	H	14	1.098423	11	109.8725	8	-58.7591
	16	H	14	1.098436	11	109.7194	8	58.23894
	17	C	14	1.545991	11	111.9703	8	179.7494
	18	H	17	1.097582	14	109.3552	11	58.45462
	19	H	17	1.098322	14	109.0959	11	-57.7237
	20	C	17	1.536885	14	112.2198	11	-179.599
	21	H	20	1.095299	17	110.5399	14	-59.4749
	22	H	20	1.09402	17	111.0232	14	60.36723
	23	P	20	1.952088	17	111.1114	14	-176.69
	24	H	23	1.457674	20	96.52149	17	-167.983
	25	H	23	1.458712	20	96.30986	17	-73.4034
A4'	1	Pd						
	2	H	1	1.581962				
	3	P	1	2.489323	2	172.8591		
	4	H	3	1.445343	1	123.4541	2	168.5632
	5	H	3	1.437879	1	119.0004	2	45.24423
	6	P	1	2.460825	3	95.77463	5	-175.191
	7	H	6	1.439573	1	118.6914	3	-173.935
	8	H	6	1.44685	1	117.1561	3	69.70489
	9	C	3	1.937423	1	111.2933	6	68.72852
	10	H	9	1.093543	3	105.4597	1	86.82715
	11	H	9	1.094051	3	109.2508	1	-156.99
	12	C	9	1.538054	3	111.0467	1	-32.5485
	13	H	12	1.09754	9	107.8334	3	56.82303
	14	H	12	1.097421	9	108.3656	3	171.3179
	15	C	6	1.937987	1	120.4194	3	-50.6172
	16	H	15	1.094833	6	106.7238	1	-79.0305
	17	H	15	1.093289	6	108.027	1	165.0767
	18	C	15	1.541859	6	111.5263	1	41.96748
	19	H	18	1.099159	15	109.2424	6	50.02682
	20	H	18	1.097201	15	108.3286	6	164.2675
	21	C	18	7.953931	15	78.27819	6	-18.4065
(HF=-204.9770792 au)	22	C	21	1.218857	18	27.6746	15	-115.177
	23	H	21	1.064088	18	152.0883	15	63.80435
	24	C	22	1.445185	21	177.1582	18	5.173348
	25	O	24	1.256963	22	120.6734	21	-165.74
A5'	1	Pd						
	2	C	1	3.108509				
	3	C	2	1.343509	1	155.6149		
	4	H	3	1.085278	2	120.9813	1	-11.0192
	5	P	1	2.498434	2	112.0788	3	-7.12665
	6	H	5	1.438922	1	113.4705	2	-39.8775
	7	H	5	1.439054	1	118.4534	2	73.8492
	8	P	1	2.474869	5	96.08669	2	172.4447
	9	H	8	1.445756	1	118.6108	5	-112.525
(HF=-206.2340552 au)	10	H	8	1.442048	1	115.3861	5	132.8334
	11	C	2	1.499259	1	33.37209	8	172.6472

	12	O	11	1.258993	2	119.2638	1	178.5224
	13	H	1	1.578503	11	86.13488	2	-20.2881
	14	H	3	1.08552	2	121.5158	1	169.0002
	15	H	2	1.083579	1	82.42624	11	-173.979
	16	C	5	1.934779	1	121.7726	11	-168.913
	17	H	16	1.092918	5	108.2023	1	157.6453
	18	H	16	1.095165	5	106.83	1	-87.513
	19	C	16	1.550245	5	111.9002	1	34.61526
	20	H	19	1.096588	16	109.1598	5	131.12
	21	H	19	1.098824	16	110.1536	5	15.63572
	22	C	8	1.935653	1	122.3373	11	-152.998
	23	H	22	1.09361	8	108.3362	1	161.54
	24	H	22	1.095103	8	105.1598	1	46.91509
	25	C	22	1.541285	8	114.4914	1	-75.6358
	26	H	25	1.099291	22	107.2864	8	176.6079
	27	H	25	1.098054	22	108.9875	8	-68.8502

[a] bond length connection, [b] bond length in (Å),[c] atoms angle connection, [d] atoms angle in (degree), [e] dihedral angle connection, and [f] dihedral angle

Table B5: The optimized geometrical parameters of bidentate ligand of transition states in cycle A (path A') using B3LYP/SDDAll level of theory.

Structure of Intermediates	Optimized Geometrical Parameters							
	#	Type	BL-C[a]	BL[b]	BA-C[c]	BA[d]	DA-C[e]	DA[f]
TSA1	1	Pd						
	2	H	1	1.608431				
	3	P	1	2.498571	2	153.0298		
	4	H	3	1.443612	1	118.6714	2	23.3145
	5	P	1	2.427496	3	100.2173	4	-159.928
	6	H	5	1.442891	1	121.7769	3	175.6775
	7	C	1	2.001313	5	155.2911	3	179.8675
	8	C	3	4.469434	1	44.94374	7	0.042391
	9	H	8	1.064995	3	141.4036	1	179.7667
	10	H	3	1.447473	1	114.0583	7	-92.7469
	11	H	5	1.446696	1	117.7198	7	113.5206
	12	C	5	1.944081	1	117.2807	7	-126.185
	13	C	12	3.837109	5	87.9107	1	-41.4444
	14	H	12	1.094256	5	105.8784	1	94.13785
	15	H	12	1.094124	5	109.0886	1	-149.899
	16	C	12	1.53698	5	111.0948	1	-25.7102
	17	H	13	1.094967	12	100.7731	5	126.4017
	18	H	13	1.093036	12	139.6103	5	-98.6907
(HF=-183.2881787 au)	19	C	13	1.541	12	29.1664	5	-120.195
	20	H	16	1.097501	12	107.9799	5	54.84945
	21	H	16	1.097934	12	108.6756	5	169.6408
	22	H	19	1.098974	13	109.1168	12	93.05454
	23	H	19	1.097533	13	108.9391	12	-152.224
TSA2	1	Pd						
	2	C	1	2.146762				
	3	O	2	1.165364	1	144.7689		
	4	H	1	3.713889	2	87.13401	3	141.1823
	5	P	1	2.756205	2	98.93027	3	156.7535
	6	H	5	1.446133	1	109.4077	2	-163.573
	7	C	1	1.98593	2	93.91774	3	65.18839
	8	C	7	1.227402	1	178.4397	2	84.93084
	9	H	8	1.064861	7	179.2954	1	-62.2845
	10	H	1	1.553163	7	77.05555	8	-150.318
	11	C	5	1.948951	1	125.7896	7	173.861
	12	C	11	1.541691	5	109.7458	1	20.61
	13	C	12	1.551894	11	112.6763	5	-71.5627
	14	H	12	1.099256	11	108.9819	5	51.35753
	15	H	12	1.097568	11	109.2665	5	166.2312
	16	C	13	1.536675	12	114.9141	11	140.9444
	17	H	13	1.096795	12	109.5173	11	19.03026
(HF=-204.9569549 au)	18	H	13	1.097782	12	109.388	11	-96.8737
	19	P	16	1.939105	13	111.7617	12	-67.7138

	20	H	16	1.094342	13	110.4876	12	174.8178
	21	H	16	1.094221	13	112.2326	12	54.19278
	22	H	19	1.438474	16	100.2682	13	-160.908
	23	H	19	1.439487	16	101.6257	13	99.07084
	24	H	11	1.09499	5	107.3952	1	-99.7108
	25	H	11	1.092817	5	109.3636	1	143.5026
TSA3'	1	Pd						
	2	C	1	2.223535				
	3	C	2	1.229284	1	151.751		
	4	H	1	1.610151	2	106.7186	3	0.585941
	5	H	3	1.066048	2	179.4102	1	-176.142
	6	C	2	1.798589	1	57.3146	3	-179.803
	7	O	6	1.197099	2	119.0789	1	179.9031
	8	P	1	2.440001	6	106.8183	2	121.3956
	9	H	8	1.445201	1	120.5061	6	19.83625
	10	H	8	1.441998	1	119.7595	6	-99.9862
	11	C	8	1.947496	1	115.0355	6	140.794
	12	H	11	1.093927	8	108.1016	1	-135.037
	13	H	11	1.093403	8	106.6545	1	109.018
	14	C	11	1.537319	8	111.3793	1	-11.8253
	15	C	14	1.548125	11	114.0646	8	-66.7842
	16	H	14	1.096456	11	107.9181	8	55.69761
	17	H	14	1.098457	11	108.743	8	170.6723
	18	C	15	1.538008	14	113.6065	11	147.5717
	19	H	15	1.097895	14	110.1198	11	25.81785
	20	H	15	1.098445	14	109.6777	11	-90.5078
	21	P	18	1.952877	15	111.4695	14	-69.0714
	22	H	18	1.093328	15	110.9563	14	171.9023
	23	H	18	1.093929	15	111.402	14	51.58968
	24	H	21	1.444703	18	99.62296	15	-134.106
	25	H	21	1.44169	18	100.7364	15	126.9758
$TSA4'_a$	1	Pd						
	2	P	1	2.518457				
	3	H	2	1.442734	1	120.2262		
	4	H	2	1.445826	1	113.2788	3	-113.666
	5	H	1	1.756308	2	99.2777	3	17.00631
	6	C	1	2.046042	2	165.9172	3	20.73505
	7	C	6	1.393965	1	91.30984	2	-3.81919
	8	C	7	1.322961	6	144.4924	1	179.8297
	9	H	8	1.093871	7	121.7343	6	-179.909
	10	O	6	1.236092	1	131.0478	7	-179.682
	11	P	1	2.430098	6	94.64224	10	-0.2392
	12	H	11	1.435402	1	114.9192	6	-4.21928
	13	H	11	1.443236	1	119.0585	6	112.2986
	14	C	11	1.936441	1	117.3429	6	-124.443
	15	H	14	1.093766	11	106.1206	1	92.99728
	16	H	14	1.093927	11	109.0793	1	-150.878
	17	C	14	1.537916	11	110.7312	1	-27.0003

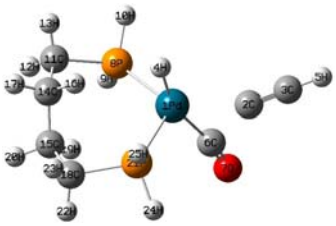

(HF=-204.9274241 au)

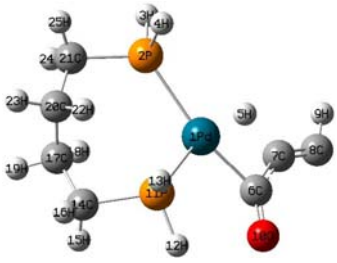

(HF=-204.9241392 au)

	18	H	2	3.053896	1	68.42148	4	-136.531
	19	H	17	1.097384	14	108.6957	11	170.0817
	20	C	17	1.553097	14	114.6162	11	-67.2273
	21	C	20	1.540301	17	113.1902	14	137.4108
	22	H	20	1.099124	17	110.474	14	14.66417
	23	H	20	1.097203	17	109.6086	14	-101.083
	24	H	21	1.094746	20	110.8335	17	43.82706
	25	H	21	1.092902	20	111.8256	17	164.2916
TSA4'$_b$ 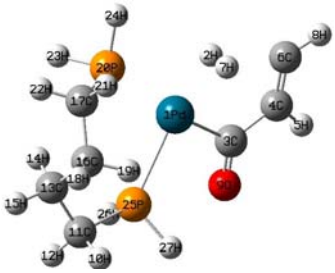 (HF=-206.1186799 au)	1	Pd						
	2	H	1	1.822449				
	3	C	1	2.094978	2	76.51764		
	4	C	3	1.507218	1	118.956	2	14.49785
	5	H	4	1.09134	3	109.0546	1	-179.814
	6	C	4	1.337191	3	126.1053	1	-0.38388
	7	H	6	2.09458	4	91.66221	3	10.72978
	8	H	6	1.094229	3	149.029	1	179.9604
	9	O	3	1.242411	1	118.5159	6	-178.058
	10	H	1	4.524246	3	107.6418	9	26.66409
	11	C	1	4.001782	3	111.3556	9	13.45866
	12	H	11	1.09322	1	129.3675	3	-63.0285
	13	C	11	1.540081	1	82.79476	3	-175.012
	14	H	13	1.09884	11	109.0389	1	60.24971
	15	H	13	1.097478	11	109.0338	1	175.0378
	16	C	1	3.91328	3	142.9276	9	40.97888
	17	C	16	1.536541	1	78.33856	3	168.0355
	18	H	13	2.17855	11	113.5203	1	-93.7563
	19	H	13	2.180141	11	85.77615	1	-54.236
	20	P	17	1.943262	1	34.60551	3	175.4616
	21	H	1	4.338845	3	157.5553	9	97.08564
	22	H	17	1.093799	16	112.1131	1	136.1278
	23	H	20	1.446417	17	100.5411	1	126.7022
	24	H	20	1.445264	17	99.13733	1	-135.203
	25	P	11	1.942301	13	111.285	16	-71.438
	26	H	11	2.616759	16	121.8445	17	33.96326
	27	H	11	2.636432	16	112.1827	17	88.05063

[a] bond length connection, [b] bond length in (Å),[c] atoms angle connection, [d] atoms angle in (degree), [e] dihedral angle connection, and [f] dihedral angle

Appendix B- (bidentate ligand)
Cycle B

Table B6: The optimized geometrical parameters of bidentate ligand of intermediates in cycle B (path B) using B3LYP/SDDAll level of theory.

Structure of Intermediates	Optimized Geometrical Parameters							
	#	Type	BL-C[a]	BL[b]	BA-C[c]	BA[d]	DA-C[e]	DA[f]
B2 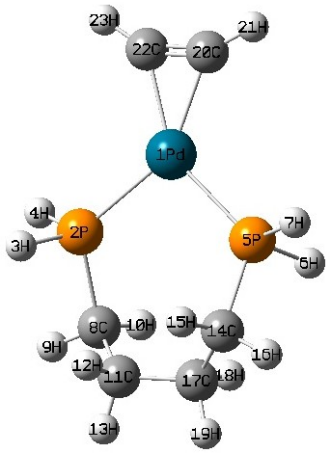 (HF=-183.3244779 au)	1	Pd						
	2	P	1	2.41452				
	3	H	2	1.451498	1	120.1724		
	4	H	2	1.448775	1	118.6898	3	116.9358
	5	P	1	2.414506	2	98.89268	4	-146.262
	6	H	5	1.451492	1	120.1503	2	96.93683
	7	H	5	1.448778	1	118.7055	2	-146.132
	8	C	2	1.939002	1	121.9011	5	-25.3437
	9	H	8	1.093964	2	106.7021	1	-167.693
	10	H	8	1.095397	2	106.1802	1	-53.0906
	11	C	8	1.545027	2	115.5202	1	70.16992
	12	H	11	1.099431	8	110.2275	2	39.6526
	13	H	11	1.098277	8	106.2674	2	153.457
	14	C	5	1.938997	1	121.9055	2	-25.1918
	15	H	14	1.095397	5	106.1811	1	-53.1424
	16	H	14	1.093962	5	106.7026	1	-167.744
	17	C	11	1.551277	8	117.8564	2	-86.9467
	18	H	17	1.099428	11	109.4544	8	-35.4284
	19	H	17	1.098272	11	106.7548	8	-149.115
	20	C	1	2.101294	5	112.9348	14	155.1242
	21	H	20	1.074008	1	137.0271	5	0.739708
	22	C	20	1.272612	1	72.37176	5	-179.238
	23	H	2	4.107855	1	45.7846	22	-0.18716
B3  (HF=-205.0196738 au)	1	Pd						
	2	P	1	2.47148				
	3	H	2	1.445925	1	118.5336		
	4	H	2	1.445979	1	120.7532	3	118.2719
	5	C	1	2.13604	2	103.034	4	167.2844
	6	H	5	1.072706	1	136.3518	2	-1.60688
	7	C	5	1.265437	1	72.18467	2	178.9132
	8	H	7	1.071697	5	154.3978	1	179.7199
	9	C	2	1.926436	1	118.4578	7	-69.9128
	10	H	9	1.095249	2	105.7339	1	54.00216
	11	H	9	1.095338	2	105.813	1	-59.3625
	12	C	9	1.535517	2	115.003	1	177.3004
	13	H	12	1.098516	9	109.6376	2	-57.9862
	14	H	12	1.098358	9	109.6998	2	58.69906

	15	C	12	1.54697	9	112.2588	2	-179.592
	16	H	15	1.0983	12	109.2305	9	57.68846
	17	H	15	1.098227	12	109.3	9	-58.4241
	18	P	15	2.961571	12	148.5904	9	179.2932
	19	H	18	1.459214	15	77.49954	12	-131.052
	20	H	18	1.459044	15	77.38204	12	132.3606
	21	C	15	1.535501	12	112.4053	9	179.597
	22	H	21	1.095684	15	111.0009	12	59.65899
	23	H	21	1.095696	15	110.9802	12	-59.1633
	24	C	1	1.927352	7	115.4789	5	179.6536
	25	O	2	4.474512	1	41.59454	24	-0.06943
A4 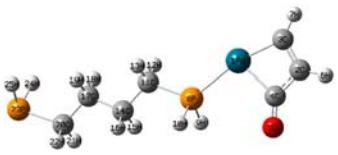 (HF=-205.0037039 au)	1	Pd						
	2	C	1	2.592763				
	3	C	2	1.375287	1	51.67008		
	4	C	2	1.442637	1	51.76559	3	179.998
	5	O	4	1.224782	2	138.3818	1	179.9994
	6	H	2	1.090832	1	176.7338	3	179.9853
	7	H	3	1.090228	2	123.3046	1	179.9985
	8	P	1	2.436703	3	167.2204	2	0.010331
	9	H	8	1.440849	1	115.3617	3	-56.4296
	10	H	8	1.440848	1	115.3394	3	56.37653
	11	C	8	1.921981	1	123.9329	3	179.9651
	12	H	11	1.095442	8	106.1537	1	56.95849
	13	H	11	1.095445	8	106.1565	1	-56.9194
	14	C	11	1.536369	8	114.5308	1	-179.983
	15	H	14	1.098288	11	109.6765	8	-58.3595
	16	H	14	1.098281	11	109.6775	8	58.36231
	17	C	14	1.546847	11	112.2043	8	-179.997
	18	H	17	1.098285	14	109.2596	11	58.06708
	19	H	17	1.098282	14	109.2604	11	-58.0724
	20	C	17	1.535408	14	112.351	11	179.9966
	21	H	20	1.095648	17	110.9827	14	-59.3999
	22	H	20	1.095643	17	110.9828	14	59.3949
	23	P	20	1.946047	17	116.0716	14	179.9978
	24	H	23	1.459225	20	96.32366	17	47.15556
	25	H	23	1.459222	20	96.32414	17	-47.161
A5  (HF=-206.2256647 au)	1	Pd						
	2	C	1	1.968409				
	3	C	2	1.469195	1	136.995		
	4	O	2	1.259178	1	100.6826	3	-179.909
	5	C	3	1.341261	2	122.6597	1	-0.04503
	6	H	1	1.560747	2	93.90135	4	-179.96
	7	P	1	2.465047	2	170.0557	4	-3.65221
	8	H	7	1.443969	1	117.2096	2	102.7842
	9	H	7	1.446626	1	122.2901	2	-16.3948
	10	C	7	1.921135	1	116.6119	2	-139.014
	11	H	10	1.095181	7	105.7471	1	59.24423
	12	H	10	1.094856	7	105.4605	1	-53.9438

	13	C	10	1.535092	7	115.1022	1	-177.325
	14	H	13	1.098321	10	109.7794	7	-58.7608
	15	H	13	1.098388	10	109.7531	7	58.08817
	16	C	13	1.547143	10	112.075	7	179.6594
	17	H	16	1.098123	13	109.2197	10	-58.2786
	18	H	16	1.098185	13	109.2324	10	57.81802
	19	C	16	1.535336	13	112.4095	10	179.7599
	20	H	19	1.095712	16	110.9718	13	-59.3397
	21	H	19	1.095723	16	110.9934	13	59.45834
	22	P	19	1.946103	16	116.1174	13	-179.919
	23	H	22	1.459099	19	96.35898	16	47.1146
	24	H	22	1.459157	19	96.37612	16	-47.2171
	25	H	5	1.086051	3	120.5143	2	0.050721
	26	H	5	1.084712	3	121.6633	2	-179.953
	27	H	3	1.08824	2	115.7172	1	179.9925
[a] bond length connection, [b] bond length in (Å),[c] atoms angle connection, [d] atoms angle in (degree), [e] dihedral angle connection, and [f] dihedral angle								

Table B7: The optimized geometrical parameters of bidentate ligand of transition states in cycle B (path B) using B3LYP/SDDAll level of theory.

Structure of Intermediates	Optimized Geometrical Parameters							
	#	Type	BL-C[a]	BL[b]	BA-C[c]	BA[d]	DA-C[e]	DA[f]
TSB1 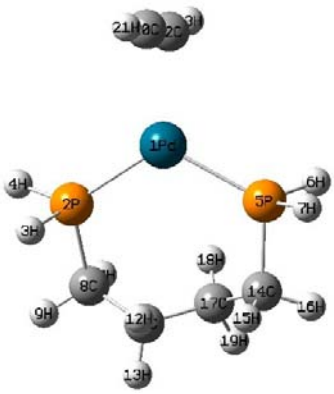 (HF=-183.2967865 au)	1	Pd						
	2	P	1	2.39411				
	3	H	2	1.454324	1	113.8298		
	4	H	2	1.458253	1	130.3772	3	120.0811
	5	P	1	2.397527	2	117.8789	4	-144.977
	6	H	5	1.45504	1	116.1477	2	111.3969
	7	H	5	1.457087	1	130.134	2	-125.797
	8	C	2	1.946701	1	117.3429	5	-16.3112
	9	H	8	1.093876	2	107.8808	1	161.4471
	10	H	8	1.09539	2	106.9981	1	-82.8567
	11	C	8	1.542786	2	111.7296	1	38.85987
	12	H	11	1.098441	8	109.6248	2	39.98649
	13	H	11	1.09819	8	108.0477	2	154.5499
	14	C	5	1.948888	1	114.5716	2	-0.45096
	15	H	14	1.09506	5	106.3641	1	-87.5604
	16	H	14	1.093623	5	108.2533	1	157.0374
	17	C	14	1.546446	5	111.7183	1	33.75207
	18	H	17	1.098287	14	109.6906	5	29.00097
	19	H	17	1.097693	14	108.3073	5	144.0381
	20	C	1	2.642998	5	121.1101	14	168.5375
	21	H	20	1.064587	1	116.5099	5	-92.5997
	22	C	20	1.226176	1	63.4723	5	87.39803
	23	H	20	2.275344	1	70.17371	5	87.41335
TSB2 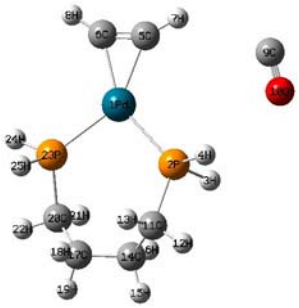 (HF=-204.9863232 au)	1	Pd						
	2	P	1	2.418813				
	3	H	2	1.449374	1	120.7859		
	4	H	2	1.448165	1	119.041	3	117.938
	5	C	1	2.10731	2	115.4105	4	43.01024
	6	C	5	1.273054	1	71.82518	2	-179.064
	7	H	5	1.074228	1	138.1133	6	-179.856
	8	H	6	1.074151	5	150.5152	1	-179.977
	9	C	5	3.602064	1	103.6949	6	-162.295
	10	O	9	1.15236	5	111.716	1	-1.89302
	11	C	2	1.937649	1	120.7209	6	162.2876
	12	H	11	1.093798	2	106.7022	1	-168.384
	13	H	11	1.095365	2	106.3684	1	-53.8741
	14	C	11	1.547811	2	115.1507	1	69.45865
	15	H	14	1.097979	11	106.5559	2	146.866
	16	H	14	1.099416	11	110.4812	2	32.84665
	17	C	14	1.550505	11	117.5219	2	-93.617

	18	H	17	1.099475	14	109.4275	11	-37.1617
	19	H	17	1.09868	14	106.8778	11	-150.977
	20	C	17	1.542969	14	118.0316	11	89.67123
	21	H	20	1.095416	17	110.6915	14	40.55701
	22	H	20	1.094056	17	109.3961	14	159.1053
	23	P	20	1.939543	17	115.8387	14	-80.248
	24	H	23	1.448181	20	97.3846	17	-156.08
	25	H	23	1.451781	20	97.28457	17	-59.1752
TSB3 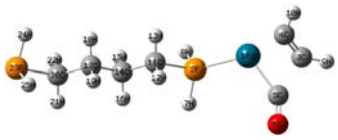 (HF=-204.9334819 au)	1	Pd						
	2	P	1	2.339642				
	3	C	1	2.297367	2	165.3234		
	4	C	3	1.307744	1	71.56541	2	-136.008
	5	C	3	1.865459	1	55.50029	4	143.435
	6	O	5	1.189376	3	134.5624	1	-149.958
	7	H	2	1.443267	1	119.0293	4	-129.315
	8	H	2	1.443303	1	115.9128	4	114.4652
	9	H	3	1.081692	1	135.2556	4	-145.908
	10	H	4	1.084362	3	128.2398	1	-155.331
	11	C	2	1.922188	1	120.2161	4	-6.12697
	12	H	11	1.095032	2	105.7425	1	-57.7775
	13	H	11	1.094914	2	105.67	1	55.6104
	14	C	11	1.535182	2	114.5198	1	178.9265
	15	H	14	1.098654	11	109.7435	2	-58.4793
	16	H	14	1.098487	11	109.767	2	58.39291
	17	C	14	1.547211	11	112.1214	2	179.9921
	18	H	17	1.09815	14	109.2116	11	57.84372
	19	H	17	1.098079	14	109.2386	11	-58.253
	20	C	17	1.535344	14	112.4038	11	179.7656
	21	H	20	1.095701	17	111.021	14	59.6661
	22	H	20	1.095709	17	110.9947	14	-59.1876
	23	P	20	1.946328	17	116.0345	14	-179.739
	24	H	23	1.459084	20	96.31624	17	46.81381
	25	H	23	1.458993	20	96.33704	17	-47.505
TSB4  (HF=-206.1107755 au)	1	Pd						
	2	H	1	1.824879				
	3	P	1	2.470986	2	117.9901		
	4	H	3	1.4444	1	117.9865	2	-136.666
	5	H	3	1.444405	1	117.9959	2	107.5145
	6	C	1	2.02912	3	164.1446	4	58.16636
	7	C	6	1.515635	1	122.5522	3	179.9727
	8	H	7	1.088991	6	110.053	1	179.9996
	9	C	7	1.324544	6	124.0104	1	-0.0003
	10	H	1	1.82495	6	77.39856	7	-13.355
	11	O	6	1.22996	1	110.6246	3	-0.02898
	12	C	3	1.924565	1	120.5639	6	-179.751
	13	H	12	1.095235	3	105.7469	1	56.73084
	14	H	12	1.095236	3	105.7432	1	-56.7331
	15	C	12	1.535263	3	114.8722	1	-179.998

	16	H	15	1.098386	12	109.6781	3	-58.3562
	17	H	15	1.098386	12	109.6763	3	58.37598
	18	C	15	1.546849	12	112.1736	3	-179.99
	19	H	18	1.09822	15	109.264	12	-58.0507
	20	H	18	1.098219	15	109.2631	12	58.07254
	21	C	18	1.535394	15	112.4234	12	-179.988
	22	H	21	1.09567	18	111.0161	15	-59.4132
	23	H	21	1.095666	18	111.0168	15	59.45243
	24	P	21	1.9465	18	116.0264	15	-179.976
	25	H	24	1.459152	21	96.30857	18	-47.1445
	26	H	24	1.459133	21	96.30219	18	47.15991
	27	H	9	1.088728	7	125.2998	6	-179.997

[a] bond length connection, [b] bond length in (Å),[c] atoms angle connection, [d] atoms angle in (degree), [e] dihedral angle connection, and [f] dihedral angle

Appendix B- (bidentate ligand)
Cycle B

Table B8: The optimized geometrical parameters of bidentate ligand of intermediates in cycle B (path B') using B3LYP/SDDAll level of theory.

Structure of Intermediates	Optimized Geometrical Parameters							
	#	Type	BL-C[a]	BL[b]	BA-C[c]	BA[d]	DA-C[e]	DA[f]
B2 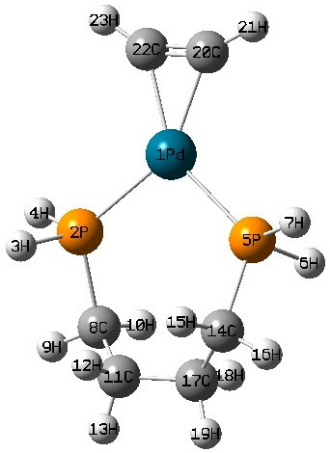 (HF=-183.3244779 au)	1	Pd						
	2	P	1	2.41452				
	3	H	2	1.451498	1	120.1724		
	4	H	2	1.448775	1	118.6898	3	116.9358
	5	P	1	2.414506	2	98.89268	4	-146.262
	6	H	5	1.451492	1	120.1503	2	96.93683
	7	H	5	1.448778	1	118.7055	2	-146.132
	8	C	2	1.939002	1	121.9011	5	-25.3437
	9	H	8	1.093964	2	106.7021	1	-167.693
	10	H	8	1.095397	2	106.1802	1	-53.0906
	11	C	8	1.545027	2	115.5202	1	70.16992
	12	H	11	1.099431	8	110.2275	2	39.6526
	13	H	11	1.098277	8	106.2674	2	153.457
	14	C	5	1.938997	1	121.9055	2	-25.1918
	15	H	14	1.095397	5	106.1811	1	-53.1424
	16	H	14	1.093962	5	106.7026	1	-167.744
	17	C	11	1.551277	8	117.8564	2	-86.9467
	18	H	17	1.099428	11	109.4544	8	-35.4284
	19	H	17	1.098272	11	106.7548	8	-149.115
	20	C	1	2.101294	5	112.9348	14	155.1242
	21	H	20	1.074008	1	137.0271	5	0.739708
	22	C	20	1.272612	1	72.37176	5	-179.238
	23	H	2	4.107855	1	45.7846	22	-0.18716
B3  (HF=-205.0196738 au)	1	Pd						
	2	P	1	2.47148				
	3	H	2	1.445925	1	118.5336		
	4	H	2	1.445979	1	120.7532	3	118.2719
	5	C	1	2.13604	2	103.034	4	167.2844
	6	H	5	1.072706	1	136.3518	2	-1.60688
	7	C	5	1.265437	1	72.18467	2	178.9132
	8	H	7	1.071697	5	154.3978	1	179.7199
	9	C	2	1.926436	1	118.4578	7	-69.9128
	10	H	9	1.095249	2	105.7339	1	54.00216
	11	H	9	1.095338	2	105.813	1	-59.3625
	12	C	9	1.535517	2	115.003	1	177.3004
	13	H	12	1.098516	9	109.6376	2	-57.9862
	14	H	12	1.098358	9	109.6998	2	58.69906

	15	C	12	1.54697	9	112.2588	2	-179.592
	16	H	15	1.0983	12	109.2305	9	57.68846
	17	H	15	1.098227	12	109.3	9	-58.4241
	18	P	15	2.961571	12	148.5904	9	179.2932
	19	H	18	1.459214	15	77.49954	12	-131.052
	20	H	18	1.459044	15	77.38204	12	132.3606
	21	C	15	1.535501	12	112.4053	9	179.597
	22	H	21	1.095684	15	111.0009	12	59.65899
	23	H	21	1.095696	15	110.9802	12	-59.1633
	24	C	1	1.927352	7	115.4789	5	179.6536
	25	O	2	4.474512	1	41.59454	24	-0.06943
A4'  (HF=-205.0156822 au)	1	Pd						
	2	C	1	2.626951				
	3	C	2	1.371412	1	50.80761		
	4	C	2	1.453398	1	51.5192	3	-179.691
	5	O	4	1.241688	2	132.6	1	179.5291
	6	H	2	1.093302	1	178.3795	3	178.7006
	7	H	3	1.091803	2	124.155	1	179.9722
	8	P	1	2.430308	3	159.6684	2	-3.49563
	9	H	8	1.444342	1	120.5235	3	118.6456
	10	H	8	1.435988	1	114.5508	3	1.600287
	11	C	8	1.936994	1	117.2674	3	-117.477
	12	H	11	1.093909	8	106.067	1	90.13859
	13	H	11	1.094091	8	109.2026	1	-153.75
	14	C	11	1.538259	8	110.8647	1	-29.733
	15	H	14	1.097694	11	108.0022	8	56.04439
	16	H	14	1.097593	11	108.6118	8	170.7736
	17	C	14	1.5542	11	114.7364	8	-66.5411
	18	C	17	1.54095	14	113.317	11	134.8472
	19	H	17	1.099111	14	110.4367	11	11.98309
	20	H	17	1.097324	14	109.6084	11	-103.704
	21	P	18	1.944039	17	111.0898	14	-74.1661
	22	H	18	1.094909	17	110.7437	14	44.48682
	23	H	18	1.093118	17	111.7461	14	164.8246
	24	H	21	1.44405	18	99.54515	17	169.5515
	25	H	21	1.44751	18	98.58619	17	-92.1385
B5' 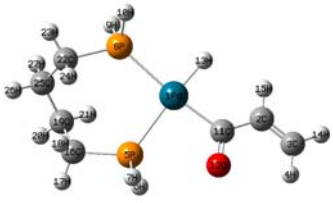 (HF=-206.2340552 au)	1	Pd						
	2	C	1	3.108509				
	3	C	2	1.343509	1	155.6149		
	4	H	3	1.085278	2	120.9813	1	-11.0192
	5	P	1	2.498434	2	112.0788	3	-7.12665
	6	H	5	1.438922	1	113.4705	2	-39.8775
	7	H	5	1.439054	1	118.4534	2	73.8492
	8	P	1	2.474869	5	96.08669	2	172.4447
	9	H	8	1.445756	1	118.6108	5	-112.525
	10	H	8	1.442048	1	115.3861	5	132.8334
	11	C	2	1.499259	1	33.37209	8	172.6472
	12	O	11	1.258993	2	119.2638	1	178.5224

	13	H	1	1.578503	11	86.13488	2	-20.2881
	14	H	3	1.08552	2	121.5158	1	169.0002
	15	H	2	1.083579	1	82.42624	11	-173.979
	16	C	5	1.934779	1	121.7726	11	-168.913
	17	H	16	1.092918	5	108.2023	1	157.6453
	18	H	16	1.095165	5	106.83	1	-87.513
	19	C	16	1.550245	5	111.9002	1	34.61526
	20	H	19	1.096588	16	109.1598	5	131.12
	21	H	19	1.098824	16	110.1536	5	15.63572
	22	C	8	1.935653	1	122.3373	11	-152.998
	23	H	22	1.09361	8	108.3362	1	161.54
	24	H	22	1.095103	8	105.1598	1	46.91509
	25	C	22	1.541285	8	114.4914	1	-75.6358
	26	H	25	1.099291	22	107.2864	8	176.6079
	27	H	25	1.098054	22	108.9875	8	-68.8502
[a] bond length connection, [b] bond length in (Å),[c] atoms angle connection, [d] atoms angle in (degree), [e] dihedral angle connection, and [f] dihedral angle								

Table B9: The optimized geometrical parameters of bidentate ligand of transition states in cycle B (path B') using B3LYP/SDDAll level of theory.

Structure of Intermediates	Optimized Geometrical Parameters							
	#	Type	BL-C[a]	BL[b]	BA-C[c]	BA[d]	DA-C[e]	DA[f]
TSB1 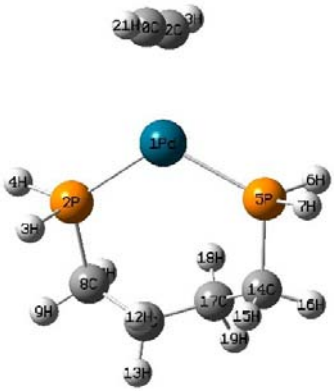 (HF=-183.2967865 au)	1	Pd						
	2	P	1	2.39411				
	3	H	2	1.454324	1	113.8298		
	4	H	2	1.458253	1	130.3772	3	120.0811
	5	P	1	2.397527	2	117.8789	4	-144.977
	6	H	5	1.45504	1	116.1477	2	111.3969
	7	H	5	1.457087	1	130.134	2	-125.797
	8	C	2	1.946701	1	117.3429	5	-16.3112
	9	H	8	1.093876	2	107.8808	1	161.4471
	10	H	8	1.09539	2	106.9981	1	-82.8567
	11	C	8	1.542786	2	111.7296	1	38.85987
	12	H	11	1.098441	8	109.6248	2	39.98649
	13	H	11	1.09819	8	108.0477	2	154.5499
	14	C	5	1.948888	1	114.5716	2	-0.45096
	15	H	14	1.09506	5	106.3641	1	-87.5604
	16	H	14	1.093623	5	108.2533	1	157.0374
	17	C	14	1.546446	5	111.7183	1	33.75207
	18	H	17	1.098287	14	109.6906	5	29.00097
	19	H	17	1.097693	14	108.3073	5	144.0381
	20	C	1	2.642998	5	121.1101	14	168.5375
	21	H	20	1.064587	1	116.5099	5	-92.5997
	22	C	20	1.226176	1	63.4723	5	87.39803
	23	H	20	2.275344	1	70.17371	5	87.41335
TSA2 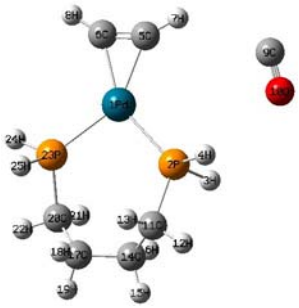 (HF=-204.9863232 au)	1	Pd						
	2	P	1	2.418813				
	3	H	2	1.449374	1	120.7859		
	4	H	2	1.448165	1	119.041	3	117.938
	5	C	1	2.10731	2	115.4105	4	43.01024
	6	C	5	1.273054	1	71.82518	2	-179.064
	7	H	5	1.074228	1	138.1133	6	-179.856
	8	H	6	1.074151	5	150.5152	1	-179.977
	9	C	5	3.602064	1	103.6949	6	-162.295
	10	O	9	1.15236	5	111.716	1	-1.89302
	11	C	2	1.937649	1	120.7209	6	162.2876
	12	H	11	1.093798	2	106.7022	1	-168.384
	13	H	11	1.095365	2	106.3684	1	-53.8741
	14	C	11	1.547811	2	115.1507	1	69.45865
	15	H	14	1.097979	11	106.5559	2	146.866
	16	H	14	1.099416	11	110.4812	2	32.84665
	17	C	14	1.550505	11	117.5219	2	-93.617

	18	H	17	1.099475	14	109.4275	11	-37.1617
	19	H	17	1.09868	14	106.8778	11	-150.977
	20	C	17	1.542969	14	118.0316	11	89.67123
	21	H	20	1.095416	17	110.6915	14	40.55701
	22	H	20	1.094056	17	109.3961	14	159.1053
	23	P	20	1.939543	17	115.8387	14	-80.248
	24	H	23	1.448181	20	97.3846	17	-156.08
	25	H	23	1.451781	20	97.28457	17	-59.1752
TSB3' 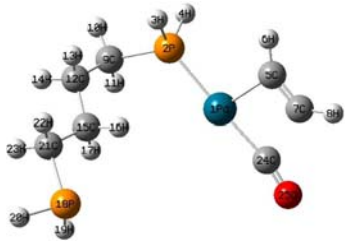 (HF=-204.9345599 au)	1	Pd						
	2	P	1	2.358804				
	3	H	2	1.442802	1	118.6872		
	4	H	2	1.440687	1	115.6275	3	116.4421
	5	C	1	2.039355	2	99.46603	4	64.25045
	6	H	5	1.082054	1	118.6945	2	0.816347
	7	C	5	1.298849	1	98.2154	2	-179.226
	8	H	7	1.086585	5	135.2808	1	-179.919
	9	C	2	1.928194	1	119.8479	7	-175.683
	10	H	9	1.094009	2	106.6087	1	-160.365
	11	H	9	1.094526	2	105.9717	1	-45.2102
	12	C	9	1.539358	2	113.951	1	77.31479
	13	H	12	1.099025	9	109.6802	2	57.26672
	14	H	12	1.099126	9	107.2458	2	172.0101
	15	C	12	1.543354	9	115.085	2	-66.7987
	16	H	15	1.097926	12	110.2021	9	62.78756
	17	H	15	1.098715	12	109.174	9	-53.4137
	18	P	15	2.893247	12	150.3284	9	178.0997
	19	H	18	1.458947	15	84.61664	12	123.0527
	20	H	18	1.458488	15	124.2951	12	32.19066
	21	C	15	1.53707	12	111.7466	9	-174.865
	22	H	21	1.095589	15	110.5232	12	-57.3012
	23	H	15	2.180418	12	97.18604	9	-150.094
	24	C	1	2.051295	7	47.94373	5	179.478
	25	O	7	2.640585	5	128.7168	1	0.757595
TSB4' 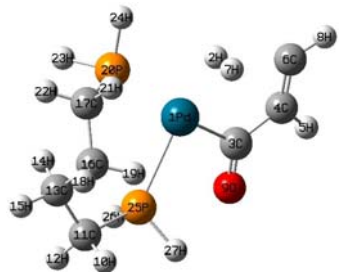 (HF=-206.1186799 au)	1	Pd						
	2	H	1	1.822449				
	3	C	1	2.094978	2	76.51764		
	4	C	3	1.507218	1	118.956	2	14.49785
	5	H	4	1.09134	3	109.0546	1	-179.814
	6	C	4	1.337191	3	126.1053	1	-0.38388
	7	H	6	2.09458	4	91.66221	3	10.72978
	8	H	6	1.094229	3	149.029	1	179.9604
	9	O	3	1.242411	1	118.5159	6	-178.058
	10	H	1	4.524246	3	107.6418	9	26.66409
	11	C	1	4.001782	3	111.3556	9	13.45866
	12	H	11	1.09322	1	129.3675	3	-63.0285
	13	C	11	1.540081	1	82.79476	3	-175.012
	14	H	13	1.09884	11	109.0389	1	60.24971
	15	H	13	1.097478	11	109.0338	1	175.0378

	16	C	1	3.91328	3	142.9276	9	40.97888
	17	C	16	1.536541	1	78.33856	3	168.0355
	18	H	13	2.17855	11	113.5203	1	-93.7563
	19	H	13	2.180141	11	85.77615	1	-54.236
	20	P	17	1.943262	1	34.60551	3	175.4616
	21	H	1	4.338845	3	157.5553	9	97.08564
	22	H	17	1.093799	16	112.1131	1	136.1278
	23	H	20	1.446417	17	100.5411	1	126.7022
	24	H	20	1.445264	17	99.13733	1	-135.203
	25	P	11	1.942301	13	111.285	16	-71.438
	26	H	11	2.616759	16	121.8445	17	33.96326
	27	H	11	2.636432	16	112.1827	17	88.05063

[a] bond length connection, [b] bond length in (Å),[c] atoms angle connection, [d] atoms angle in (degree), [e] dihedral angle connection, and [f] dihedral angle

Appendix C
Unsaturated Amide Product

Table C1: The optimized geometrical parameters of the product (unsaturated amide) using B3LYP/SDDAll level of theory.

Structure Product	Optimized Geometrical Parameters							
	Atom #	Atom Type	BL-C[a]	BL[b]	AA-C[c]	AA[d]	DA-C[e]	DA[f]
Amide 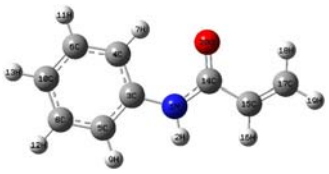 (HF=-82.3462551 au)	1	N						
	2	H	1	1.01155				
	3	C	1	1.418517	2	114.6812		
	4	C	3	1.406997	1	123.3074	2	179.9971
	5	C	3	1.408708	1	117.0057	4	-179.999
	6	C	4	1.399488	3	119.1707	1	-180
	7	H	4	1.079439	3	119.4816	1	-0.0042
	8	C	5	1.395302	3	120.3764	1	-179.999
	9	H	5	1.087214	3	119.7632	1	0.002942
	10	C	8	1.400678	5	120.1961	3	-0.00157
	11	H	6	1.084912	4	118.797	3	179.9989
	12	H	8	1.08489	5	119.5212	3	-179.999
	13	H	10	1.084435	8	120.2959	5	179.9997
	14	C	1	1.381307	3	129.1391	5	179.9799
	15	C	14	1.487375	1	113.8442	3	-179.986
	16	H	15	1.088029	14	117.9115	1	-0.02808
	17	C	15	1.33899	14	121.4521	1	179.974
	18	H	17	1.084896	15	120.3609	14	-0.00399
	19	H	17	1.084208	15	121.6707	14	179.9988
	20	O	14	1.256289	1	123.4475	3	0.01403

[a] bond length connection (BL-C)
[b] bond length (BL) in (Å)
[c] atoms angle connection (AA-C)
[d] atoms angle (AA) in (degree)
[e] dihedral angle connection (DA-C)
[f] dihedral angle (DA)

REFERENCES

1. Parshall, George W., *Homogeneous Catalysis*; John Wiley & Sons, Inc.: New York, 1981. 80.
2. Fable, J., *New Syntheses with Carbon Monoxide*; Springer-Verlag: Berlin, 1980.
3. Cenini, S.; Ragaini, F., *Catalytic Reductive Carbonylation of Organic Nitro Compounds*; Kluwer Academic Publishers: Dordrecht, 1997. 1.
4. Tijani, Jimoh, *Palladium-Catalyzed Regionselective Carbonylation of Coupling of Alkynes with Aniline Derivatives*; K.F.U.P.M.: Dhahran, 2001.
5. Copenhaver, J.,W.; Bigelow, M., H., *Acetylene and Carbon Monoxide Chemistry*; Reinhold Publishing Corporation: New York, 1949. 246.
6. Masters, C. *Homogeneous Transition-metal Catalysis*; Chapman and Hall Ltd: London, 1981.
7. Tsuji, J. *Perspectives in Organopalladium Chemistry for the XXI Century*, Krips Repro B.V., Netherlands, 1999
8. Kiss, G., *Chem. Rev*. 101 (2001) 3435
9. Sheldon, R. A. *Chemicals from Synthesis Gas*; Reifel Publishing Company: Netherlands, 1983, 104.
10. Heck, R. *Palladium Reagents in Organic Syntheses*, Academic Press Inc, London, 1985
11. Tsuji, Jiro, *Organic Synthesis with Palladium Compounds*; Springer-Verlag: Berlin, 1980. 81,161.
12. Vasapollo, G.; Somasunderam, A.; El Ali, B. Alper, H. *Tetrahedron Lett*. 1994, 35, 6203.
13. Cornils, B; Herrmann, W. A., *Applied Homogenous Catalysis with Organmetallic Compounds*; VCH Weinhein: Germany, 1996; Vol. 1.

14. Wender, I.; Pino, P. *Organic Syntheses via Metal Carbonyls*; John Wiley & Sons: New York, 1977.

15. El Ali, B.; Alper, H. *J. Mol. Catal*. 1991, 67, 29

16. El Ali, B.; Alper, H. *J. Mol. Catal*. 1995, 96, 197.

17. Torii, S.; Okumoto, H.; Sadakane, M; He Xu, L.; *Chem Lett*. 1991, 10, 1673.

18. Murahashi, S.; Imada, Y; Nishimura, K; *Tetrahedron*, 1994, 50, 2453.

19. Jensen, F. *Introduction to Computational Chemistry*, John Wiley & Sons Ltd., London 1999.

20. Dolg, M. in *Modern Methods and Algorithms of Quantum Chemistry*, J. Grotendorst, John von Neumann Institute for Computing, Julich, NIC Series, Vol. 1, P. 479-508, 2000.

21. Wadt, W. R.; Hay, P. *J. Chem. Phys*. 1985, 82,284.

22. Hay, P. J.; Wadt, W. R. *J. Chem. Phys*. 1985, 82,299.

23. Young, D. *Computational Chemistry*, John Wiley & Sons Ltd., New York, 2001.

24. Woo, T.K.; Margl, P.M.; Deng, L.; Cavallo, L.; Ziegler, T. *Catalysis Today*.1999, 50, 479.

25. Hagelin, H.; Akermark, B.; Norrby, P. *Organometallics*. 1999, 18, 2884.

26. Hagelin, H.; Svensson, M.; Akermark, B.; Norrby, P. *Organometallics*. 1999, 18, 4574.

27. Torii, S.; Okumoto, H.; Xu, L. H.; Sadakane, M.; Shostakovsky, M. V.; Ponomaryov, A. B.; Kalinin, V. N. *Tetrahedron*. 1993, 49(31), 6773.

28. Tanaka, H.; Hai, A. K. M. A.; Sadakane, M.; Okumoto, H.; Torii, S. *J. Org. Chem*. 1994, 59(11), 3040.

29. El Ali, B.; Tijani, J.; El-Ghanam, A. *J. Mol. Catal*. 2002, 187, 17.

30. Cui, Q.; Musaev, D. G.; Morokuma, K. *Organometallics*. 1998, 17, 742.

31. Cui, Q.; Musaev, D. G.; Morokuma, K. *Organometallics*. 1998, 17, 1383.

32. Jakt, M.; Johannissen, L.; Rzepa, H. S.; Widdowson, D. A.; Wilhelm, R. *J. Chem. Soc. Perkin Trans. 2*. 2002, 576.

33. Matsibara, T. *Organometallics*. 2003, 22, 4297.

34. Laird, B., B.; Ross, R., B.; Ziegler, T. *Chemical Applications of Density-Functional Theory*; American Chemical Society: Washington, DC, 1996.

35. Frisch, Æ.; Frisch, M. J.; Trucke, G. W. *Gaussian 03 User's Reference*; Gaussian, Inc.: Carnegie, 2003 and reference therein.

36. Gonzalez, C.; Schlegel, H. B. *J. Chem. Phys.* 1989, 90, 2154.

37. Gonzalez, C.; Schlegel, H. B. *J. Phys. Chem.* 1990, 94, 5523.

38. Leeuwen, P.; Morokuma, K.; Lenthe, J. *Theoretical Aspects of Homogeneous Catalysis*, Kluwer Academic Publishers, Netherlands, 1995.

39. Thomas, R. *Computational Organometallic Chemistry*, Marcel Dekker Inc., New York, 2001.

40. Thomas, R. *J. Chem. Inf Comput. Sci* 39 (1999) 376.

41. *HyperChem. Reference Manual*; Hypercube, Inc.: Canada, 1996.

42. *CS Chem3D Pro*. Cambridge Soft Corporation: 1999.

43. *Titan. Tutorial and User's Guide*; Wavefunction Inc. Schrödinger Inc.: USA, 1999.

44. *Gaussian 98*, Revision A.6, M. J. Frisch, G. W. Trucks, H. B. Schlegel, G. E. Scuseria, M. A. Robb, J. R. Cheeseman, V. G. Zakrzewski, J. A. Montgomery, Jr.,R. E. Stratmann, J. C. Burant, S. Dapprich, J. M. Millam, A. D. Daniels, K. N. Kudin, M. C. Strain, O. Farkas, J. Tomasi, V. Barone, M. Cossi, R. Cammi, B. Mennucci, C. Pomelli, C. Adamo, S. Clifford, J. Ochterski, G. A. Petersson, P. Y. Ayala, Q. Cui, K. Morokuma, D. K. Malick, A. D. Rabuck, K. Raghavachari, J. B. Foresman, J. Cioslowski, J. V. Ortiz, B. B. Stefanov, G. Liu, A. Liashenko, P. Piskorz, I. Komaromi, R. Gomperts, R. L. Martin, D. J. Fox, T. Keith, M. A. Al-Laham, C. Y. Peng, A. Nanayakkara, C. Gonzalez, M. Challacombe, P. M. W. Gill, B. Johnson, W. Chen, M. W. Wong, J. L. Andres, C. Gonzalez, M. Head-Gordon, E. S. Replogle, and J. A. Pople, Gaussian, Inc., Pittsburgh PA, 1998.

45. *Gaussian 03*, Revision B.04, M. J. Frisch, G. W. Trucks, H. B. Schlegel, G. E. Scuseria, M. A. Robb, J. R. Cheeseman, J. A. Montgomery, Jr., T. Vreven, K. N. Kudin, J. C. Burant, J. M. Millam, S. S. Iyengar, J. Tomasi, V. Barone, B. Mennucci, M. Cossi, G. Scalmani, N. Rega, G. A. Petersson, H. Nakatsuji, M. Hada, M. Ehara, K. Toyota, R. Fukuda, J. Hasegawa, M. Ishida, T. Nakajima, Y. Honda, O. Kitao, H. Nakai, M. Klene, X. Li, J. E. Knox, H. P. Hratchian, J. B. Cross, C. Adamo, J. Jaramillo, R. Gomperts, R. E. Stratmann, O. Yazyev, A. J. Austin, R. Cammi, C. Pomelli, J. W. Ochterski, P. Y. Ayala, K. Morokuma, G. A. Voth, P. Salvador, J. J. Dannenberg,V. G. Zakrzewski, S. Dapprich, A. D. Daniels, M. C. Strain, O. Farkas, D. K. Malick, A. D. Rabuck, K. Raghavachari, J. B. Foresman, J. V. Ortiz, Q. Cui, A. G. Baboul, S. Clifford, J. Cioslowski, B. B. Stefanov, G. Liu, A. Liashenko, P. Piskorz, I. Komaromi, R. L. Martin, D. J. Fox, T. Keith, M. A. Al-Laham, C. Y. Peng, A. Nanayakkara, M. Challacombe, P. M. W. Gill, B. Johnson, W. Chen, M. W. Wong, C. Gonzalez, and J. A. Pople, Gaussian, Inc., Pittsburgh PA, 2003.

46. *GaussView*, Gaussian, Inc. Carnegie Office Park, Bldg. 6, Carnegie, PA 15106 USA.

47. Becke, A. D. *Phys. Rev. A.* 1988, 38, 3098.

48. Becke, A. D. *J. Chem. Phys.* 1993, 98, 5648.

49. Lee, C.; Yang, W.; Parr, R. G. *Phys. Rev. B.* 1988, 37, 785.

50. Frisch, Æ.; Frisch, M. J. *Gaussian 98 User's Reference*; Gaussian, Inc.: Carnegie, 1998.

51. Frisch, Æ.; Dennington II, R.; Keith, T. *GaussView Reference*; Gaussian, Inc.: Carnegie, 2003.

52. Szentpaly, L. V. Fuentealba, P.; Preuss, H.; Stoll, H. *Chem. Phys. Lett.* 1982, 93, 555.

53. Fuentealba, P.; Stoll, H.; Szentpaly, L. V.; Schwerdtfeger, P.; Preuss, H. *J. Phys. B.* 1983, 16, 1323.

54. Stoll, H.; Fuentealba, P.; Schwerdtfeger, P.; Flad, J.; Szentpaly, L. V.; Preuss, H. *J. Chem. Phys.* 1984, 81, 2732.

55. Fuentealba, P.; Szentpaly, L. V.; Preuss, H.; Stoll, H.; *J. Phys.B* 1985, 18, 1287.

56. Fuentealba, P.; Preuss, H.; Stoll, H.; Szentpaly, L. V. *Chem. Phys. Lett.* 1989, 89, 418.

57. Stevens, W.; Basch, H.; Krauss, M. *J. Chem. Phys*. 1984, 81, 6026.

58. Stevens, W.; Krauss, M.; Basch, H.; Jasien, P.G. *Can. J. Chem*. 1992, 70, 612.

59. Cundari, T.R.; Stevens, W. J. *J. Chem. Phys*. 1993, 98, 5555.

60. Bottoni, A.; Higueruelo, A. P.; Miscione, G. P. *J. Am. Chem. Soc*. 2002, 124, 5506.

61. March, J. *Advanced Organic Chemistry* 3rd ed. John wily & Sons, New York, 1985

Vitae

Jameel Al- Thagfi

Born in Taif, Kingdom of Saudi Arabia, 1979.

Received B.S. in chemistry from King Fahad University of Petroleum and Minerals in June 2001.

Started M.S. program in chemistry at KFUPM in September 2001.

Joined KFUPM as graduate assistant in March 2002.

M.S. degree in chemistry in May 2004.

Conferences and publications contribution:

1- J. R. Al-Thagfi, M. A. Morsy* and Bassam El Ali

"Towards Unforced Density Functional Theory Computational Modeling of Homogeneous Catalysis of Palladium-Phosphine Complexes". The 14th International Symposium on Homogeneous Catalysis, Munich, July 5-9, 2004.

2- M. A. Morsy,* J. R. Al-Thagfi, and Bassam El Ali

"Computational Study on the Origin of the Regio-Selectivity in the formation of unsaturated amides from terminal alkyne using Palladium Catalyst". The Second Workshop on Catalysts Application in The GCC Countries: New Trends in the chemistry of catalysis, Sharjah, UAE, December, 13-15, 2004.